Deliverable No. 9.1
User requirements for the visualization toolkit and image analysis toolkits

Grant Agreement No.:	600841
Deliverable No.:	D9.1
Deliverable Name:	User requirements for the visualization toolkit and image analysis toolkits
Contractual Submission Date:	30/09/2013
Actual Submission Date:	01/10/2013

Dissemination Level		
PU	Public	**X**
PP	Restricted to other programme participants (including the Commission Services)	
RE	Restricted to a group specified by the consortium (including the Commission Services)	

CO	Confidential, only for members of the consortium (including the Commission Services)	

COVER AND CONTROL PAGE OF DOCUMENT	
Project Acronym:	**CHIC**
Project Full Name:	Computational Horizons In Cancer (CHIC): Developing Meta- and Hyper-Multiscale Models and Repositories for In Silico Oncology
Deliverable No.:	D9.1
Document name:	Requirement Analysis for Computational Horizons In Cancer (CHIC)
Nature (R, P, D, O)[1]	R
Dissemination Level (PU, PP, RE, CO)[2]	PU
Version:	5
Actual Submission Date:	01/10/2013
Editor: Institution: E-Mail:	Nikolaos Ersotelos University of Bedfordshire Nikolaos.Ersotelos@beds.ac.uk

ABSTRACT:

This deliverable focuses on the analysis of the requirements for the Computational Horizons In Cancer project. The analysis, initially reviews related approaches from currently running research project. Then it specifies the methodology that will be followed and presents the first two phases: i.e. the purpose and scope specification and the knowledge acquisition. In the first phase the description of the work and the use-cases are analyzed to identify the domain of interest whereas in the second phase relevant domains are analyzed and evaluated. In the following months the outcomes of this deliverable will be used to specify the Computational Horizons In Cancer (CHIC).

KEYWORD LIST:

Requirement Analysis, VPH, multiscale model, repository, metamodel, hypermodel, cancer, in silico oncology, oncosimulator

The research leading to these results has received funding from the European Community's Seventh Framework Programme (FP7/2007-2013) under grant agreement n° 600841.

[1] **R**=Report, **P**=Prototype, **D**=Demonstrator, **O**=Other

[2] **PU**=Public, **PP**=Restricted to other programme participants (including the Commission Services), **RE**=Restricted to a group specified by the consortium (including the Commission Services), **CO**=Confidential, only for members of the consortium (including the Commission Services)

The author is solely responsible for its content, it does not represent the opinion of the European Community and the Community is not responsible for any use that might be made of data appearing therein.

MODIFICATION CONTROL			
Version	**Date**	**Status**	**Author**
1.0	01/09/2013	Draft	Nikolaos Ersotelos
2.0	13/09/2013	Draft	Nikolaos Ersotelos
3.0	30/09/2013	Pre final	Nikolaos Ersotelos
4.0	01/10/2013	Final	Nikolaos Ersotelos

List of contributors

- Feng Dong, BED
- Kostas Marias, FORTH
- Mauricio Reyes, UBern
- Kontopodis Eleftherios, FORTH
- George Manikis, FORTH
- Dimitra Dionysiou, ICCS
- Georgios S. Stamatakos, ICCS
- Norbert Graf, USAAR

Contents

1 Executive Summary

This deliverable focuses on the analysis of the requirements of visualization and image processing for the Computational Horizons In Cancer project. The analysis, initially reviews related approaches from currently running research project. Then it specifies the methodology that will be followed and presents the first two phases: i.e. the purpose and scope specification and the knowledge acquisition. In the first phase the description of the work and the use-cases are analyzed to identify the domain of interest whereas in the second phase relevant domains are analyzed and evaluated. In the following months the outcomes of this deliverable will be used to specify the Computational Horizons In Cancer (CHIC).

2 Introduction

Developing robust, reproducible, interoperable and collaborative hyper-models of diseases and normal physiology is a sine qua non necessity if rational, coherent and comprehensive exploitation of the invaluable information hidden within human multiscale biological data is envisaged. Responding to this imperative in the context of both the broad Virtual Physiological Human (VPH) initiative and the paradigmatic cancer domain, CHIC proposes the development of a suite of tools, services and secure infrastructure that will support accessibility and reusability of VPH mathematical and computational hypermodels. These will include a hypermodelling infrastructure consisting primarily of a hypermodelling editor and a hypermodelling execution environment, an infrastructure for semantic metadata management, a hypermodel repository, a hypermodel-driven clinical data repository, a distributed metadata repository and an in silico trial repository for the storage of executed simulation scenarios. Multiscale models and data will be semantically annotated using the ontological and annotating tools to be developed.

An image processing and visualization toolkit will be developed. They will reside in the CHIC model repository, which will store the multiscale models, the complimentary tools and modules. The CHIC image processing tools (e.g. brain tumour image analysis framework, general image processing development toolkit, image registration tools, software platform for the assessment of tumour treatment response) will be used in the preprocessing of imaging data in order to be prepared for usage in the simulations. The results of the simulations will use the CHIC visualization tools in order to be presented to the user. The visualization toolkit will offer general development environment for visualization, visual analysis suite for model repositories, visual analysis suite for data repositories

The image processing and visualization toolkits will be integrated into CHIC tools, services, infrastructure and repositories to provide the community with a collaborative interface for exchanging knowledge and sharing work in an effective and standardized way. A number of open source features and tools will enhance usability and accessibility.

2.1 Purpose of this document

This document will gather user requirement on the visual analysis suite and image analysis tools. Typical approaches and examples that are expected to receive benefit from the use of visualization and image analysis are identified and analysed. The document will look into current problems and needs in the model and data analysis and understand the scales of the model and data repositories.

According to the aforementioned claims, the purpose of this deliverable is to establish the methodology for the visualization development of the Computational Horizons In Cancer (CHIC) project. The first step towards this direction is to identify the purpose and the scope of this project and then to reuse existing approaches that can model the needed information. The development of the Computational Horizons In Cancer (CHIC) visualization project will be based on the following three principles:

- **Reuse**: Avoid “reinventing the wheel” and reuse already established high quality models for identifying visually the tumor's shape and growth.
- **Granularity**: Usually in health-care domain, annotations or mappings cannot be extracted from a model. So, multiple models should be used.

Those principles are already extensively used in similar research projects.

2.2 Structure of this document

The structure of this document is the following: Sections 3 reviews similar approaches from research projects. Then Section 4 defines the models which will be included for the visualization and image processing CHIC's project Section 5 describes the analysis of images in the brain tumor domain, whereas Section 6 gives an overview of MRI data used in CHIC and their implementation. Finally, Section 7 concludes this deliverable.

3 Recent approaches of visualization and image processing

3.1 Visualization

Information visualization has been an interesting topic that attracts user attentions for many years with a wide range of techniques available nowadays, including scatterplots [Utts05, Cle88], parallel coordinates [INS85], trees[SHN92, FEK02] and graphs[Lan10], etc.

This project involves a significant amount of models and data from the repositories. Visualization will be useful in terms of enhancing user understanding towards the model and data structures and helping the retrieval of relevant information from the model and data. While most of the visualization techniques deal with datasets, this project will need visualization on both model and data repository. Therefore, the target of the visualization task is a complex mixture of highly heterogeneous information, including the structures of model/data repository, model information, data information and data itself (e.g. images).

To support the visualization of large information set, we need to address the scalability issues. While significant progresses have been made in visual representation and exportation of large datasets, scalability still remains as a challenging issue. Indeed, large amount of datasets can lead to overplotting, which significantly hampers the capability of human vision in identifying data patterns and hence reduces the effectiveness of visualization. While great efforts have been made towards the scalability issue [PIR11], the techniques that deal with large datasets still attract a lot of research attentions. The relevant techniques include:

- Filtering techniques [LES06], which allow users to focus on their selected targeted data;
- Aggregation [ELM08] is also important as it allows us to combine details and create different levels of overviews in hierarchies, which support users to perform "overviews first and details on demand". Hierarchical clustering techniques can be used to create effective aggregation of data at different levels of details. Also, uncertainty-based aggregation creates data aggregation with uncertainty information to enhance user understanding towards the aggregated data.
- Dimension reduction is very useful in reducing data volumes. Subspace clustering helps identify the meaningful cohort of patients in a subset of relevant dimensions [KRI09]. Given a dataset with high dimensionality, the number of possible sub feature space is exponentially high. Fully automatic machine learning normally does not do a good job in terms of identifying the clusters. A recent trend is to involve human experts [FER10], which couples user interaction with the subspace clustering process.
- Data analysis techniques, such as data fitting, regression, graph structure analysis [GRE07, vLan09], comparison [AND09] can also be used to assist the process of large data.
- Processing of large dataset is time consuming. Multi-threading and parallel processing (e.g. GPGPU) could be the solution.

In addition, the prediction of tumour development is clearly an area of high uncertainty, and the development of means by which the uncertainty can be made evident and be taken into account within the clinical process would be very useful. Also, data aggregation involved in large scale visualization produces a considerable amount of uncertainty, which can be

originated from the aggregation techniques (e.g. binning, clustering). The uncertainty-aware visualization techniques inlucde:

- Visualization of uncertainty related to data aggregation – the technique will need to visually present the uncertainty within aggregated data (e.g. mean, standard deviation, etc..). This helps to present a faithful picture of the dataset after the aggregation.

- Presentation of uncertainty information within a graph. Typical techniques to portray graphs include node-link, matrix view, etc. [HER00, SCH09, NEU06, BAT99]. Nowadays a typical graph visualization contains multiple types of nodes (i.e. so call multiple mode), which reflects the heterogeneous nature of the data. While various techniques and tools exist for visualizing uncertainty in scientific visualizations [Ced00,Pot10], little attention has been paid towards the uncertainty information in graphs. Finally, user interaction with data has always been an interesting research issue. The interaction techniques are categorized as select, explore, reconfigure, encode, abstract,/elaborate, filter, and connect[Yi07]. An important task of user interaction is to help user navigation of the data. To this end, the interaction should follow the recommendation of "overviews first and details-on-demands" by working together with the data aggregation. Also, techniques that support zoom in within local areas, such as focus+cotext, coordinate views, help users to interactively explore data details without losing the perception towards the overall data structure.

3.2 Image processing

Image segmentation has been a classic problem in image analysis and computer vision [Pal93]. Some recent work has made good progresses (e.g. the mean-shift based segmentations [JEN08]). The advance of pattern recognition and machine learning techniques with respect to data clustering (unsupervised) and classification (supervised) has pushed the state of the art of image segmentation greatly forward, especially owing to the adaptation of training datasets to assist the performance. Also, special attentions have been paid towards a group of global energy minimization based methods that cast the segmentation into an energy minimization problem and search for a global energy minimal point, which lead to improved results due to the consideration of the segmentation at a global scale [SZE08]. Different energy minimization approaches such as graph cut [BOY01, BOY04], belief propagation [FEL04, YAN10], tree reweighted message passing [WAI05, KOL06] have been investigated.

Different modalities of imaging techniques (e.g. T1 MRI, T1 contrast enhanced MRI, T2 MRI, T2 flair MRI, CT, PET, etc) are required when diagnosing disease such as gliomas. Even so, it is very difficult for a radiologist to define the exact margins of bulk tumor. For example, even with four different modalities (T1, T1 contrast enhanced, T2, T2 flair), glioma boundaries are not easily discernible and within each boundary different pathophysiological information is contained. The clinician needs to understand the complex interplay between these multi-modal boundaries in order to gather information concerning the individual tumor properties. To date current available systems for automatic morphometric analysis of brain tumors, patient follow-up, radiotherapy planning, and decision support based systems do not provide effective knowledge of the tumor and its surroundings, unless manual techniques are used, which are highly time consuming and user-dependent, hindering their use in practice. However, the state of the art shows that there is an increasing interest in developing advanced tissue classification techniques (also called image segmentation) for healthy and pathological

brain tissues, as well as tumor growth models that aim to characterize the complex pathophysiological scenario of gliomas and its surroundings.

Current segmentation methods can be divided into two different categories: In most cases, classification methods with some degree of spatial regularization are employed for the segmentation of multimodal datasets [VER08], [WEL08], [BAU11], while atlas-based segmentation is an established way for segmenting monomodal image [ZAC09], [GOO11], [BAU12]. Using atlas-based segmentation on the high-resolution monomodal image is attractive thanks to its robustness and its versatile usability because it allows to overlay DTI maps or subcortical label maps on the patient image, which is important information in neurosurgery and radiotherapy. Most atlas based segmentation methods establish initial correspondence between a healthy atlas and a pathologic patient image by seeding the atlas with a patient-specific tumor prior, which is often based on a tumor-growth model. The deformation field, which is obtained after non-rigid registration of the modified atlas to the patient can be used for warping the atlas label image, thus obtaining an implicit segmentation of the patient image. The shortcomings of most current approaches include the need for a manual segmentation of the tumor area as an input for the tumor growth process and no optimal utilization of the segmented healthy tissues during atlas-based segmentation. In addition, in order to bring these emerging technologies into clinical practice it is crucial to design and develop them taking into account current clinical imaging protocols.

4 Requirement of visualization and image processing from cancer models

Image processing and visualization utilities will be developed. They will reside in the CHIC model repository, which will store the multiscale models, the complimentary tools and modules. Hence, this section will review the cancer models that are to be included in the CHIC model repository in terms of their requirement on visualization and image processing. Notably, each model can be studied from multiple perspectives, in which different visualization and image processing techniques are applied. In the rest of this section, it will presented studies of each model by providing a brief summary of the study and by reviewing their requirement on visualization and image processing.

4.1 UPENN - Molecular Dynamics of clinical mutations in oncogenic receptors

Model description
All-atom molecular dynamics simulations are performed and analyzed for 30 mutations found in neuroblastoma patients to determine potential of kinase activation

4.1.1 Study 1: All-atom molecular dynamics simulations using orientational constraints from anisotropic NMR samples

[STE07] Orientational constraints obtained from solid state NMR experiments on anisotropic samples are used here in molecular dynamics (MD) simulations for determining the structure and dynamics of several different membrane-bound molecules. The new MD technique is based on the inclusion of orientation dependent pseudoforces in the COSMOS-NMR force field. These forces drive molecular rotations and re-orientations in the simulation, such that the motional time-averages of the tensorial NMR properties approach the experimentally measured parameters. The orientational-constraint-driven MD simulations are universally applicable to all NMR interaction tensors, such as chemical shifts, dipolar couplings and quadrupolar interactions. The strategy does not depend on the initial choice of coordinates, and is in principle suitable for any flexible molecule. To test the method on three systems of increasing complexity, they were used as constraints some deuterium quadrupolar couplings from the literature on pyrene, cholesterol and an antimicrobial peptide embedded in oriented lipid bilayers. The MD simulations were able to reproduce the NMR parameters within experimental error. The alignment of the three membranebound molecules and some aspects of their conformation were thus derived from the NMR data, in good agreement with previous analyses. Furthermore, the new approach yielded for the first time the distribution of segmental orientations with respect to the membrane and the order parameter tensors of all three systems.

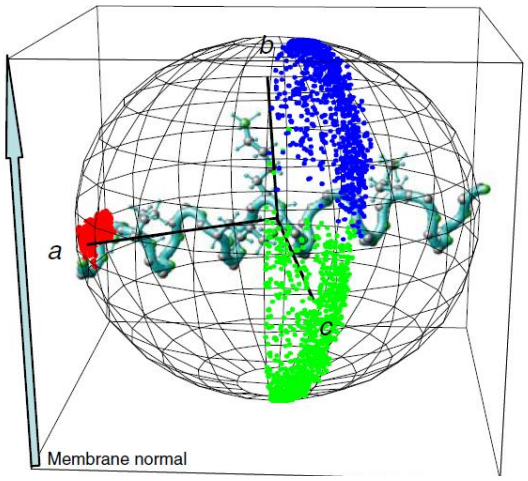

Fig. 1. Visualization of the alignment and motional behaviour of the a-helical peptide PGLa (only lysine side chains shown) in a DMPC membrane, as determined by a 1 ns MD simulation using experimental ^{2}H-NMR constraints (Strandberg et al. 2005) The instantaneous orientation of the three axes of inertia a, b and c is displayed as a scatter plot on a sphere, representing snapshots of these axes orientations every picosecond. The poles of the sphere are oriented parallel to the membrane normal. The helix long axis displays only a small scatter with a mean tilt angle of 99^{o}, while the two other axes oscillate about this direction producing a large scatter.

4.2 UPENN - Autodock

Model description
AutoDock is a suite of automated docking tools. It is designed to predict how small molecules, such as substrates or drug candidates, bind to a receptor of known 3D structure.

4.2.1 Study 1: AutoDock4 and AutoDockTools4: Automated Docking with Selective Receptor Flexibility

[MOR09] This study describes the testing and release of AutoDock4 and the accompanying graphical user interface AutoDockTools. AutoDock4 incorporates limited flexibility in the receptor. Several tests are reported here, including a redocking experiment with 188 diverse ligand-protein complexes and a cross-docking experiment using flexible sidechains in 87 HIV protease complexes. it is also reported its utility in analysis of covalently-bound ligands, using both a grid-based docking method and a modification of the flexible sidechain technique.
Docking of penicillin in a covalent complex with D-alanyl-D-alanine carboxypeptidase
The results are shown in Fig. 2 are for docking of penicillin in a covalent complex with D-alanyl-D-alanine carboxypeptidase. In the first two experiments, a Gaussian map was created and centered on the CB or OG atoms of SER62 (Fig. 2A and 2B). afterwards they were performed docking experiments with the appropriate atoms in the ligand targeted to that map. Poor results were obtained: a wide range of conformation was found and the conformation of best energy showed only slight resemblance to the crystallographic conformation. Better results were obtained when two Gaussian maps were used, corresponding to CB and OG of the serine (Fig. 2C). This forced the docked ligand to adopt the appropriate geometry of bonding with the serine, and resulted in docked conformations that were much more similar

to the crystallographic conformation. Use of a flexible sidechain to model the covalent ligand gave excellent results. All 10 docking runs gave similar conformations, all of which were very similar to the crystallographic conformation (Fig. 2D).

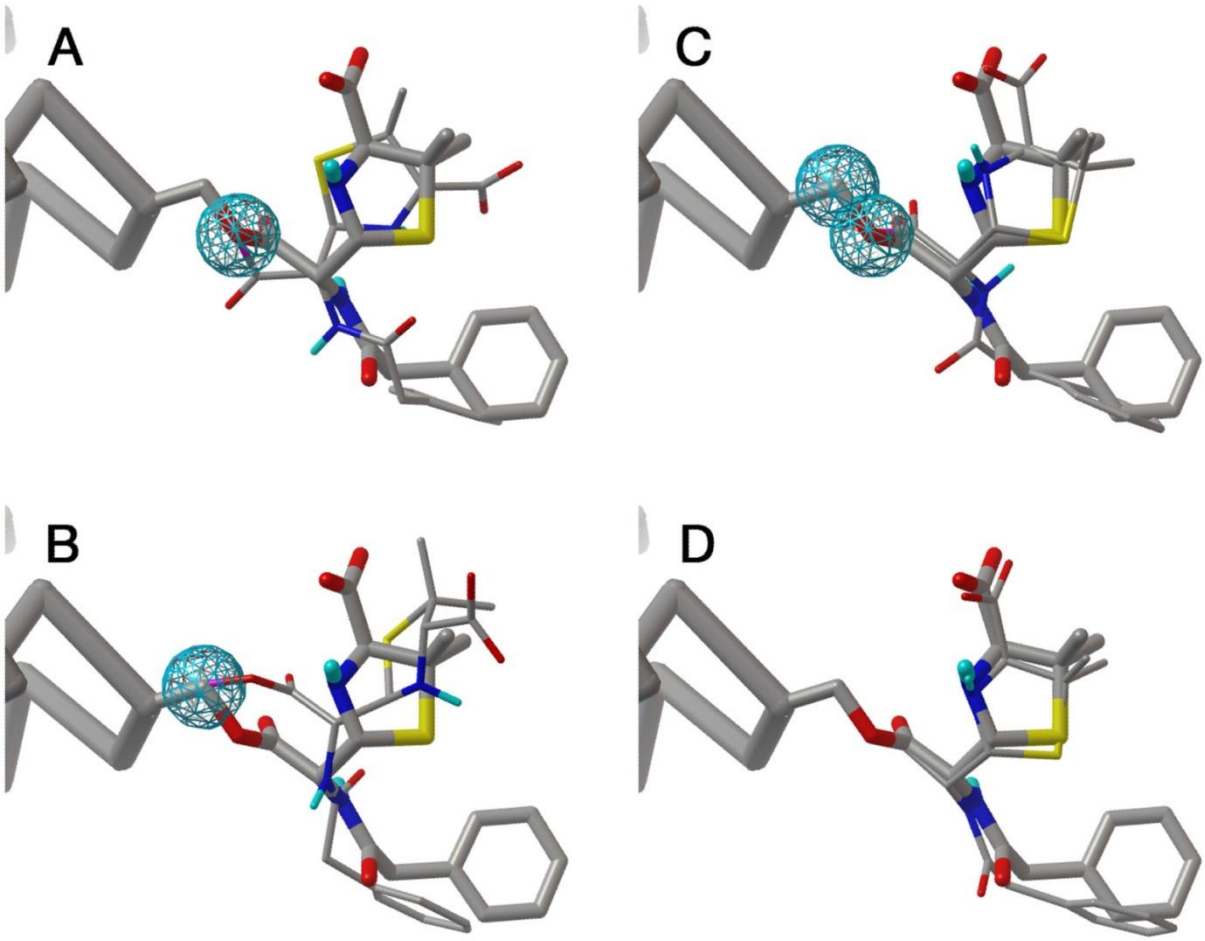

Fig. 2. Results of covalent docking: (A) Using a Gaussian map centered on serine OG. The crystallographic structure is shown in large bonds and the best docked conformation is shown in thinner bonds. The blue sphere surrounds the region of most favorable energy in the Gaussian map. (B) Using a Gaussian map centered on serine CB. (C) Using two Gaussian maps. (D) Using a flexible sidechain to model the covalent ligand.

4.2.2 Study 2: A Semiempirical Free Energy Force Field with Charge-Based Desolvation

[HUE07] This study describes the development and testing of a semiempirical free energy force field for use in AutoDock4 and similar grid-based docking methods. The force field is based on a comprehensive thermodynamic model that allows incorporation of intramolecular energies into the predicted free energy of binding. It also incorporates a charge-based method for evaluation of desolvation designed to use a typical set of atom types. The method has been calibrated on a set of 188 diverse protein–ligand complexes of known structure and binding energy, and tested on a set of 100 complexes of ligands with retroviral proteases. The force field shows improvement in redocking simulations over the previous AutoDock3 force field.

This following diagram Fig. 3 describes an assignment of an unbound state for the ligand and protein. In this work, they were tested three approaches to the unbound state, as shown in Fig.

3. These states are simple approximations to the ensemble of unbound conformations, making a few extreme assumptions about which conformations dominate the energetics of the ensemble.
The first approach (the ‘‘extended’’ state) is a fully extended conformation, which models a fully solvated conformation with few internal contacts. A short optimization was performed on the ligand in isolation using a uniform potential inversely proportional to the distance between each pair of atoms. This pushes all atoms as far away from one another as possible.
The second approach (the ‘‘compact’’ state) is a minimized conformation that has substantial internal contacts, modeling a folded state for the unbound ligand. AutoDock4 was used with values of the energetic parameters taken from the calibration using the extended state in order the new solvation model in the determination of this unbound state to be included. A short Lamarckian genetic algorithm conformational search was performed, using an empty affinity grid. As expected, these conformations tend to bury hydrophobic portions inside and form internal hydrogen bond interactions.
The final approach (the ‘‘bound’’ state) uses the assumption used in AutoDock3 and many other docking methods. In this, it is assumed that the conformation of the unbound state is identical to the conformation of the bound state.

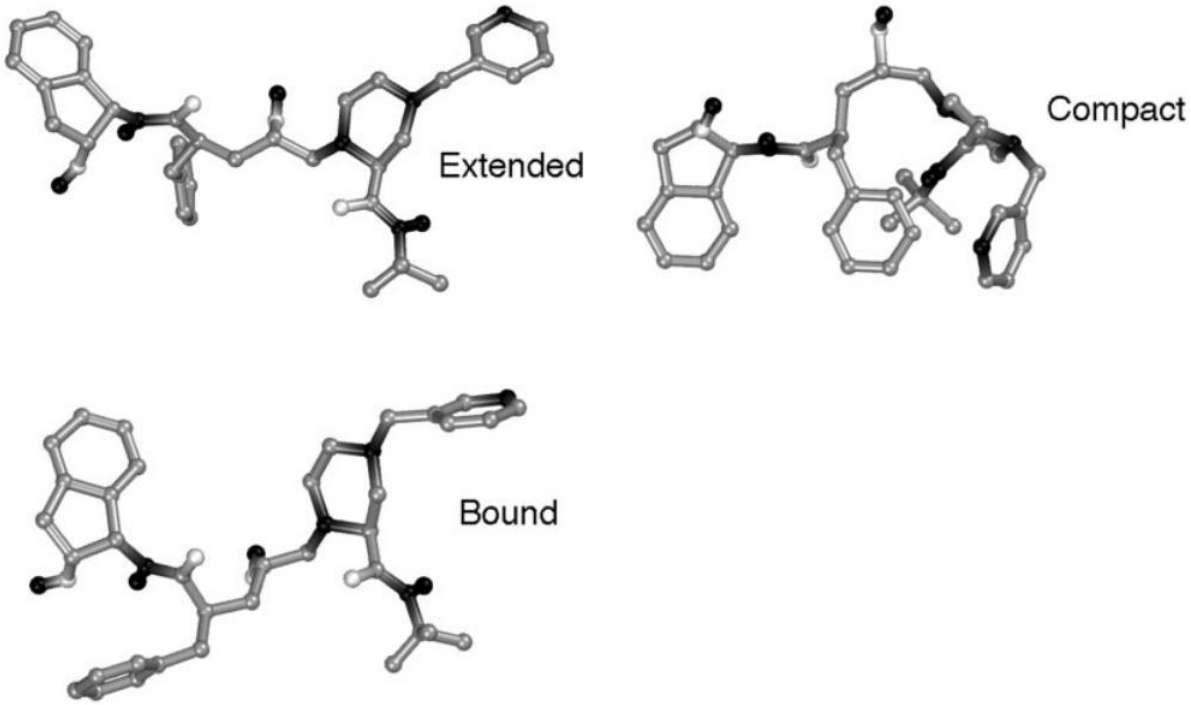

Fig. 3. Comparison of the extended, compact, and bound conformations of the HIV protease inhibitor indinavir, taken from PDB entry 1hsg. Note that the extended and bound states are quite similar, and that the hydrophobic groups have formed a cluster in the compact state.

4.3 UPPENN - Shape Signatures

Model description

computer-aided ligand- and receptor-based drug design.

4.3.1 Study 1: Shape Signatures: A New Approach to Computer-Aided Ligand- and Receptor-Based Drug Design

[ZAU03] A unifying principle of rational drug design is the use of either shape similarity or complementarity to identify compounds expected to be active against a given target. Shape similarity is the underlying foundation of ligand-based methods, which seek compounds with structure similar to known actives, while shape complementarity is the basis of most receptor based design, where the goal is to identify compounds complementary in shape to a given receptor. These approaches can be extended to include molecular descriptors in addition to shape, such as lipophilicity or electrostatic potential. Here it is introduced a new technique, which it calls shape signatures, for describing the shape of ligand molecules and of receptor sites. The method uses a technique akin to ray-tracing to explore the volume enclosed by a ligand molecule, or the volume exterior to the active site of a protein. Probability distributions are derived from the ray-trace, and can be based solely on the geometry of the reflecting ray, or may include joint dependence on properties, such as the molecular electrostatic potential, computed over the surface. Our shape signatures are just these probability distributions, stored as histograms. They converge rapidly with the length of the ray-trace, are independent of molecular orientation, and can be compared quickly using simple metrics. Shape signatures can be used to test for both shape similarity between compounds and for shape complementarity between compounds and receptors and thus can be applied to problems in both ligand- and receptor-based molecular design. this study presents results for comparisons between small molecules of biological interest and the NCI Database using shape signatures under two different metrics. The results show that the method can reliably extract compounds of shape (and polarity) similar to the query molecules. It will be also presented initial results for a receptor-based strategy using shape signatures, with application to the design of new inhibitors predicted to be active against HIV protease.

Receptor-Based Design

Fig. 4. shows the receptor subsite created by removing the R2 substituent (tert-butyl formamide) from the Indinavir framework, along with the associated ray-trace. Subsites were created using the same approach at the R3 (phenyl) and R4 (benzocyclopentanol) positions (not shown).

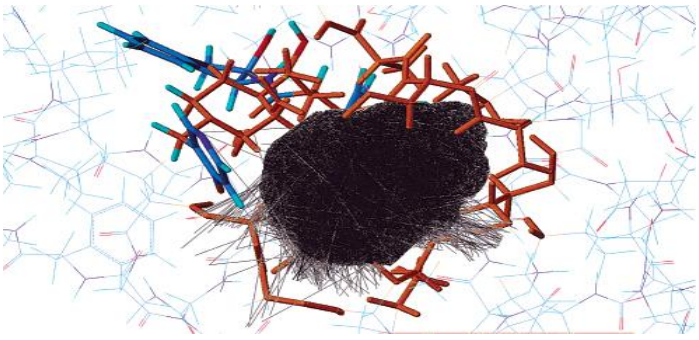

Fig. 4. Ray-traces in HIV protease subsite R2 (as defined in the text). Protein atoms involved in defining a site are orange; framework atoms are colored by atom type. All subsite atoms appear in capped-stick rendering.

4.4 UOXF - Cell cycle model for Wnt signalling pathway

Model description
ODE model of cell cycle at subcellular level; focus on influence of local oxygen concentration on cell cycle progression; distinguish between normal and cancer cells Ode model for wnt signalling pathway at subcellular level; model accounts for competition for beta-catenin between nucleus and cell membrane

4.4.1 Study 1: Elucidating the interactions between the adhesive and transcriptional functions of β-caterin in normal and cancerous cells

[LEE07] Wnt signalling is involved in a wide range of physiological and pathological processes. The presence of an extracellular Wnt stimulus induces cytoplasmic stabilisation and nuclear translocation of β-catenin, a protein that also plays an essential role in cadherin-mediated adhesion. Two main hypotheses have been proposed concerning the balance between β-catenin's adhesive and transcriptional functions: either β-catenin's fate is determined by competition between its binding partners, or Wnt induces folding of β-catenin into a conformation allocated preferentially to transcription. The experimental data supporting each hypotheses remain inconclusive. In this paper it will be presented a new mathematical model of the Wnt pathway that incorporates β-catenin's dual function. We use this model to carry out a series of in silico experiments and compare the behaviour of systems governed by each hypothesis. Our analytical results and model simulations provide further insight into the current understanding of Wnt signalling and, in particular, reveal differences in the response of the two modes of interaction between adhesion and signalling in certain in silico settings. It also be exploited a model to investigate the impact of the mutations most commonly observed in human colorectal cancer. Simulations show that the amount of functional APC required to maintain a normal phenotype increases with increasing strength of the Wnt signal, a result which illustrates that the environment can substantially influence both tumour initiation and phenotype.

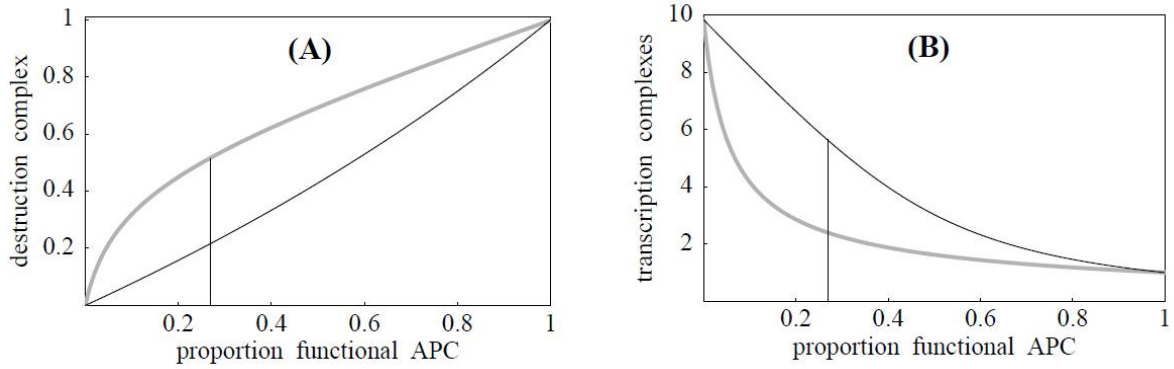

Fig. 5. Effects of continuous Wnt-exposure on gene expression. The Wnt signal S∞ __≡1 starts at time τ=0. The Wnt-induced increase in the rate of Tyr-phosphorylation, $\widehat{\mu}_c(1) - \mu_c$, is given by bottom-up values of 0 (*H*.I; dashed lines), 25 (*H*.II) and 175 (*H*.II), respectively. The higher the rate of Tyr-phosphorylation, the quicker is the initial response to the Wnt stimulus. (A) Normalised level of transcription complexes, $C_T(\tau)/C_T^{\star\star}$. (B) Normalised level of target protein, $Y(\tau)/Y^{**}$. The **'s denote steady-state values in the absence of Wnt. For the parameter values chosen, 1500 dimensionless-time units correspond to 2 h.

4.5 ICCS - NTUA - ISOG - Untreated Tumor Growth. Spatial code

Model description
The model simulates the spatiotemporal growth of untreated clinical tumors. It is based on the consideration of a discrete time and space stochastic cellular automaton, representing the tumor region. More specifically, the tumor region can be considered as a grid of "geometrical cells" (GCs, the elementary volume of the grid). Each GC corresponds to a cluster of heterogeneous cells found in various states. Specific rules regulate the transition between these states, as well as cell movement throughout the tumor volume; the aim is a realistic, conformal to the initial shape of the tumor, simulation of spatial evolution.
The adopted cytokinetic model incorporates the biological mechanisms of cell cycling, quiescence, differentiation and loss. Stem, LIMP, DIFF, apoptotic and necrotic cells represent the distinct cell categories of the model. More specifically, tumor sustenance is attributed to the presence of a cell population that exhibits stem cell like properties. Specifically, cancer stem cells have the ability to preserve their own population, as well as give birth to cells of limited mitotic potential (LIMP cells) that follow the path towards terminal differentiation (DIFF cells). A proliferating tumor cell (stem or LIMP) passes through the successive cell cycle phases. Phases within or out of the cell cycle (G1, S, G2, M, G0) constitute different states in which cells may be found. After the completion of mitosis a fraction of newborn cells will enter the dormant phase, whereas the rest will continue to cycle. Transition to quiescence (dormant, G0, phase) and "awakening" of dormant cells are regulated by local metabolic conditions. All cell categories may die through spontaneous apoptosis. However, for dormant and differentiated cells necrosis is the main cell loss mechanism caused by inadequate nutrients' and oxygen supply.

4.5.1 Study 1: A four-dimensional simulation model of tumour response to radiotherapy in vivo: parametric validation considering radiosensitivity, genetic profile and fractionation

[DIO04] The aim of this study is to present the current state of a four-dimensional simulation model of solid tumour growth and response to radiotherapy developed by our group. The most prominent points of the algorithms describing the fundamental biological phenomena involved are outlined. A specific application of the model to a selected clinical case of glioblastoma multiforme is described and comparative studies are performed, using various exploratory values of the model parameters. Qualitative agreement with clinical observations has been achieved. Special emphasis is laid on the variability of radiosensitivity parameters throughout the cell cycle and on the influence of the genetic profile of the tumour on its radiosensitivity. The results of the simulation are three dimensionally reconstructed. A valuable tool for getting insight into the biology of tumour growth and response to radiotherapy and at the same time an advanced patient specific decision support system is expected to emerge after the completion of the necessary extensive clinical evaluation.
Visualization of three-dimensional sections of tumour produced with AVS/Express
Radiation therapy deals with the use of ionizing radiations in the treatment of patients with malignant neoplasias. The aim of radiation therapy is to deliver the highest possible dose of irradiation to a defined tumour volume to ensure maximum tumour control, while keeping at the lowest possible level the damage to surrounding healthy tissue (Perez and Brady, 1998). The major advances in imaging and treatment delivery, spanning approximately the last 20 years, have allowed for improved targeting and increased sparing of normal tissues. In order

to ensure the best possible treatment strategy for a cancer patient, an optimization process of the treatment planning should take place before the radiation delivery.
The imaging data (e.g. CT, MRI, PET slices, possibly fused), including the definition of the tumour contour, its metabolically active sub-regions, and the anatomical structures of interest, the histopathologic (e.g. type of tumour) and genetic data (e.g. p53 status, if available) of the patient are collected. The clinician delineates the tumour and the anatomical structures of interest by using a dedicated computer tool. In the case of radiotherapy, the planned distribution of the absorbed dose (e.g. in Gy) in the region of interest is also acquired. For the purpose of the 3D reconstruction and visualization of both the initial tumour and the simulation outcome, the 3D visualization package AVS/Express 4.2 (Stamatakoset al., 2002) is used.
The 3D behaviour of the tumour (Fig.6) has been simulated according to the AVS/Express 4.2 simulation software, and the most likely spatio-temporal response of the tumour to irradiation for each simulated case has been ‘‘predicted’’.

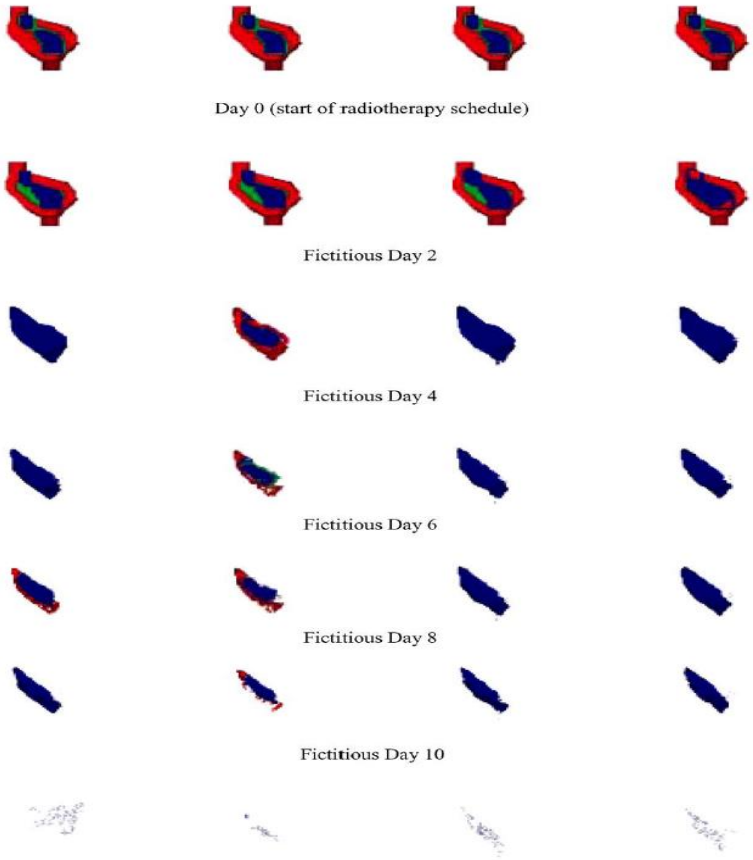

Fig.6. Fictitious day 42 (end of radiotherapy schedule. Three-dimensional sections of tumour produced with AVS/Express.

4.6 ICCS - NTUA - ISOG - Untreated Tumor Growth. Non Spatial code

Model description
The non-spatial model constitutes a variation/simplification of the previous model (ICCS-NTUA-ISOG-Untreated Tumor Growth. Spatial code). Its crucial new features consist in a. omitting the simulation of the spatial evolution of the tumor and b. considering more compartments that the proliferating cells can be found. The omission of the simulation of the

three dimensional expansion of the tumor allows a more realistic modeling of the cell cycle, in terms of available computational resources. The exclusion of the spatial evolution of the tumor does not affect the temporal evolution of the various cancerous cell categories and the total cell population. Subsequently, the time course of the tumor volume can be easily derived assuming typical cell densities, e.g. 109 biological cells/cm3 (Steel, 1997). In the non-spatial model the cycling and dormant cancerous cells are distributed in a number of classes/compartments that equals the duration of the relevant phase (see paragraph 1.2). Each compartment corresponds to an hour-long interval.

4.6.1 Study 1: A four-dimensional simulation model of tumour response to radiotherapy in vivo: parametric validation considering radiosensitivity, genetic profile and fractionation

This study has been referred in 4.5.1 chapter

4.7 ICCS - NTUA - ISOG - Single Agent Chemotherapy. Spatial code

Model description

The model simulates the spatiotemporal response of clinical tumors to chemotherapeutic treatment. It is based on the consideration of a discrete time and space stochastic cellular automaton, representing the tumor region. More specifically, the tumor region can be considered as a grid of "geometrical cells" (GCs, the elementary volume of the grid). Each GC corresponds to a cluster of heterogeneous cells found in various states. Specific rules regulate the transition between these states, as well as cell movement throughout the tumor volume; the aim is a realistic, conformal to the initial shape of the tumor, simulation of spatial evolution.

Free Growth: The adopted cytokinetic model incorporates the biological mechanisms of cell cycling, quiescence, differentiation and loss. Stem, LIMP, DIFF, apoptotic and necrotic cells represent the distinct cell categories of the model. More specifically, tumor sustenance is attributed to the presence of a cell population that exhibits stem cell like properties. Specifically, cancer stem cells have the ability to preserve their own population, as well as give birth to cells of limited mitotic potential (LIMP cells) that follow the path towards terminal differentiation (DIFF cells). A proliferating tumor cell (stem or LIMP) passes through the successive cell cycle phases. Phases within or out of the cell cycle (G1, S, G2, M, G0) constitute different states in which cells may be found. After the completion of mitosis a fraction of newborn cells will enter the dormant phase, whereas the rest will continue to cycle. Transition to quiescence (dormant, G0, phase) and "awakening" of dormant cells are regulated by local metabolic conditions. All cell categories may die through spontaneous apoptosis. However, for dormant and differentiated cells necrosis is the main cell loss mechanism caused by inadequate nutrients' and oxygen supply.

Treatment: The model addresses the case of cell-cycle non-specific chemotherapeutic agents. When a tumor is chemotherapeutically treated, a fraction of cancerous proliferating cells are lethally hit by the drug. These cells enter a rudimentary cell cycle that leads to apoptotic death through a cell cycle phase depending each time on the specific chemotherapeutic agent. In the simulation model the case of drugs that primarily inhibit the DNA synthesis and lead to apoptotic death at the end of the S phase is addressed. The effect of the drug is considered instantaneous at the time of its administration.

4.7.1 Study 1: An advanced discrete state–discrete event multiscale simulation model of the response of a solid tumor to chemotherapy: Mimicking a clinical study

[STA10] In this paper an advanced, clinically oriented multiscale cancer model of breast tumor response to chemotherapy is presented. The paradigm of early breast cancer treated by epirubicin according to a branch of an actual clinical trial (the Trial of Principle, TOP trial) has been addressed. The model, stemming from previous work of the In Silico Oncology Group, National Technical University of Athens, is characterized by several crucial new features, such as the explicit distinction of proliferating cells into stem cells of infinite mitotic potential and cells of limited proliferative capacity, an advanced generic cytokinetic model and an improved tumor constitution initialization technique. A sensitivity analysis regarding critical parameters of the model has revealed their effect on the behavior of the biological system. The favorable outcome of an initial step towards the clinical adaptation and validation of the simulation model, based on the use of anonymized data from the TOP clinical trial, is presented and discussed. Two real clinical cases from the TOP trial with variable molecular profile have been simulated. A realistic time course of the tumor diameter and a reduction in tumor size in agreement with the clinical data has been achieved for both cases by selection of reasonable model parameter values, thus demonstrating a possible adaptation process of the model to real clinical trial data. Available imaging, histological, molecular and treatment data are exploited by the model in order to strengthen patient individualization modeling. The expected use of the model following thorough clinical adaptation, optimization and validation is to simulate either several candidate treatment schemes for a particular patient and support the selection of the optimal one or to simulate the expected extent of tumor shrinkage for a given time instant and decide on the adequacy or not of the simulated scheme.

Time interval M between consecutive calculations of the average values of the relative population of cells clustered in a given mitotic potential category.

The average value of N consecutive values of the relative population of cells clustered in a given mitotic potential category is compared with its predecessor every M time steps (hours). It has been shown again that the most effective M value so that good convergence is achieved, is the value of the cell cycle duration in h (Fig. 7). Fig. 7 triangles shows the exemplary case of the relative variation of the average of N¼Tc (¼96) consecutive instantaneous values of the relative population of stem cells, taken every M¼Tc (¼96) time steps (hours) overtime. The curve is fairly smooth and tends to zero. On the contrary, Fig. 7 circles depicts the same case in which M has not been set to Tc. A small fluctuation of the relative variation over time (about2%) is apparent. Here again the fluctuation is still not significant.

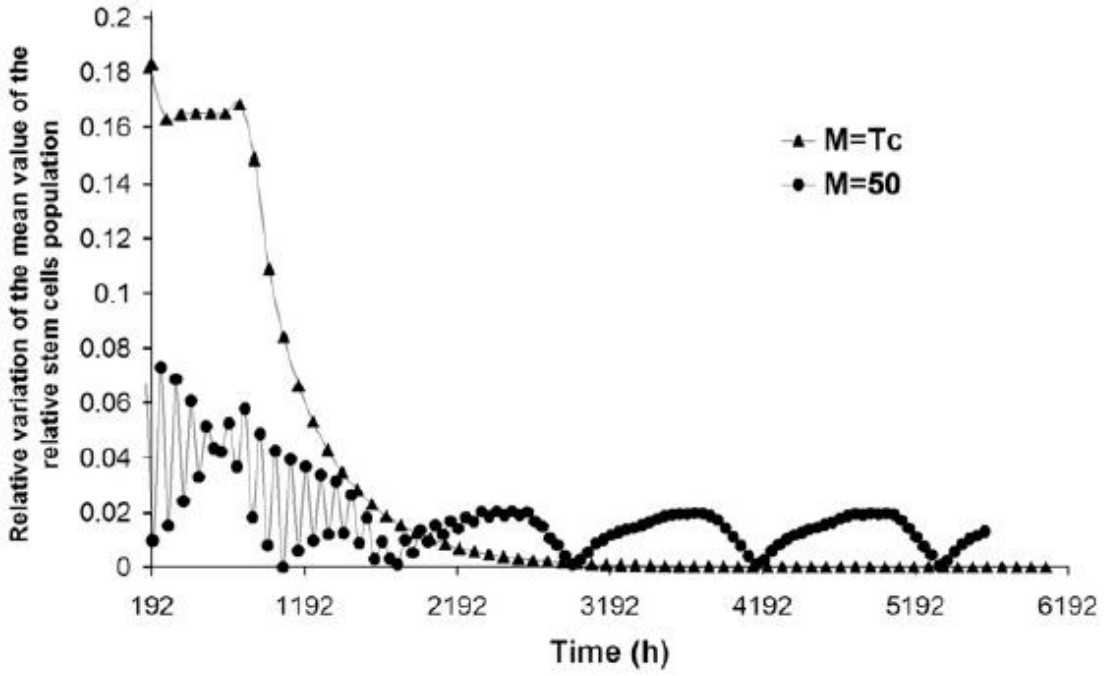

Fig. 7. Study of the model convergence. Relative variation of the average of N¼Tc¼96 consecutive instantaneous values of the relative population of stem cells taken every M time steps (hours) over time. Triangles correspond to M equal to the numerical value of the cell cycle duration (96h). Circles correspond to M¼50. Both curves correspond to the same tumor. The convergence of this parameter to zero is essential for the equilibrium condition.

4.8 ICCS - NTUA-ISOG- Single Agent Chemotherapy. Non Spatial code

Model description

The non-spatial model constitutes a variation/simplification of the previous model (ICCS-NTUA-ISOG- Single Agent Chemotherapy. Spatial code). Its crucial new features consist in a. omitting the simulation of the spatial evolution of the tumor and b. considering more compartments that the proliferating cells can be found. The omission of the simulation of the three dimensional expansion of the tumor, in the case of free growth, or shrinkage, in the case of therapy, allows a more realistic modeling of the cell cycle, in terms of available computational resources. The exclusion of the spatial evolution of the tumor does not affect the temporal evolution of the various cancerous cell categories and the total cell population. Subsequently, the time course of the tumor volume can be easily derived assuming typical cell densities, e.g. 109 biological cells/cm3 (Steel, 1997). In the non-spatial model the cycling and dormant cancerous cells are distributed in a number of classes/compartments that equals the duration of the relevant phase (see paragraph 1.2). Each compartment corresponds to an hour-long interval.

4.8.1 Study 1: An advanced discrete state–discrete event multiscale simulation model of the response of a solid tumor to chemotherapy: Mimicking a clinical study

This study has been referred in 4.7.1 chapter

4.9 ICCS - NTUA-ISOG-Radiotherapy. Spatial code

Model description

The model simulates the spatiotemporal response of clinical tumors to chemotherapeutic treatment. It is based on the consideration of a discrete time and space stochastic cellular automaton, representing the tumor region. More specifically, the tumor region can be considered as a grid of "geometrical cells" (GCs, the elementary volume of the grid). Each GC corresponds to a cluster of heterogeneous cells found in various states. Specific rules regulate the transition between these states, as well as cell movement throughout the tumor volume; the aim is a realistic, conformal to the initial shape of the tumor, simulation of spatial evolution.

Free Growth: The adopted cytokinetic model incorporates the biological mechanisms of cell cycling, quiescence, differentiation and loss. Stem, LIMP, DIFF, apoptotic and necrotic cells represent the distinct cell categories of the model. More specifically, tumor sustenance is attributed to the presence of a cell population that exhibits stem cell like properties. Specifically, cancer stem cells have the ability to preserve their own population, as well as give birth to cells of limited mitotic potential (LIMP cells) that follow the path towards terminal differentiation (DIFF cells). A proliferating tumor cell (stem or LIMP) passes through the successive cell cycle phases. Phases within or out of the cell cycle (G1, S, G2, M, G0) constitute different states in which cells may be found. After the completion of mitosis a fraction of newborn cells will enter the dormant phase, whereas the rest will continue to cycle. Transition to quiescence (dormant, G0, phase) and "awakening" of dormant cells are regulated by local metabolic conditions. All cell categories may die through spontaneous apoptosis. However, for dormant and differentiated cells necrosis is the main cell loss mechanism caused by inadequate nutrients' and oxygen supply.

Treatment: In the case of radiation therapy lethally damaged cells die through a radiation-induced mitotic necrotic mechanism. These cells enter a rudimentary cell cycle and die after undergoing a few mitotic divisions. The probability of cells to be hit by irradiation depends primarily on the phase they reside. Cell killing by irradiation is described by the Linear Quadratic or LQ Model.

4.9.1 Study 1: An advanced discrete state–discrete event multiscale simulation model of the response of a solid tumor to chemotherapy: Mimicking a clinical study

This study has been referred in 4.7.1 chapter

4.9.2 Study 2: Critical Parameters Determining Standard Radiotherapy Treatment Outcome for Glioblastoma Multiforme: A Computer Simulation

[DIO08] The aim of this paper is to investigate the most critical parameters determining radiotherapy treatment outcome in terms of tumor cell kill for glioblastoma multiforme tumors by using an already developed simulation model of in vivo tumor response to radiotherapy.

In Fig. 8. it is observed that as time increases the absolute difference between the numbers of surviving cells is constantly decreasing. Therefore, it is becoming progressively easier for the curves corresponding to different growth fractions to coincide at certain points if the stochasticity of the mathematical treatment is taken into account. It is obvious that after a point at which the number of surviving cells of two initially different tumors becomes the same their further relative time course is random given that the same treatment scheme is applied. It should be noted that different values of the growth fraction are computed in the model by appropriately adjusting the number of dead cells so as to have the same total number of cells (i.e. the hypoxic fraction remains the same).

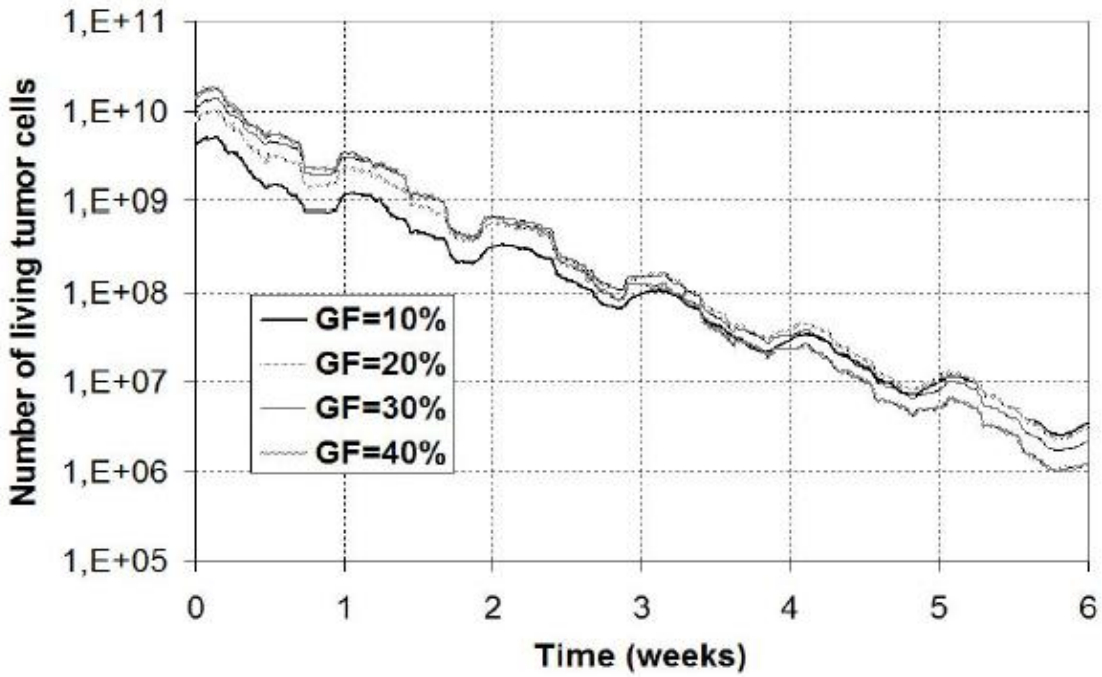

Fig. 8. Number of living tumor cells as a function of time from the start of radiotherapy treatment (at t=0), for hypothetical GBM tumors differing in their growth fraction.

4.9.3 Study 3: In Silico Radiation Oncology: Combining Novel Simulation Algorithms With Current Visualization Techniques

[STA02] The concept of in silico radiation oncology is clarified in this paper. A brief literature review points out the principal domains in which experimental, mathematical, and three-dimensional (3-D) computer simulation models of tumor growth and response to radiation therapy have been developed. Two paradigms of 3-D simulation models developed by our research group are concisely presented. The first one refers to the in vitro development and radiation response of a tumor spheroid whereas the second one refers to the fractionated radiation response of a clinical tumor in vivo based on the patient's imaging data. In each case, a description of the salient points of the corresponding algorithms and the visualization techniques used takes place. Specific applications of the models to experimental and clinical

cases are described and the behavior of the models is two- and three-dimensionally visualized by using virtual reality techniques. Good qualitative agreement with experimental and clinical observations strengthens the applicability of the models to real situations. A protocol for further testing and adaptation is outlined. Therefore, an advanced integrated patient specific decision support and spatio–temporal treatment planning system is expected to emerge after the completion of the necessary experimental tests and clinical evaluation.

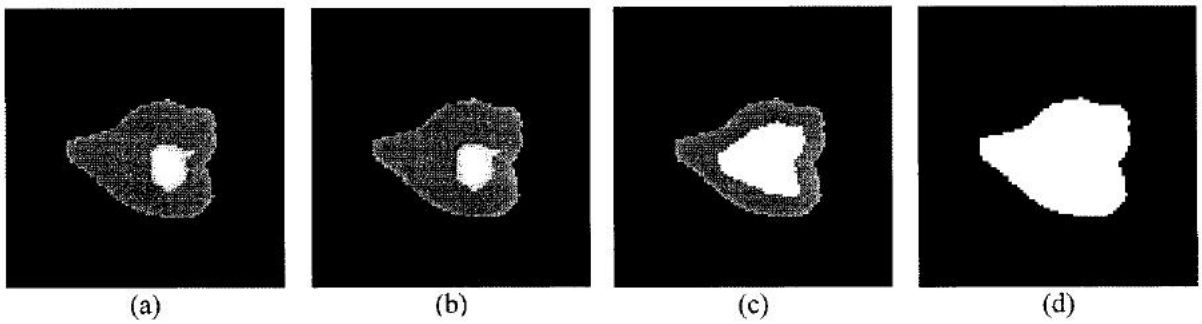

Fig. 9. Simulation results using a reduced value for the cell loss factor (0.5). Standard dose fractionation is considered. A centrally located slice of the tumor (a) before the beginning of the radiotherapy course and (b) one, (c) two, and (d) three fictitious days after the beginning of the radiotherapy course. Due to a reduced cell loss factor, there is no observable shrinkage of the tumor. This seems to be a more clinically compatible scenario in the case of astrocytoma.

4.10 ICCS - NTUA - ISOG - Radiotherapy. Non Spatial code

Model description

The non-spatial model constitutes a variation/simplification of the previous model (ICCS-NTUA-ISOG- Radiotherapy. Spatial code). Its crucial new features consist in a. omitting the simulation of the spatial evolution of the tumor and b. considering more compartments that the proliferating cells can be found. The omission of the simulation of the three dimensional expansion of the tumor, in the case of free growth, or shrinkage, in the case of therapy, allows a more realistic modeling of the cell cycle, in terms of available computational resources. The exclusion of the spatial evolution of the tumor does not affect the temporal evolution of the various cancerous cell categories and the total cell population. Subsequently, the time course of the tumor volume can be easily derived assuming typical cell densities, e.g. 109 biological cells/cm3 (Steel, 1997). In the non-spatial model the cycling and dormant cancerous cells are distributed in a number of classes/compartments that equals the duration of the relevant phase (see paragraph 1.2). Each compartment corresponds to an hour-long interval.

4.10.1 Study 1: An advanced discrete state–discrete event multiscale simulation model of the response of a solid tumor to chemotherapy: Mimicking a clinical study

This study has been referred in 4.7.1 chapter

4.10.2 Study 2: Critical Parameters Determining Standard Radiotherapy Treatment Outcome for Glioblastoma Multiforme: A Computer Simulation

This study has been referred in 4.9.2 chapter

4.10.3 Study 3: In Silico Radiation Oncology: Combining Novel Simulation Algorithms With Current Visualization Techniques

This study has been referred in 4.9.3 chapter

4.11 ICCS - NTUA-ISOG-Breast Cancer Therapy: Epirubicin

Model description

The model simulates the spatiotemporal response of breast cancer clinical tumors to chemotherapeutic treatment with single agent Epirubicin. It is based on the consideration of a discrete time and space stochastic cellular automaton, representing the tumor region. More specifically, the tumor region can be considered as a grid of "geometrical cells" (GCs, the elementary volume of the grid). Each GC corresponds to a cluster of heterogeneous cells found in various states. Specific rules regulate the transition between these states, as well as cell movement throughout the tumor volume; the aim is a realistic, conformal to the initial shape of the tumor, simulation of spatial evolution.

Free Growth: The adopted cytokinetic model incorporates the biological mechanisms of cell cycling, quiescence, differentiation and loss. Stem, LIMP, DIFF, apoptotic and necrotic cells represent the distinct cell categories of the model. More specifically, tumor sustenance is attributed to the presence of a cell population that exhibits stem cell like properties. Specifically, cancer stem cells have the ability to preserve their own population, as well as give birth to cells of limited mitotic potential (LIMP cells) that follow the path towards terminal differentiation (DIFF cells). A proliferating tumor cell (stem or LIMP) passes through the successive cell cycle phases. Phases within or out of the cell cycle (G1, S, G2, M, G0) constitute different states in which cells may be found. After the completion of mitosis a fraction of newborn cells will enter the dormant phase, whereas the rest will continue to cycle. Transition to quiescence (dormant, G0, phase) and "awakening" of dormant cells are regulated by local metabolic conditions. All cell categories may die through spontaneous apoptosis. However, for dormant and differentiated cells necrosis is the main cell loss mechanism caused by inadequate nutrients' and oxygen supply.

Treatment: The model addresses the case of Epirubicin agent. When a tumor is chemotherapeutically treated, a fraction of cancerous proliferating cells are lethally hit by the drug. These cells enter a rudimentary cell cycle that leads to apoptotic death through a cell cycle phase depending each time on the specific chemotherapeutic agent. In the simulation model the case of Epirubicin agent that primarily inhibits the DNA synthesis and lead to apoptotic death at the end of the S phase is addressed. The effect of the drug is considered instantaneous at the time of its administration.

4.11.1 Study 1: An advanced discrete state–discrete event multiscale simulation model of the response of a solid tumor to chemotherapy: Mimicking a clinical study

This study has been referred in 4.7.1 chapter

4.11.2 Study 2: Studying the growth kinetics of untreated clinical tumors by using an advanced discrete simulation model

[KOL11] Prior to an eventual clinical adaptation and validation of any clinically oriented model, a thorough study of its dynamic behavior is a sine qua non. Such a study can also elucidate aspects of the interplay of the involved biological mechanisms. Toward this goal, the paper focuses on an in-depth investigation of the free growth behavior of a macroscopically homogeneous malignant tumor system, using a discrete model of tumor growth. this study demonstrates that when a clinical tumor grows exponentially, the following preconditions must be fulfilled: (a) time- and space-independent tumor dynamics, in terms of the transition rates among the considered cell categories and the duration of the cell cycle phases, and (b) a umor system in a state of population equilibrium. Moreover, constant tumor dynamics during the simulation are assumed. In order to create a growing tumor, a condition that the model parameters must fulfill has been derived based on an analytical treatment of the model's assumptions. A detailed parametric analysis of the model has been performed, in order to determine the impact and the interdependences of its parameters with focus on the free growth rate and the composition of cell population. Constraining tumor cell kinetics, toward limiting the number of possible solutions (i.e., sets of parameters) to the problem of adaptation to the real macroscopic features of a tumor, is also discussed. After completing all parametric studies and after adapting and validating the model on clinical data, it is envisaged to end up with a reliable tool for supporting clinicians in selecting the most appropriate pattern, extracted from several candidate therapeutic schemes, by exploiting tumor- and patient-specific imaging, molecular and histological data.

Visualization of patient's molecular and treatment data.

The model addresses tumors well beyond their initiation phase and aims at simulating their spatiotemporal evolution. It has been designed to incorporate patient-specific data such as imaging based, histopathological, molecular and treatment data.

The model is based on the consideration of a discrete time and space stochastic cellular automaton, representing the tumor region. More specifically, the tumor region can be considered as a grid (or ‘‘mesh’’) of ‘‘Geometrical Cells’’ (GCs, the elementary volume of the grid). Each GC corresponds to a cluster of heterogeneous cells found in various states. Specific rules regulate the transitions between these states, as well as the cell movement throughout the tumor volume.

In order to demonstrate the tumor growth several parameters are taken under consideration. More specifically each model parameter is represented according to a doubling time condition. For a given doubling time more than one solutions exist, corresponding to different possible combinations of model parameter values. In the Fig. 10, different ‘solutions’, characterized by the same doubling time, by varying each time two model parameters. These solutions, although having the same growth rate, are expected to differ in the cell population composition, i.e., the fraction of the various cell categories. More specifically, the interdependences of the following pairs of parameters with respect to the tumor's doubling time have been examined (Fig. 10). The two parameters considered each time vary in combination so as to maintain a constant Td (equal to 50, 100 and 300 days).

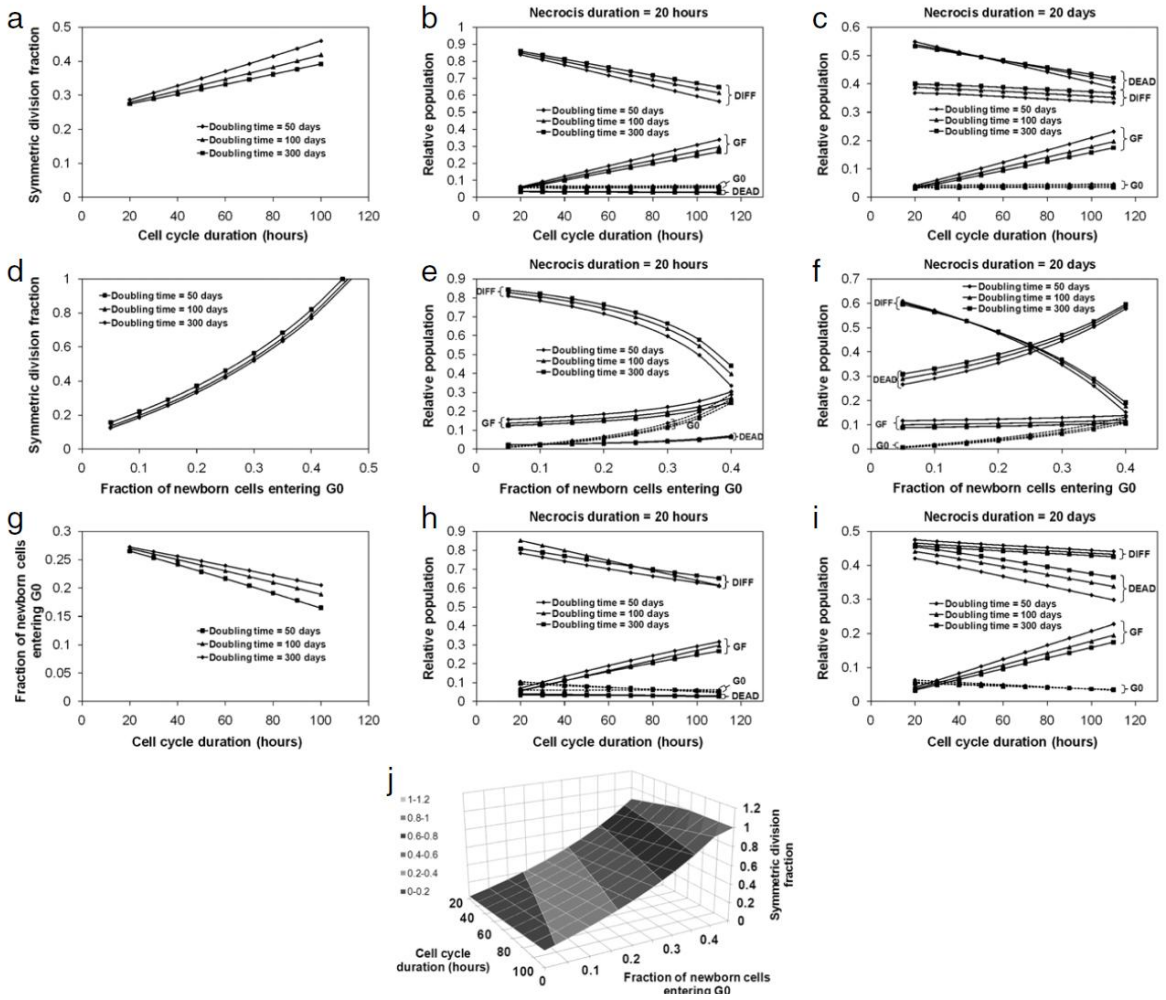

Fig. 10. Joint effect of three pairs of model input parameters on volume doubling time (Td) and relative population of the various cell categories. The two parameters considered at each time vary in combination so as to maintain a constant Td (equal to 50, 100 and 300 days). The three-dimensional graph corresponds to a Td equal to 50 days. Two values of necrosis phase duration are considered (20 h and 20 days). The latter parameter does not affect the results in terms of volume doubling time (first column of panels).

4.12 ICCS - NTUA - ISOG - Lung Cancer Therapy: Cisplatin and Docetaxel

Model description

The model simulates the spatiotemporal response of lung cancer to combination chemotherapy treatment with the regimens Cisplatin and Docetaxel. In accordance to clinical practice the cisplatin/docetaxel regimen is given as a three-week cycle and is administrated usually three times. On the first day of each cycle the patient is given both the docetaxel and cisplatin.

It is based on the consideration of a discrete time and space stochastic cellular automaton, representing the tumor region. More specifically, the tumor region can be considered as a grid of "geometrical cells" (GCs, the elementary volume of the grid). Each GC corresponds to a cluster of heterogeneous cells found in various states. Specific rules regulate the transition

between these states, as well as cell movement throughout the tumor volume; the aim is a realistic, conformal to the initial shape of the tumor, simulation of spatial evolution.
Free Growth: The adopted cytokinetic model incorporates the biological mechanisms of cell cycling, quiescence, differentiation and loss. Stem, LIMP, DIFF, apoptotic and necrotic cells represent the distinct cell categories of the model. More specifically, tumor sustenance is attributed to the presence of a cell population that exhibits stem cell like properties. Specifically, cancer stem cells have the ability to preserve their own population, as well as give birth to cells of limited mitotic potential (LIMP cells) that follow the path towards terminal differentiation (DIFF cells). A proliferating tumor cell (stem or LIMP) passes through the successive cell cycle phases. Phases within or out of the cell cycle (G1, S, G2, M, G0) constitute different states in which cells may be found. After the completion of mitosis a fraction of newborn cells will enter the dormant phase, whereas the rest will continue to cycle. Transition to quiescence (dormant, G0, phase) and "awakening" of dormant cells are regulated by local metabolic conditions. All cell categories may die through spontaneous apoptosis. However, for dormant and differentiated cells necrosis is the main cell loss mechanism caused by inadequate nutrients' and oxygen supply.
Treatment: When a tumor is chemotherapeutically treated, a fraction of cancerous proliferating cells are lethally hit by the drug. These cells enter a rudimentary cell cycle that leads to apoptotic death through a cell cycle phase depending each time on the specific chemotherapeutic agent. The effect of the drug is considered instantaneous at the time of its administration.

4.12.1 Study 1: Studying the growth kinetics of untreated clinical tumors by using an advanced discrete simulation model

This study has been referred in 4.11.2 chapter

4.13 ICCS - NTUA-ISOG-Lung Cancer Therapy: Cisplatin and Gemcitabine

Model description
The model simulates the spatiotemporal response of lung cancer to combination chemotherapy treatment with the regimens Cisplatin and Gemcitabine. In accordance to clinical practice the cisplatin/ gemcitabine regimen is given as a three-week cycle and is administrated usually two or three times. On the first day of treatment the patient is given both the gemcitabine and cisplatin. On the same day of the following week (day eight) only gemcitabine is adminstrated.
It is based on the consideration of a discrete time and space stochastic cellular automaton, representing the tumor region. More specifically, the tumor region can be considered as a grid of "geometrical cells" (GCs, the elementary volume of the grid). Each GC corresponds to a cluster of heterogeneous cells found in various states. Specific rules regulate the transition between these states, as well as cell movement throughout the tumor volume; the aim is a realistic, conformal to the initial shape of the tumor, simulation of spatial evolution.
Free Growth: The adopted cytokinetic model incorporates the biological mechanisms of cell cycling, quiescence, differentiation and loss. Stem, LIMP, DIFF, apoptotic and necrotic cells represent the distinct cell categories of the model. More specifically, tumor sustenance is attributed to the presence of a cell population that exhibits stem cell like properties. Specifically, cancer stem cells have the ability to preserve their own population, as well as give birth to cells of limited mitotic potential (LIMP cells) that follow the path towards

terminal differentiation (DIFF cells). A proliferating tumor cell (stem or LIMP) passes through the successive cell cycle phases. Phases within or out of the cell cycle (G1, S, G2, M, G0) constitute different states in which cells may be found. After the completion of mitosis a fraction of newborn cells will enter the dormant phase, whereas the rest will continue to cycle. Transition to quiescence (dormant, G0, phase) and "awakening" of dormant cells are regulated by local metabolic conditions. All cell categories may die through spontaneous apoptosis. However, for dormant and differentiated cells necrosis is the main cell loss mechanism caused by inadequate nutrients' and oxygen supply.
Treatment: When a tumor is chemotherapeutically treated, a fraction of cancerous proliferating cells are lethally hit by the drug. These cells enter a rudimentary cell cycle that leads to apoptotic death through a cell cycle phase depending each time on the specific chemotherapeutic agent. The effect of the drug is considered instantaneous at the time of its administration.

4.13.1 Study 1: Studying the growth kinetics of untreated clinical tumors by using an advanced discrete simulation model

This study has been referred in 4.11.2 chapter

4.14 ICCS - NTUA-ISOG-Lung Cancer Therapy: Cisplatin and Vinorelbine

Model description
The model simulates the spatiotemporal response of lung cancer to combination chemotherapy treatment with the regimens Cisplatin and Vinorelbine. In accordance to clinical practice the cisplatin/vinorelbine regimen is given as a three-week cycle and is administrated usually two or three times. On the first day of treatment the patient is given both the vinorelbine and cisplatin. On the same day of the following week (day eight) only vinorelbine is adminstrated.
It is based on the consideration of a discrete time and space stochastic cellular automaton, representing the tumor region. More specifically, the tumor region can be considered as a grid of "geometrical cells" (GCs, the elementary volume of the grid). Each GC corresponds to a cluster of heterogeneous cells found in various states. Specific rules regulate the transition between these states, as well as cell movement throughout the tumor volume; the aim is a realistic, conformal to the initial shape of the tumor, simulation of spatial evolution.
Free Growth: The adopted cytokinetic model incorporates the biological mechanisms of cell cycling, quiescence, differentiation and loss. Stem, LIMP, DIFF, apoptotic and necrotic cells represent the distinct cell categories of the model. More specifically, tumor sustenance is attributed to the presence of a cell population that exhibits stem cell like properties. Specifically, cancer stem cells have the ability to preserve their own population, as well as give birth to cells of limited mitotic potential (LIMP cells) that follow the path towards terminal differentiation (DIFF cells). A proliferating tumor cell (stem or LIMP) passes through the successive cell cycle phases. Phases within or out of the cell cycle (G1, S, G2, M, G0) constitute different states in which cells may be found. After the completion of mitosis a fraction of newborn cells will enter the dormant phase, whereas the rest will continue to cycle. Transition to quiescence (dormant, G0, phase) and "awakening" of dormant cells are regulated by local metabolic conditions. All cell categories may die through spontaneous apoptosis. However, for dormant and differentiated cells necrosis is the main cell loss mechanism caused by inadequate nutrients' and oxygen supply.

Treatment: When a tumor is chemotherapeutically treated, a fraction of cancerous proliferating cells are lethally hit by the drug. These cells enter a rudimentary cell cycle that leads to apoptotic death through a cell cycle phase depending each time on the specific chemotherapeutic agent. The effect of the drug is considered instantaneous at the time of its administration.

4.14.1 Study 1: Studying the growth kinetics of untreated clinical tumors by using an advanced discrete simulation model

This study has been referred in 4.11.2 chapter

4.14.2 Study 2: Clinically driven design of multi-scale cancer models: the ContraCancrum project paradigm

[MAR07] The challenge of modelling cancer presents a major opportunity to improve our ability to reduce mortality from malignant neoplasms, improve treatments and meet the demands associated with the individualization of care needs. This is the central motivation behind the ContraCancrum project. By developing integrated multi-scale cancer models, ContraCancrum is expected to contribute to the advancement of in silico oncology through the optimization of cancer treatment in the patient-individualized context by simulating the response to various therapeutic regimens. The aim of the present paper is to describe a novel paradigm for designing clinically drive multi-scale cancer modelling by bringing together basic science and information technology modules. In addition, the integration of the multi-scale tumour modelling components has led to novel concepts of personalized clinical decision support in the context of predictive oncology, as is also discussed in the paper. Since clinical adaptation is an inelastic prerequisite, a long-term clinical adaptation procedure of the models has been initiated for two tumour types, namely non-small cell lung cancer and glioblastoma multiforme; its current status is briefly summarized.

The mesoscopic cell simulator (a module which includes the development of a set of multilevel simulation models of tumour growth and response to radiotherapy and chemotherapy for the cases of GBM and lung cancer in the patient-individualized context) uses information about the direction along which new tumour cells will spread, based on the pressure gradient in the surrounding tissue. Moreover, the mechanical simulation needs information on the amount by which individual geometrical cells will expand which is, in turn, provided by the cell concentrations calculated by the cellular simulator. Initial results showed that biomechanical information leads to a 20 per cent correction of the tumour shape in terms of the ratio of smallest to largest moment of inertia compared with simulation performed without biomechanical simulations. For illustrative purposes, Fig. 11 shows biomechanical simulation results in a lung cancer case.

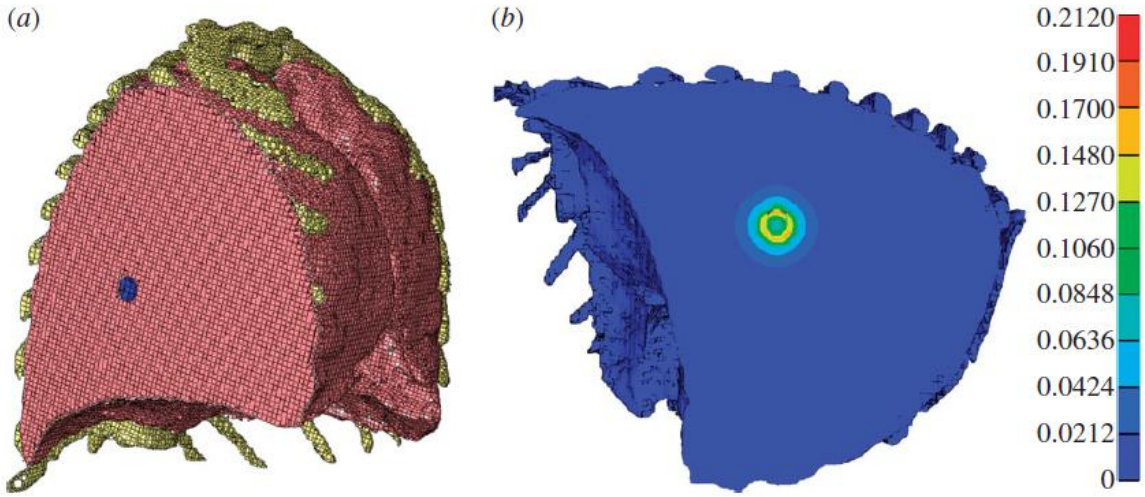

Fig. 11. (a) Biomechanical simulations in lung cancer data with different colours representing the different anatomical structures used for the simulation. (b) Calculated magnitude of displacement (colour-coded) for the growth of a tumour in the lung.

4.15 ICCS - NTUA - ISOG - Glioblastoma Therapy: Temozolomide and Radiation

Model description

The model simulates the spatiotemporal response of glioblastoma multiforme to combined modality treatment using radiation and chemotherapy with temozolomide agent. It is based on the consideration of a discrete time and space stochastic cellular automaton, representing the tumor region. More specifically, the tumor region can be considered as a grid of "geometrical cells" (GCs, the elementary volume of the grid). Each GC corresponds to a cluster of heterogeneous cells found in various states. Specific rules regulate the transition between these states, as well as cell movement throughout the tumor volume; the aim is a realistic, conformal to the initial shape of the tumor, simulation of spatial evolution.

Free Growth: The adopted cytokinetic model incorporates the biological mechanisms of cell cycling, quiescence, differentiation and loss. Stem, LIMP, DIFF, apoptotic and necrotic cells represent the distinct cell categories of the model. More specifically, tumor sustenance is attributed to the presence of a cell population that exhibits stem cell like properties. Specifically, cancer stem cells have the ability to preserve their own population, as well as give birth to cells of limited mitotic potential (LIMP cells) that follow the path towards terminal differentiation (DIFF cells). A proliferating tumor cell (stem or LIMP) passes through the successive cell cycle phases. Phases within or out of the cell cycle (G1, S, G2, M, G0) constitute different states in which cells may be found. After the completion of mitosis a fraction of newborn cells will enter the dormant phase, whereas the rest will continue to cycle. Transition to quiescence (dormant, G0, phase) and "awakening" of dormant cells are regulated by local metabolic conditions. All cell categories may die through spontaneous apoptosis. However, for dormant and differentiated cells necrosis is the main cell loss mechanism caused by inadequate nutrients' and oxygen supply.

Treatment: The model addresses the case of temozolomide chemotherapeutic agent. When a tumor is chemotherapeutically treated, a fraction of cancerous proliferating cells are lethally hit by the drug. These cells enter a rudimentary cell cycle that leads to apoptotic death through a cell cycle phase depending each time on the specific chemotherapeutic agent. The effect of the drug is considered instantaneous at the time of its administration.

In the case of radiation therapy, lethally damaged cells die through a radiation-induced mitotic necrotic mechanism after undergoing a few mitotic divisions. The probability of cells to be hit by irradiation depends primarily on the phase they reside.

4.15.1 Study 1: A Spatiotemporal, Patient Individualized Simulation Model of Solid Tumor Response to Chemotherapy in Vivo: The Paradigm of Glioblastoma Multiforme Treated by Temozolomide

[STA06] A novel four-dimensional, patient-specific Monte Carlo simulation model of solid tumor response to chemotherapeutic treatment in vivo is presented. The special case of glioblastoma multiforme treated by temozolomide is addressed as a simulation paradigm. Nevertheless, a considerable number of the involved algorithms are generally applicable. The model is based on the patient's imaging, histopathologic and genetic data. For a given drug administration schedule lying within acceptable toxicity boundaries, the concentration of the prodrug and its metabolites within the tumor is calculated as a function of time based on the drug pharamacokinetics. A discretization mesh is superimposed upon the anatomical region of interest and within each geometrical cell of the mesh the most prominent biological "laws" (cell cycling, necrosis, apoptosis, mechanical restictions, etc.) are applied. The biological cell fates are predicted based on the drug pharmacodynamics. The outcome of the simulation is a prediction of the spatiotemporal activity of the entire tumor and is virtual reality visualized. A good qualitative agreement of the model's predictions with clinical experience supports the applicability of the approach. The proposed model primarily aims at providing a platform for performing patient individualized in silico experiments as a means of chemotherapeutic treatment optimization.

In order to extend the study of the model behavior to other combinations of possible values of the model parameters, a number of further simulation runs have been performed. Fig. 12a – 12b depict the simulation predictions concerning the two fractionation schemes considered for other possible values of the cell cycle duration and clonogenic cell density. In particular Fig. 12a corresponds to TC = 48 h, mean clonogenic cell loss factor has been expressed as the sum of the cell density equal to cells/mm and dose/fraction equal to 150 mg/m . Fig. 12b corresponds to h, mean clonogenic cell density equal to cells/mm and dose/fraction equal to 200 mg/m .

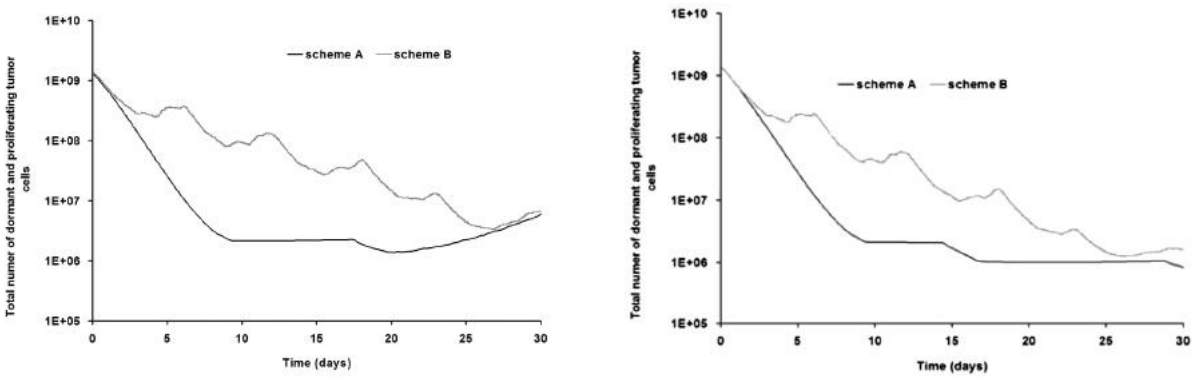

Fig. 12a: Number of surviving (metabolically living) proliferating and dormant (G0) tumor cells corresponding to the particular GBM tumor considered as a function of the time. TMZ is administered according to fractionation scheme A (bold line) or B (light line). Each chemotherapy fraction corresponds to 150 mg/m2. The

cell cycle has been assumed equal to Tc = 48 h and the mean clonogenic cell density equal to 2 x CCD = 2 x 104cells/mm3 (clonogenic cell density in the proliferating cell layer = 4 x 104cells/mm3). Only one chemotherapy cycle/scheme has been simulated.
Fig. 12b: Number of surviving (metabolically living) proliferating and dormant (G0) tumor cells corresponding to the particular GBM tumor considered as a function of the time. TMZ is administered according to fractionation scheme A (bold line) or B (light line) (Fig. 3). Each chemotherapy fraction corresponds to 200 mg/m . The cell cycle has been assumed equal to Tc = 40 h and the mean clonogenic cell density equal to 3 _ CCD = 3_10 cells/mm (clonogenic cell density in the proliferating cell layer = 6 _ 10 cells/mm). Only one chemotherapy cycle/scheme has been simulated.

4.15.2 Study 2: Studying the growth kinetics of untreated clinical tumors by using an advanced discrete simulation model

This study has been referred in 4.11.2 chapter

4.15.3 Study 3: Clinically driven design of multi-scale cancer models: the ContraCancrum project paradigm

This study has been referred in 4.14.2 chapter

4.16 ICCS - Free Growth of homogeneous solid tumors simulation model

Model description:
This is a four-dimensional discrete simulation model of solid homogeneous tumor free growth.

4.16.1 Study 1: Towards in silico oncology: Adapting a four dimensional nephroblastoma treatment model to a clinical trial case based on multi-method sensitivity analysis

[GEO12] In the past decades a great progress in cancer research has been made although medical treatment is still widely based on empirically established protocols, which have many limitations. Computational models address such limitations by providing insight into the complex biological mechanisms of tumor progression. A set of clinically - oriented, multi scale models of solid tumor dynamics has been developed by the In Silico Oncology Group (ISOG), Institute of Communication and Computer Systems (ICCS) - National Technical University of Athens (NTUA) to study cancer growth and response to treatment. Within this context using certain representative parameter values, tumor growth and response have been modeled under a cancer preoperative chemotherapy protocol in the framework of the SIOP2001/ GPOH clinical trial. A thorough cross-method sensitivity analysis of the model has been performed. Based on the sensitivity analysis results, a reasonable adaptation of the values of the model parameters to a real clinical case of bilateral nephroblastomatosis has been achieved. The analysis presented supports the potential of the model for the study and eventually the future design of personalized treatment schemes and/or schedules using the data obtained from in vitro experiments and clinical studies.
Graphical analysis of results
In Fig. 13 the effect of the most important model parameters on the initial constitution of the tumor, in terms of the four basic cell categories (proliferating, dormant, differentiated and dead cells) is presented. This image also reports the free growth behavior of the tumor for

different parameter values, as tumor constitution initialization is performed by progressive growth steps until reaching a state of population equilibrium.
The graphical method reveals that the most crucial parameters in the constitution of the initial tumor in terms of the various cell categories are the fraction of cells that enter the dormant state and the fraction of stem cells that perform symmetric division.

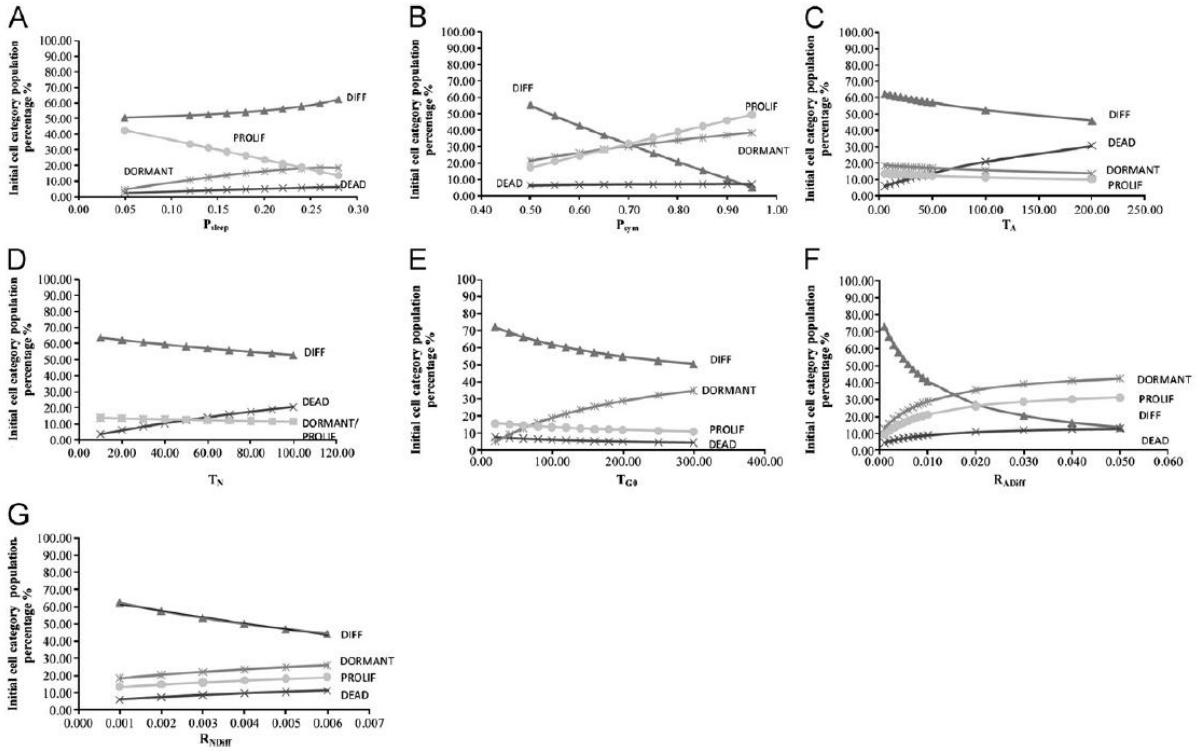

Fig. 13. Graphical representation of the effects of important input model on the constitution of the initial tumor.

Image based visualization of nephroblastoma case adaptation method

The anonymized imaging and clinical data of a bilateral nephroblastomatosis case have been collected in the framework of SIOP 2001/GPOH trial and selected to be modeled by the 'Oncosimulator'. The outer boundaries of the bilateral tumor based on MRI imaging sets have been delineated at three time instants for both kidneys (Fig. 14).
According to the imaging data, a high level of chemotherapy - induced shrinkage of the tumor has been achieved. The reduction of the tumor between the first and the second imaging data is estimated to 92% and 89% for the right and the left kidney respectively. The total reduction of the tumor volume after the completion of the chemotherapy treatment (based on the first and the third set of images) is 94% and 95% for the right and the left kidney.

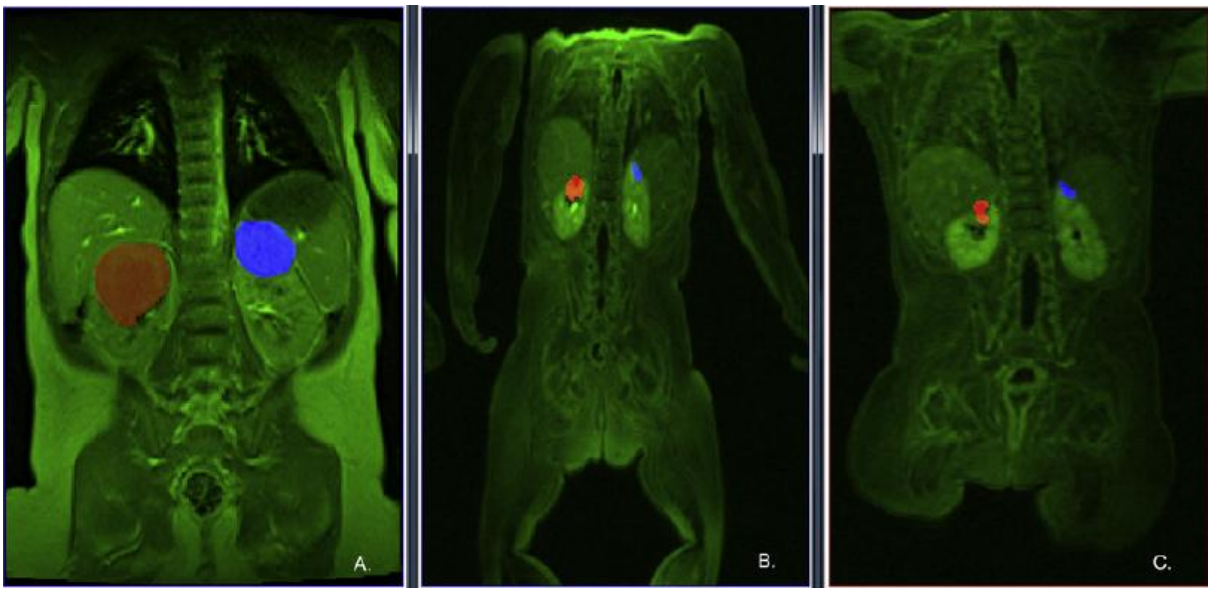

Fig. 14. Imaging data of the bilateral nephroblastomatosis case modeled. Representative MRI images merged with the tumor annotations of the right (red) and left (blue) kidney at three time instants: (A) Time of diagnosis (t¼0 day). (B) An intermediate point during chemotherapy (t¼75 day). (C) After the completion of chemotherapy (t¼108 day,). The images have been produced with ImageJ [36].

4.16.2 Study 2: Exploiting Clinical Trial Data Drastically Narrows the Window of Possible Solutions to the Problem of Clinical Adaptation of a Multiscale Cancer Model

[STA07] The development of computational models for simulating tumor growth and response to treatment has gained significant momentum during the last few decades. At the dawn of the era of personalized medicine, providing insight into complex mechanisms involved in cancer and contributing to patient-specific therapy optimization constitute particularly inspiring pursuits. The in silico oncology community is facing the great challenge of effectively translating simulation models into clinical practice, which presupposes a thorough sensitivity analysis, adaptation and validation process based on real clinical data. In this study, the behavior of a clinically-oriented, multiscale model of solid tumor response to chemotherapy is investigated, using the paradigm of nephroblastoma response to preoperative chemotherapy in the context of the SIOP/GPOH clinical trial. A sorting of the model's parameters according to the magnitude of their effect on the output has unveiled the relative importance of the corresponding biological mechanisms; major impact on the result of therapy is credited to the oxygenation and nutrient availability status of the tumor and the balance between the symmetric and asymmetric modes of stem cell division. The effect of a number of parameter combinations on the extent of chemotherapy induced tumor shrinkage and on the tumor's growth rate are discussed. A real clinical case of nephroblastoma has served as a proof of principle study case, demonstrating the basics of an ongoing clinical adaptation and validation process. By using clinical data in conjunction with plausible values of model parameters, an excellent fit of the model to the available medical data of the selected nephroblastoma case has been achieved, in terms of both volume reduction and histological constitution of the tumor. In this context, the exploitation of multiscale clinical data drastically narrows the window of possible solutions to the clinical adaptation problem.

Visualization of parametric analysis

An additional parametric analysis is presented in Fig. 15, involving the six most critical parameters which largely complete the picture of the tumor's response to treatment in terms of volume reduction (i.e. Psleep, Psym, CKRtotal, Tc, RA, PG0toG1). The combined effects of a number of parameter dyads on the reduction percentage of a chemotherapeutically treated tumor and on the growth rate constant characterizing its free growth or re-growth after completion of therapy have been studied. The considered parameter dyads are: i) Psym and Psleep, ii) TC and RA, and iii) CKRtotal and PG0toG1.
The areas that appear in the graphs of Fig. 15 show only combinations of biologically relevant parameter values leading to tumors that exhibit monotonic behavior for the case of free growth and tumors displaying volume reduction after therapy for the case of treatment.

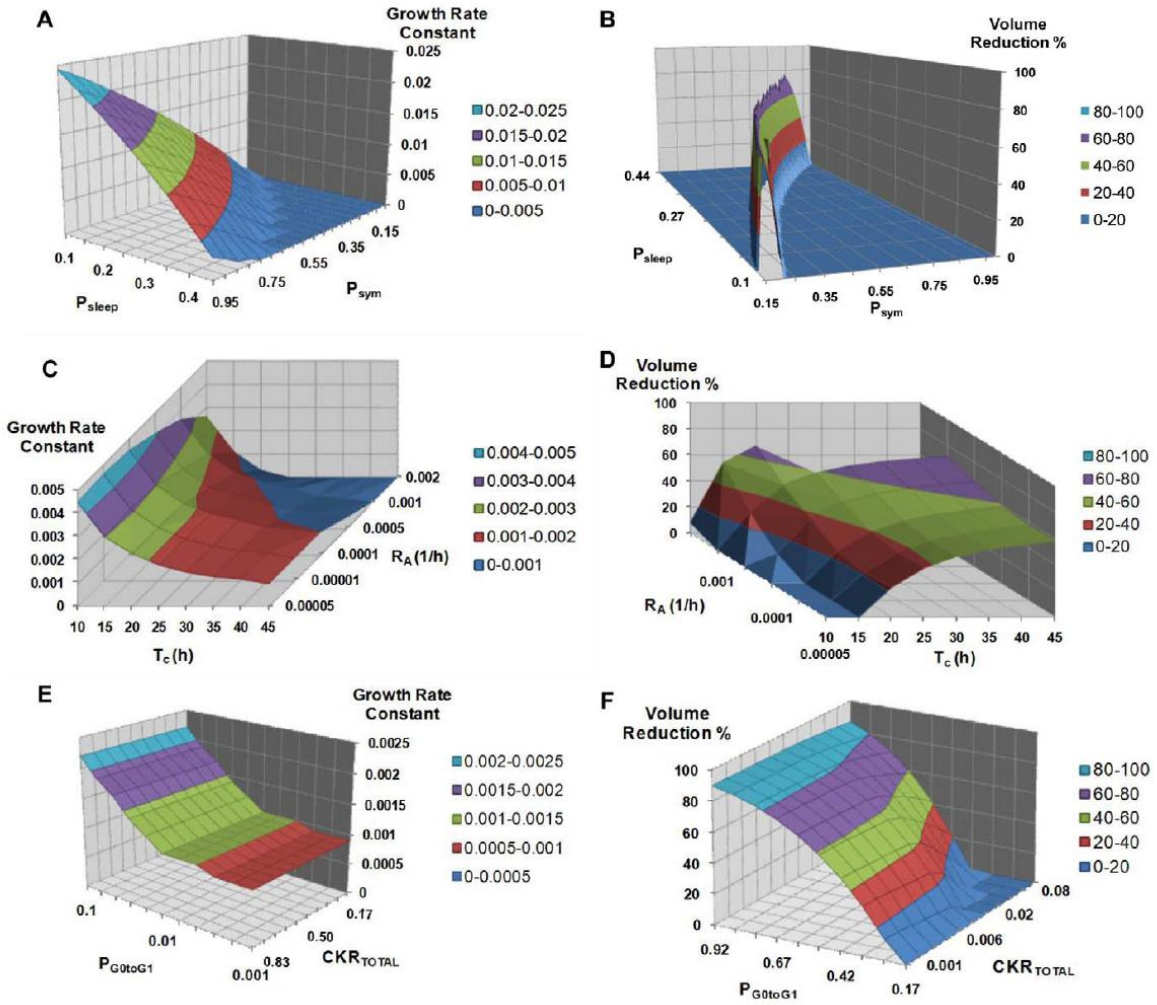

Fig. 15. Selected combined effects of several model parameter combinations. Combined effects of selected parameter combinations on tumor free growth rate (first column) and volume reduction after therapy (second column). Different colors correspond to distinct ranges of the growth rate constant value or the tumor volume reduction percentage. Panels A, B: Combined effect of Psym and Psleep. Panels C,D: Combined effect of Tc and RA. Panels E,F: Combined effect of CKRtotal and PG0toG1.

4.16.3 Study 3: Modeling Nephroblastoma Treatment Response Cases with In Silico Scenarios

[GEO12] Two blastemal nephroblastoma cases have been successfully clinically adapted under two simulation scenarios of a clinically-oriented multiscale computational model, providing insight into the tumor characteristics.

As a first adaptation scenario (A), two nephroblastoma tumors are taken under consideration, which have common growth kinetics features as they are of the same histological subtype (blastemal). The cell kill ratio of the chemotherapeutic drugs is adapted in order to simulate the volume reduction induced by chemotherapy.
As a second adaptation scenario (B), the effect of the chemotherapeutic drugs is considered common for both cases and the growth rate of the tumors is adapted within the range defined by reported literature, by perturbing the value of an important growth kinetic parameter according to model sensitivity analyses [4], the fraction of stem cells that perform symmetric division (Psym).
The above assumptions in conjunction with accumulated basic science and clinical experience-plausible values set the tumor dynamic model parameters for cases A, B and under scenarios A, B. The time course of the volume of the four virtual tumors is presented in Fig. 16. The resultant virtual tumor characteristics and volume reduction are given in table II.

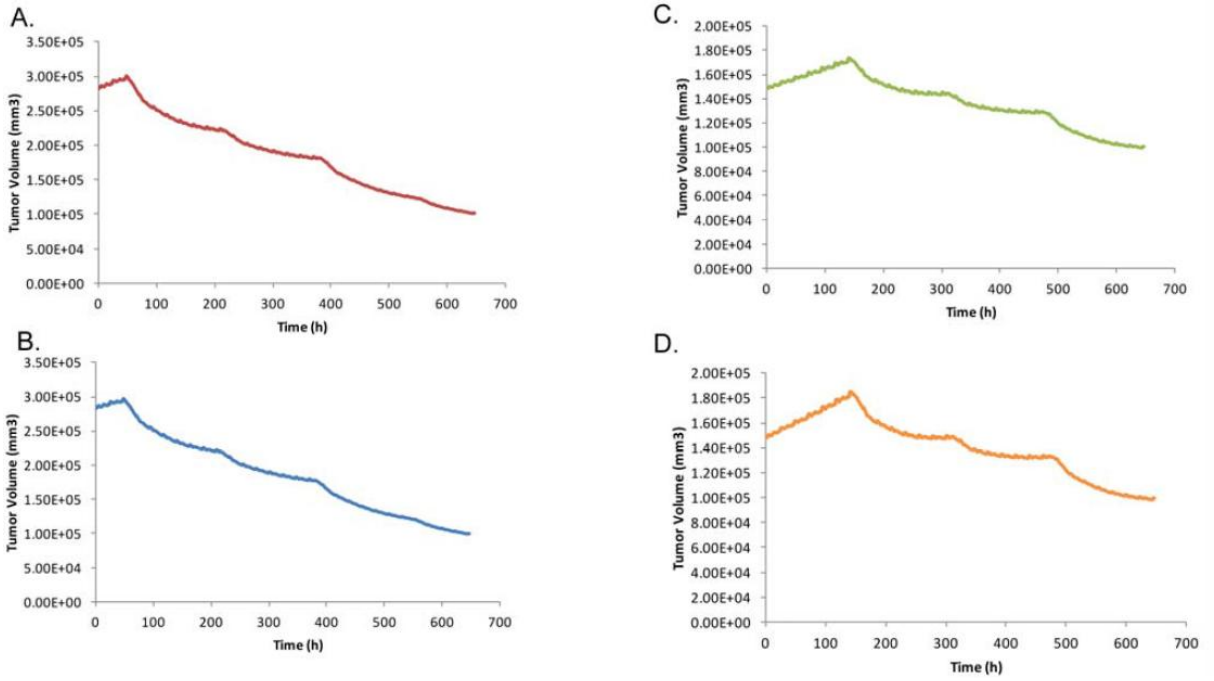

Fig. 16. Tumor volume time evolution for the four simulation scenarios (Table 1): A: T1, B: T2, C: T3, D: T4

4.16.4 Study 4: Multilevel Cancer Modeling in the Clinical Environment: Simulating the Behavior of Wilms Tumor in the Context of the SIOP 2001/GPOH Clinical Trial and the ACGT Project

[GEO08] Mathematical and computational tumor dynamics models can provide considerable insight into the relative importance and interdependence of related biological mechanisms. They may also suggest the existence of optimal treatment windows in the generic setting. Nevertheless, they cannot be translated into clinical practice unless they undergo a strict and thorough clinical validation and adaptation. In this context one of the major actions of the EC

funded project "Advancing Clinico-Genomic Trials on Cancer" (ACGT) is dedicated to the development of a patient specific four dimensional multiscale tumor model mimicking the nephroblastoma tumor response to chemotherapeutic agents according to the SIOP 2001/GPOH clinical trial. Combined administration of vincristine and dactinomycin is considered. The patient's pseudoanonymized imaging, histopathological, molecular and clinical data are carefully exploited. The paper briefly outlines the basics of the model developed by the In Silico Oncology Group and particularly stresses the effect of stem/clonogenic, progenitor and differentiated tumor cells on the overall tumor dynamics. The need for matching the cell category transition rates to the cell category relative populations of free tumor growth for an already large solid tumor at the start of simulation has been clarified. A technique has been suggested and succesfully applied in order to ensure satisfaction of this condition. The concept of a nomogram matching the cell category transition rates to the cell category relative populations at the treatment baseline is introduced. Convergence issues are addressed and indicative numerical results are presented. Qualitative agreement of the model's behavior with the corresponding clinical trial experience supports its potential to constitute the basis for an optimization system within the clinical environment following completion of its clinical validation and optimization. In silico treatment experimentation in the patient individualized context is expected to constitute the primary application of the model.

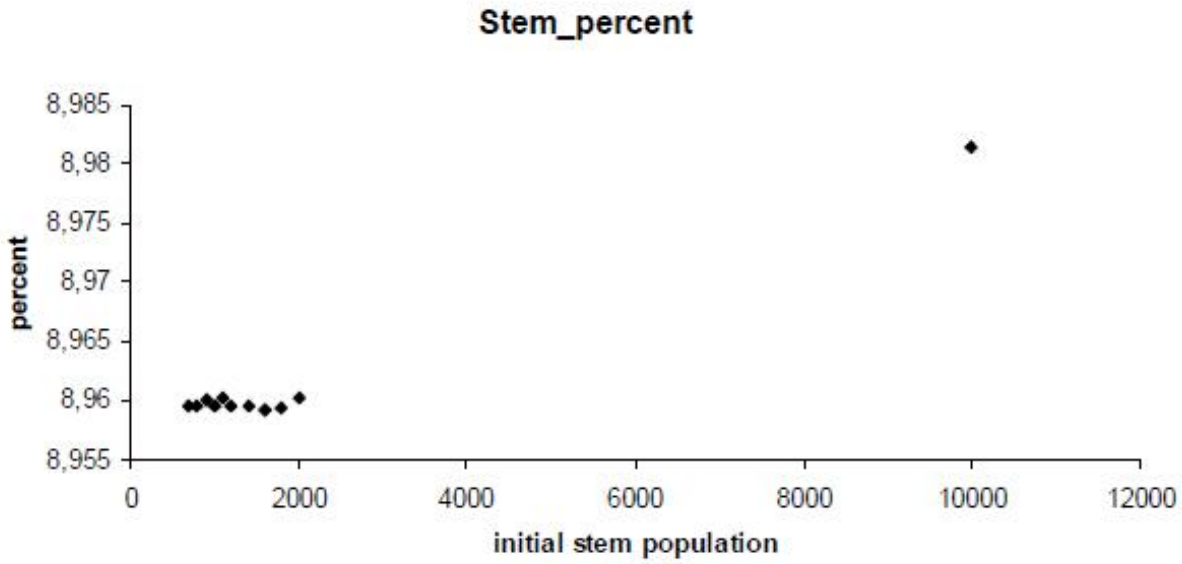

Fig. 17. Relative population of stem cells at equilibrium as a fuction of the number of initial stem cells used to produce the relative populations of each cell category at the treatment simulation starting point. The relative population of stem cells is expressed as a percentage of the total tumor cells (abbreviated here as "percent"). It can be noticed that if less than 2000 initial stem cells are used to produce all cell category relative populations and therefore initialize the clinical tumor good stabilization of the stem cell relative population is achieved (for the subspace of parameter values combinations addressed here).

4.16.5 Study 5: A four-dimensional simulation model of tumour response to radiotherapy in vivo: parametric validation considering radiosensitivity, genetic profile and fractionation

This study has been referred in 4.5.1 chapter

4.16.6 Study 6: In Silico Radiation Oncology: Combining Novel Simulation Algorithms With Current Visualization Techniques

This study has been referred in 4.9.3 chapter

4.17 ICCS - Vincristine Chemotherapy Simulation

Model description:
A generic four-dimensional simulation model of tumor response to vincristine chemotherapy. The model is based on the consideration of a discrete time and space stochastic cellular automata.

4.17.1 Study 1: Towards in silico oncology: Adapting a four dimensional nephroblastoma treatment model to a clinical trial case based on multi-method sensitivity analysis

This study has been referred in 4.16.1 chapter

4.17.2 Study 2: Modeling Nephroblastoma Treatment Response Cases with In Silico Scenarios

This study has been referred in 4.16.3 chapter

4.17.3 Study 3: Multilevel Cancer Modeling in the Clinical Environment: Simulating the Behavior of Wilms Tumor in the Context of the SIOP 2001/GPOH Clinical Trial and the ACGT Project

This study has been referred in 4.16.4 chapter

4.17.4 Study 4: In Silico Radiation Oncology: Combining Novel Simulation Algorithms With Current Visualization Techniques

This study has been referred in 4.9.3 chapter

4.18 ICCS - Actinomycin - Vincristine Combined Chemotherapy Simulation model

Model description:
A generic four-dimensional simulation model of tumor response to combined therapy of vincristine and actinomycin. The model is based on the consideration of a discrete time and space stochastic cellular automata.

4.18.1 Study 1: Towards in silico oncology: Adapting a four dimensional nephroblastoma treatment model to a clinical trial case based on multi-method sensitivity analysis: *referred in 4.16.1 chapter*

This study has been referred in 4.16.1 chapter

4.18.2 Study 2: Exploiting Clinical Trial Data Drastically Narrows the Window of Possible Solutions to the Problem of Clinical Adaptation of a Multiscale Cancer Model

This study has been referred in 4.16.2 chapter

4.18.3 Study 3: Modeling Nephroblastoma Treatment Response Cases with In Silico Scenarios

This study has been referred in 4.16.3 chapter

4.18.4 Study 4: Multilevel Cancer Modeling in the Clinical Environment: Simulating the Behavior of Wilms Tumor in the Context of the SIOP 2001/GPOH Clinical Trial and the ACGT Project

This study has been referred in 4.16.4 chapter

4.18.5 Study 5: In Silico Radiation Oncology: Combining Novel Simulation Algorithms With Current Visualization Techniques

This study has been referred in 4.9.3 chapter

4.19 UOXF - Angiogenesis

Model description:
PDE model for tumour angiogenesis.

4.20 UOXF - Angiogenesis and vasculogenesis

Model description:
ODE model that investigates how contribution from angiogenesis and vasculogenesis changes during tumour growth.

4.21 UOXF - ascular tumour growth and chemotherapy

Model description:
PDE model that investigates how interplay between vascular remodelling and tumour growth and resulting spatio-temporal dynamics influence tumour's response to chemotherapy.

4.21.1 Oscillatory dynamics in a model of vascular tumour growth--implications for chemotherapy

Investigations of solid tumours suggest that vessel occlusion may occur when increased pressure from the tumour mass is exerted on the vessel walls. Since immature vessels are frequently found in tumours and may be particularly sensitive, such occlusion may impair tumour blood flow and have a negative impact on therapeutic outcome. In order to study the effects that occlusion may have on tumour growth patterns and therapeutic response, in this paper it was developed and investigated a continuum model of vascular tumour growth.
By analysing a spatially uniform submodel, it has been identified regions of parameter space in which the combination of tumour cell proliferation and vessel occlusion give rise to sustained temporal oscillations in the tumour cell population and in the vessel density. Alternatively, if the vessels are assumed to be less prone to collapse, stable steady state solutions are observed. When spatial effects are considered, the pattern of tumour invasion depends on the dynamics of the spatially uniform submodel. If the submodel predicts a stable steady state, then steady travelling waves are observed in the full model, and the system evolves to the same stable steady state behind the invading front. When the submodel yields oscillatory behaviour, the full model produces periodic travelling waves. The stability of the waves (which can be predicted by approximating the system as one of lambda-omega type) dictates whether the waves develop into regular or irregular spatio-temporal oscillations. Simulations of chemotherapy reveal that treatment outcome depends crucially on the underlying tumour growth dynamics. In particular, if the dynamics are oscillatory, then therapeutic efficacy is difficult to assess since the fluctuations in the size of the tumour cell population are enhanced, compared to untreated controls.
it has been developed a mathematical model of vascular tumour growth formulated as a system of partial differential equations (PDEs). Employing a combination of numerical and analytical techniques, it was demonstrated how the spatio-temporal dynamics of the untreated tumour may influence its response to chemotherapy.

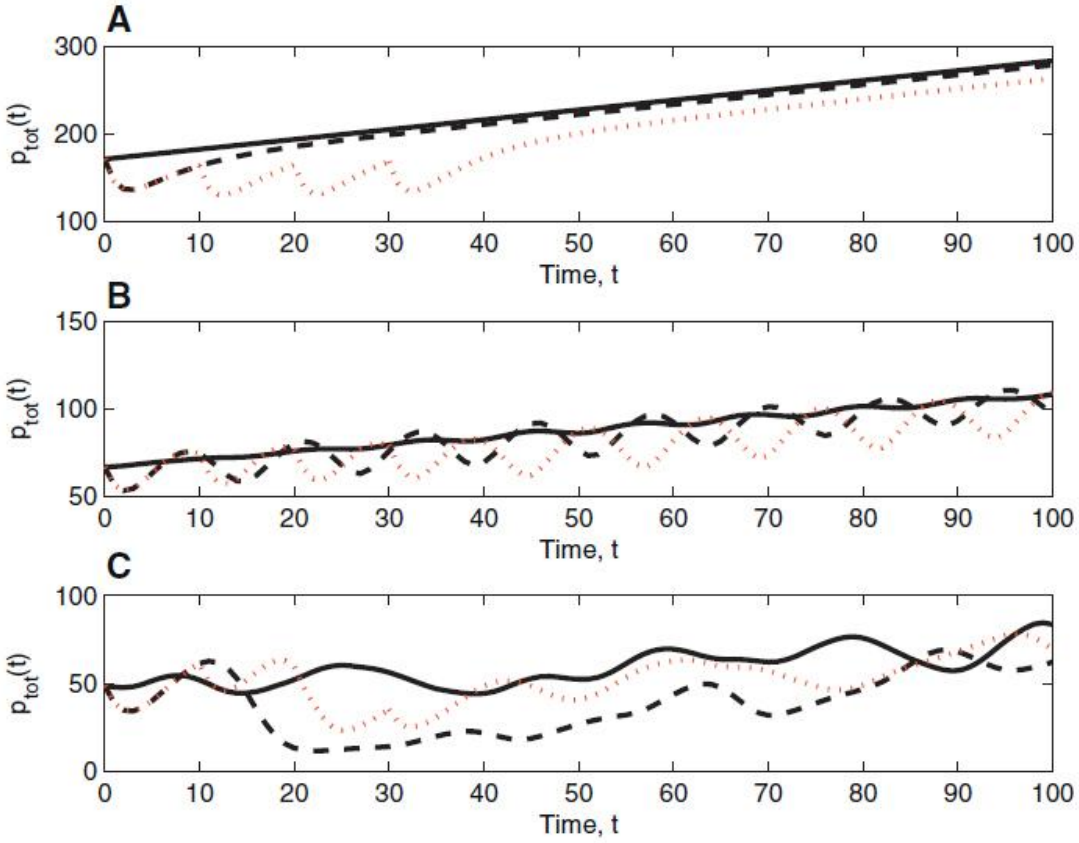

Fig. 19. System responses to therapy. Three trios of curves (calculated from solutions of (11)-(15), using (27)) showing how the tumour burden, ptot, varies after a single bolus of chemotherapy (black dashed lines) and 4 boluses of chemotherapy (red dotted lines). Here time, t, represents time since therapy was initialised. (A) In this case, before therapy is applied, the dynamics behind the invading front evolve to a stable equilibrium. Both a single bolus and multiple boluses decrease tumour burden relative to untreated control (solid line). This persists even during the recovery phase, when the effects of the therapy wane and the tumour starts to regrow. Multiple boluses are clearly more effective than a single bolus. (B) When in the absence of therapy tumour invasion results in the development of regular oscillations (solid line), the therapies induce oscillations of larger amplitude during the regrowth phase. Multiple boluses are slightly more effective than a single bolus. (C) When irregular oscillations occur in the absence of therapy (solid line), chemotherapies lead to an increase in the amplitude of these oscillations during the recovery phase. Multiple boluses do not improve the therapeutic response. Key: solid lines: no therapy; black dashed lines: single bolus; red dotted lines: 4 boluses (each separated by ten time units). Parameter values: with $dc = 2.0 \times 10^4$, $Dc = 1.6 \times 10^4$, $hc = 1.3 \times 10^3$, $k = 0.9$ and $Kc = 0.05$.

4.22 UOXF - Vascular tumour growth

Model description:
PDE model of vascular tumour growth based on the theory of mixtures

4.22.1 Study 1: Multiphase modelling of vascular tumour growth in two spatial dimensions

[HUB12] In this paper it was presented a continuum mathematical model of vascular tumour growth which is based on a multiphase framework in which the tissue is decomposed into four distinct phases and the principles of conservation of mass and momentum are applied to

the normal/healthy cells, tumour cells, blood vessels and extracellular material. The inclusion of a diffusible nutrient, supplied by the blood vessels, allows the vasculature to have a nonlocal influence on the other phases. Two-dimensional computational simulations are carried out on unstructured, triangular meshes to allow a natural treatment of irregular geometries, and the tumour boundary is captured as a diffuse interface on this mesh, thereby obviating the need to explicitly track the (potentially highly irregular and ill-defined) tumour boundary. A hybrid finite volume/finite element algorithm is used to discretise the continuum model: the application of a conservative, upwind, finite volume scheme to the hyperbolic mass balance equations and a finite element scheme with a stable element pair to the generalised Stokes equations derived from momentum balance, leads to a robust algorithm which does not use any form of artificial stabilisation. The use of a matrix-free Newton iteration with a finite element scheme for the nutrient reaction-diffusion equations allows full nonlinearity in the source terms of the mathematical model. Numerical simulations reveal that this four-phase model reproduces the characteristic pattern of tumour growth in which a necrotic core forms behind an expanding rim of well-vascularised proliferating tumour cells. The simulations consistently predict linear tumour growth rates. The dependence of both the speed with which the tumour grows and the irregularity of the invading tumour front on the model parameters is investigated.

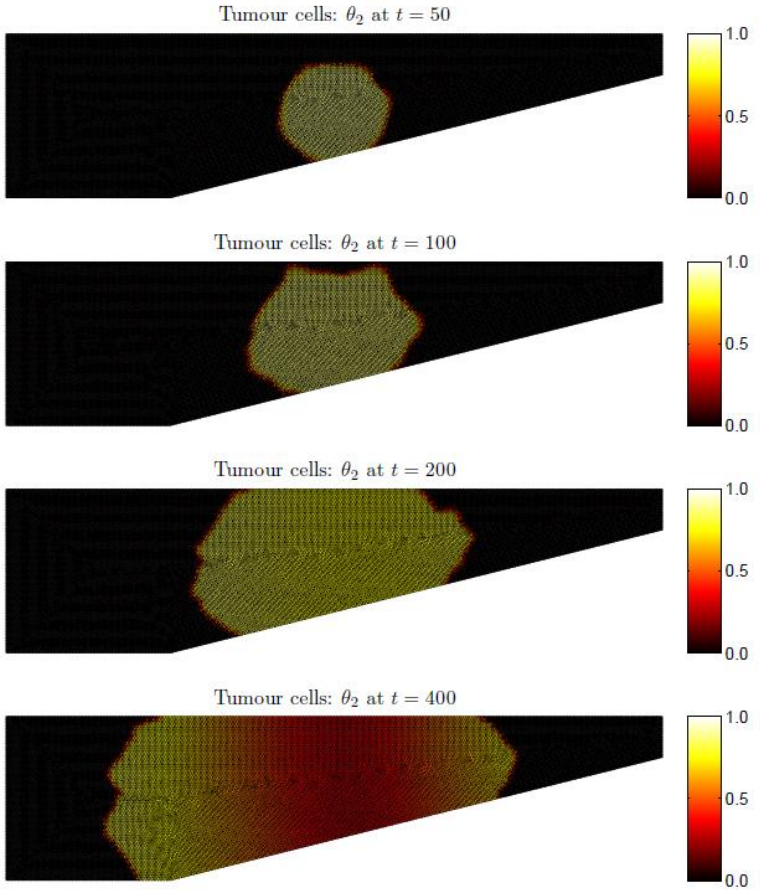

Fig. 20. Snapshots of the evolution of the tumour cell phase volume fraction, _2, when a single, circular tumour is seeded in a tapered domain. Time increases from top to bottom.

The simulation results presented in Fig. 20 exhibit behaviour similar to that described earlier. There is an initial period of rapid growth, after which a necrotic core forms behind the

proliferating rim of tumour cells. The solid walls prevent the tumour from spreading upwards and downwards, but it continues to spread laterally as time progresses.

4.23 ICCS - Untreated vascular tumour growth

Model description:
This model describes the interplay between pathological angiogenesis and solid tumour growth.

4.23.1 Study 1: Tumor development under angiogenic signaling: a dynamical theory of tumor growth, treatment response, and postvascular dormancy

[HAH99] The effects of the angiogenic inhibitors endostatin, angiostatin, and TNP-470 on tumor growth dynamics are experimentally and theoretically investigated. On the basis of the data, it was posed a quantitative theory for tumor growth under angiogenic stimulator/inhibitor control that is both explanatory and clinically implementable. Our analysis offers a ranking of the relative effectiveness of these inhibitors. Additionally, it reveals the existence of an ultimate limitation to tumor size under angiogenic control, where opposing angiogenic stimuli come into dynamic balance, which can be modulated by antiangiogenic therapy. The competitive influences of angiogenically driven growth and inhibition underlying this framework may have ramifications for tissue size regulation in general.

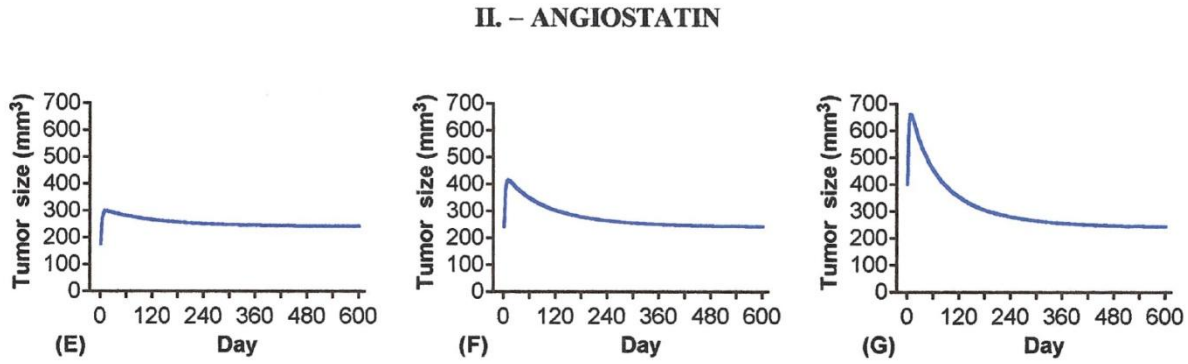

Fig 21. The set point attained by ongoing treatment is independent of the tumor volume at which treatment is initiated, depending only on how the ongoing treatment modulates the balance between angiogenic stimulators and inhibitors. The set point is determined by the point in tumor growth where stimulation and inhibition (from both endogenous and therapeutic sources) come into balance. TNP-470, the effect of beginning a TNP-470 regimen (30 mg/kg/q.o.d.) at day 0 (tumor size ~170 mm^3) on the control tumor modifies the course of growth, limiting the final size to 12,300 mm^3 (B). This final value is not sensitive to treatment start time but, rather, is determined by the average extent to which the administered inhibitor supplements endogenous inhibition. If treatment commences instead when the tumor size is already 12,300 mm^3, the tumor will remain at that size (C). Likewise, if treatment commences at a time when the tumor size is larger than this asymptotic value (example shown: V 5 17,300 mm^3), treatment brings the tumor down to, but not beyond, the asymptotic set point size V 5 12,300 mm^3 (D). ANGIOSTATIN, on the basis of the angiostatin response with 20 mg/kg/day, a calculated response to 14 mg/kg/day is shown. This dose level is insufficient to accomplish a complete regression. Instead, tumor size is driven toward a finite set point value. By starting treatment at the same 177 mm^3 tumor size as for the 20 mg/kg/day experiment, tumor size is seen to first rise, then settle back to a set point value of ~240 mm^3 (E). The consequence of initiating treatment at a later time when tumor size has reached 240 mm3 is shown (F).

Although the tumor continues to grow for a time under treatment (~10 days), it then regresses back to the 240-mm^3 set point size as before. G, consequence of starting treatment at a still larger tumor size, in this case, 400 mm^3. An initial overshoot is once again observed before final asymptotic descent to the 240- mm^3 set point. The rise and subsequent downturn in each instance is attributable to the accumulation of dose concentration as the regimen proceeds, an effect arising from the relatively slow clearance of this agent.

4.23.2 Study 2: New approach to modeling of antiangiogenic treatment on the basis of hahnfeldt et al. model

[POL11] In the paper it is proposed a new methodology in modeling of antiangiogenic treatment on the basis of well recognized model formulated by Hahnfeldt et al. in 1999. On the basis of the Hahnfeldt et al. model, with the usage of the optimal control theory, some protocols of antiangiogenic treatment were proposed. However, in our opinion the formulation of that model is valid only for the antivascular treatment, that is treatment that is focused on destroying endothelial cells. Therefore, it was proposed a modi_cation of the original model which is valid in the case of the antiangiogenic treatment, that is treatment which is focused on blocking angiogenic signaling. It analyzed basic mathematical properties of the proposed model and present some numerical simulations.

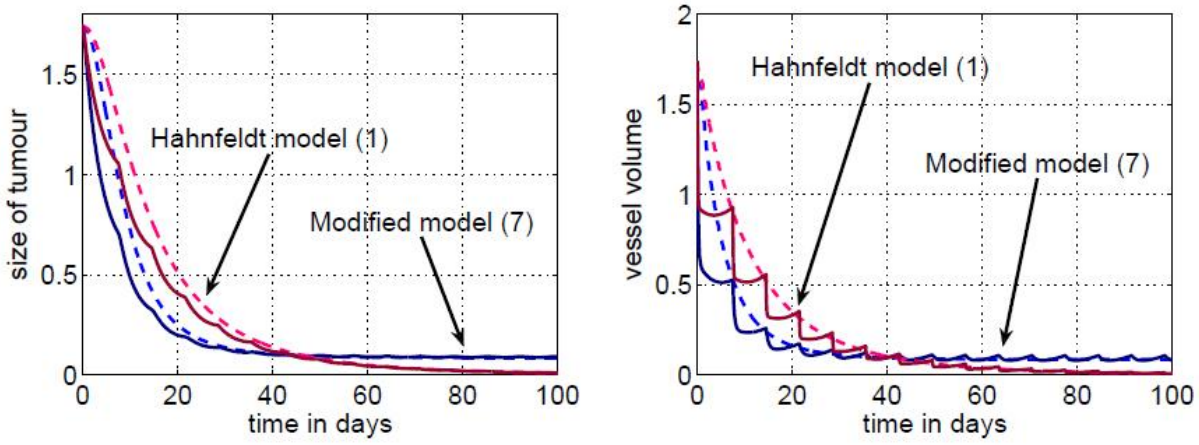

Fig. 22. Comparison of solutions to the Hahnfeldt et al.model (1) and the modi_ed model (8) for daily dose 0:7. Solid line - the solution for a dose applied once a week, dotted line - a dose applied every hour.

4.23.3 Study 3: Modeling the Interplay Between Pathological Angiogenesis and Solid Tumor Growth: the Anti-angiogenic Treatment Effect

[ARG12] In this paper, a previous continuum approach describing vascular tumor growth under angiogenic signaling is developed and extended via the inclusion of bevacizumab pharmacokinetics. The modeling approach to the problem addressed includes inter alia the building of the model (selection of equations, related assumptions, coupling with a pharmacokinetic model tailored to the bevacizumab paradigm, implementation and numerical solution) as well as a study of the vascular tumor growth model with results for free growth and an intermittent bevacizumab mono-therapy schedule.

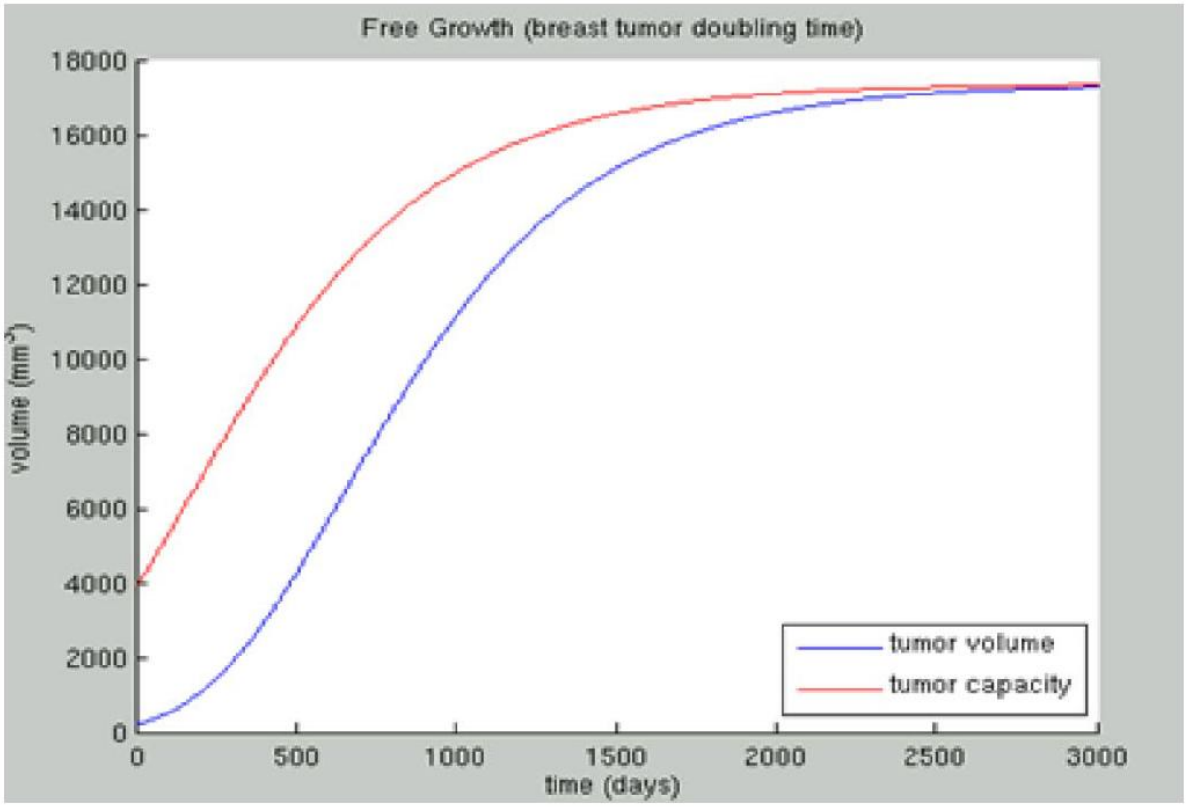

Fig. 23. Simulation results for an untreated breast tumor characterized by the parameter values

4.24 ICCS - Vascular tumour growth under bevacizumab monotherapy

Model description:
This model describes the response of a solid tumour to bevacizumab monotherapy.

4.24.1 Study 1: New approach to modeling of antiangiogenic treatment on the basis of hahnfeldt et al. model

This study has been referred in 4.23.2 chapter

4.24.2 Study 2: Modeling the Interplay Between Pathological Angiogenesis and Solid Tumor Growth: the Anti-angiogenic Treatment Effect

This study has been referred in 4.23.3 chapter

4.25 ICCS - Time-course of bevacizumab

Model description:
This model describes the time-course of bevacizumab concentration in plasma

4.26 ICCS - Bevacizumab concentration in plasma in a given time-point

Model description:
Given a specific time-point, this model computes the concentration of bevacizumab in plasma

4.27 ICCS - Time-course of vinorelbine concentration in plasma

Model description:
This model describes the time-course of vinorelbine concentration in plasma

4.28 ICCS - Vinorelbine concentration in plasma in a given time-point

Model description:
Given a specific time-point, this model computes the concentration of vinorelbine in plasma

4.29 ICCS - Diffusion-Reaction Based Glioblastoma multiforme (GBM) Invasion and Response to Treatment Model with Boundary Conditions

Model description:
The purpose of the model is to demonstrate in real time the spatiotemporal predictions of the continuous mathematics based Oncosimulator built around a multiscale model of the evolution of a highly diffusive solid tumor. The modelling approach is based on the numerical solution for a homogeneous approximation of the diffusive growth of gliomas and in particular glioblastoma multiforme (GBM). According to the diffusion based approach the tumor is considered a spatiotemporal distribution of continuous cell density which follows the general diffusion law. The crucial component is the numerical handling of the adiabatic Neumann boundary conditions since the physical processes is taking place in the vicinity of the anatomic boundaries imposed by the of the skull.

4.29.1 Study 1: A detailed numerical treatment of the boundary conditions imposed by the skull on a diffusion–reaction model of glioma tumor growth. Clinical validation aspects

[GIA12a] The study of the diffusive behavior of glioma tumor growth is an active field of biomedical research with considerable therapeutic implications. An important aspect of the corresponding computational problem is the mathematical handling of boundary conditions. This study aims at providing an explicit and thorough numerical formulation of the adiabatic Neumann boundary conditions imposed by the skull on the diffusive growth of gliomas and in particular on glioblastoma multiforme (GBM). Additionally, a detailed exposition of the numerical solution process for a homogeneous approximation of glioma invasion using the

Crank–Nicolson technique in conjunction with the Conjugate Gradient system solver is provided. The entire mathematical and numerical treatment is also in principle applicable to mathematically similar physical, chemical and biological phenomena. A comparison of the numerical solution for the special case of pure diffusion in the absence of boundary conditions or equivalently in the presence of adiabatic boundaries placed in infinity with its analytical counterpart is presented. Numerical simulations for various adiabatic boundary geometries and non zero net tumor growth rate support the validity of the corresponding mathematical treatment. Through numerical experimentation on a set of real brain imaging data, a simulated tumor has shown to satisfy the expected macroscopic behavior of glioblastoma multiforme including the adiabatic behavior of the skull. The paper concludes with a number of remarks pertaining to both the biological problem addressed and the more generic diffusion–reaction context.

Visualization for numerical validation of the adiabatic behavior of the boundary implementation

Several pertinent boundary geometry scenarios have been addressed. In order to check the correctness of the boundary treatment component of the simulation code the following two criteria have been adopted:

i. prohibition of tumor cell transfer through the skull;

ii. conservation of the total number of tumor cells within the skull cavity in the special fictitious (and exclusively mathematically relevant) case of pure diffusion with neither cell generation nor cell death. Obviously, in the biologically relevant scenarios addressed where tumor cell proliferation and loss are present this criterion is irrelevant.

A three dimensional visualization of the simulation results for an arbitrary boundary geometry is shown in Fig. 24. An initial virtual spherical tumor is supposed to lie inside the boundary cavity. As time increases, the tumor grows and diffuses over the entire mesh. However, it does not migrate beyond the boundary. Thus criterion i is satisfied. Visualization details are provided in Fig. 25.

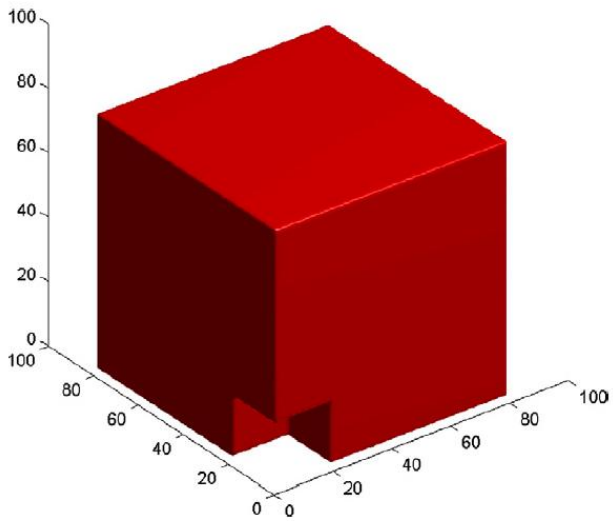

Fig.24 An arbitrary boundary geometry. An initial virtual spherical tumor is supposed to lie inside the boundary cavity.

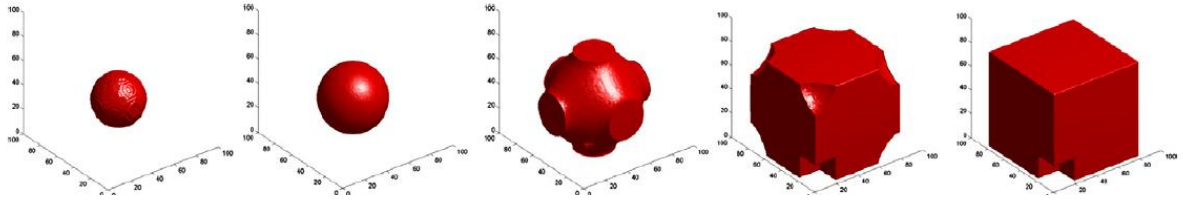

Fig. 25. An initial virtual spherical tumor of radius = 2 cm is supposed to lie inside the boundary cavity of Fig. 13. Panels from left to right correspond to days 1, 150, 299, 450, 899. For visualization purposes, for each time point considered, a concentration cutoff value has been assumed so that concentration values lower than the cutoff value are represented by white color. As time increases, the tumor diffuses over the free space of the entire mesh. However, it does not migrate beyond the boundary. A cubic mesh of 8 cm x 8 cm x8 cm has been used. The following parameter values have been used: diffusion coefficient D = 0.0065 cm2/d, cell concentration within the initial tumor equal to 106 cells/mm3, h = 0.1 cm and Dt = 1 d, net tumor growth rate ρ = 0.012 d-1 and loss rate due to treatment (arbitrary value) G = 0.0013 d-1.

4.29.2 Study 2: The Continuous Mathematics Based Glioblastoma Oncosimulator: Application of an Explicit Three Dimensional Numerical Treatment of the Skull-Glioblastoma Neumann Boundary Condition on Real Anatomical Data

[GIA12b] The Continuous Mathematics Based Glioblastoma Oncosimulator is a platform for simulating, investigating, better understanding, and exploring the natural phenomenon of glioma tumor growth. Modelling of the diffusive-invasive behaviour of glioma tumour growth may have considerable therapeutic implications. A crucial component of the corresponding computational problem is the numerical treatment of the adiabatic Neumann boundary conditions imposed by the skull on the diffusive growth of gliomas and in particular glioblastoma multiforme (GBM). In order to become clinically acceptable such a numerical handling should ensure that no potentially life-threatening glioma cells disappear artificially due to oversimplifying assumptions applied to the simulated region boundaries. However, no explicit numerical treatment of the 3D boundary conditions under consideration has appeared in the literature to the best of the authors' knowledge. Therefore, this paper aims at providing an outline of a novel, explicit and thorough numerical solution to this problem. Additionally, a brief exposition of the numerical solution process for a homogeneous approximation of glioma diffusion-invasion using the Crank – Nicolson technique in conjunction with the Conjugate Gradient system solver is outlined. The entire mathematical and numerical treatment is also in principle applicable to mathematically similar physical, chemical and biological diffusion based spatiotemporal phenomena which take place in other domains for example embryonic growth and general tissue growth and tissue differentiation. A comparison of the numerical solution for the special case of pure diffusion in the absence of boundary conditions with its analytical counterpart has been made. In silico experimentation with various adiabatic boundary geometries and non zero net tumour growth rate support the validity of the corresponding mathematical treatment. Through numerical experimentation on a set of real brain imaging data, a simulated tumour has shown to satisfy the expected macroscopic behaviour of glioblastoma multiforme, on concrete published clinical imaging data, including the adiabatic behaviour of the skull. The paper concludes with a number of remarks pertaining to the potential and the limitations of the diffusion-reaction approach to modelling multiscale malignant tumour dynamics.

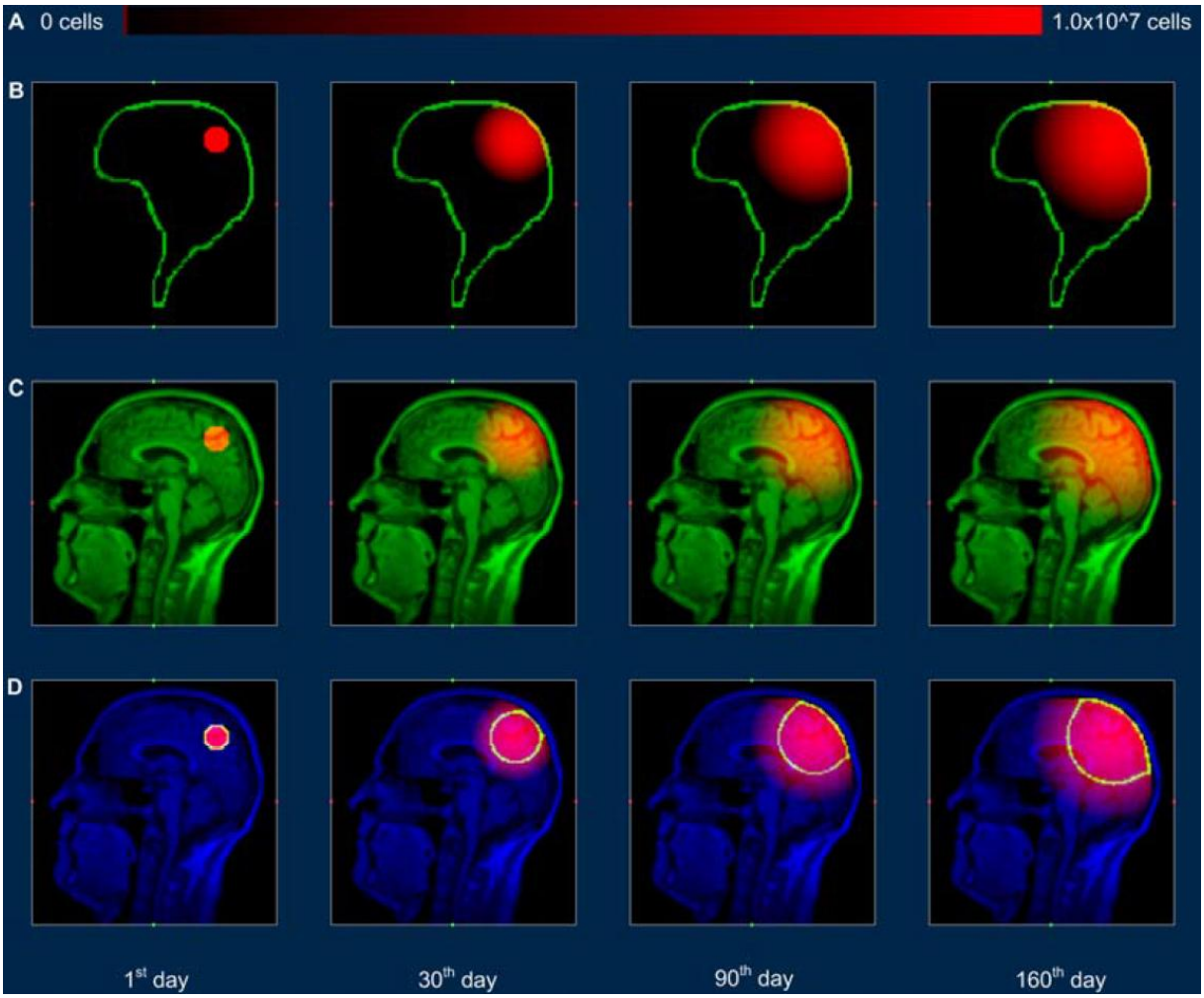

Fig. 26. Schematic representation of the growth of a virtual glioblastoma tumor in vivo in sagittal planes at various time points (panel columns from left to right correspond to days 1, 30, 90 and 160 respectively). (A) The red color intensity level I depends on cell concentration according to the function I=klog10c , where c denotes tumor cell concentration, the constant k=255/log10cmax , cmax is the maximum value of tumor cell concentration over the entire space and time range considered during all simulations that have been included in this figure. Maximum and zero cell concentration corresponds to RGB(255,0,0) and RGB(0,0,0) respectively. (B), (C) As time increases, the tumor diffuses theoretically over the interior space of the skull cavity of the human head. (D) The yellow/bright contour defines the boundary of the tumor component in 2D that is tomographically detectable and has a cell density higher than the assumed threshold of 8000 cells per cubic millimeter.

4.30 UNITO - Phenomenological universality in cancer growth

Model description:
Series expansion Un of the solution of the growth equation: exact solutions of U0 ,U1 and U2.

4.30.1 Study 1: A Classification Scheme for Phenomenological Universalities in Growth Problems

[CAS06] A classification in universality classes of broad categories of phenomenologies, belonging to different disciplines, may be very useful for a crossfertilization among them and for the purpose of pattern recognition. It was presented here a simple scheme for the classification of nonlinear growth problems. The success of the scheme in predicting and characterizing the well known Gompertz, West and logistic models, suggests to us the study of a hitherto unexplored class of nonlinear growth problems.

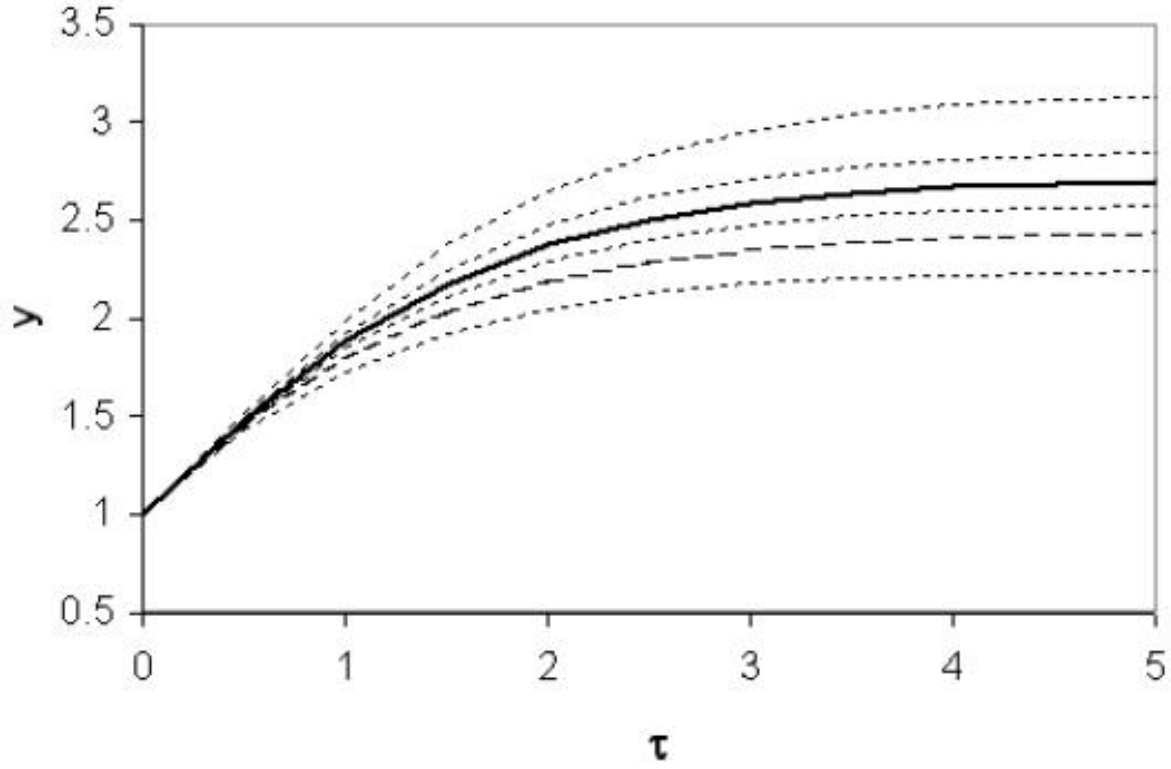

Fig. 27: - Growth curves belonging to the class U2. From the top to the bottom the values of the parameter b are −0.25,−0.1, 0.1, 0.25, 0.5 respectively. The solid curve (b = 0, p = 1) corresponds to the Gompertzian (U1), while the dashed one refers to the value proposed in [6] p = 3/4 (b = 1/4).

4.31 UNITO - cancer growth & radiotherapy

Model description:
Comparison between the predictions of U1 and U2 in different clinical schedules.

4.32 UNITO - Multipassage tumor growth

Model description:
U1 application to tumor regrowth

4.32.1 Study1: A New Computational Tool for the Phenomenological Analysis of Multipassage Tumor Growth Curves

[GLI09] Multipassage experiments are performed by subcutaneous implantation in lab animals (usually mice) of a small number of cells from selected human lines. Tumor cells are then passaged from one mouse to another by harvesting them from a growing tumor and implanting them into other healthy animals. This procedure may be extremely useful to investigate the various mechanisms involved in the long term evolution of tumoral growth. It has been observed by several researchers that, contrary to what happens in in vitro experiments, there is a significant growth acceleration at each new passage. This result is explained by a new method of analysis, based on the Phenomenological Universalities approach. It is found that, by means of a simple rescaling of time, it is possible to collapse all the growth curves, corresponding to the successive passages, into a single curve, belonging to the Universality Class U2. Possible applications are proposed and the need of further experimental evidence is discussed.

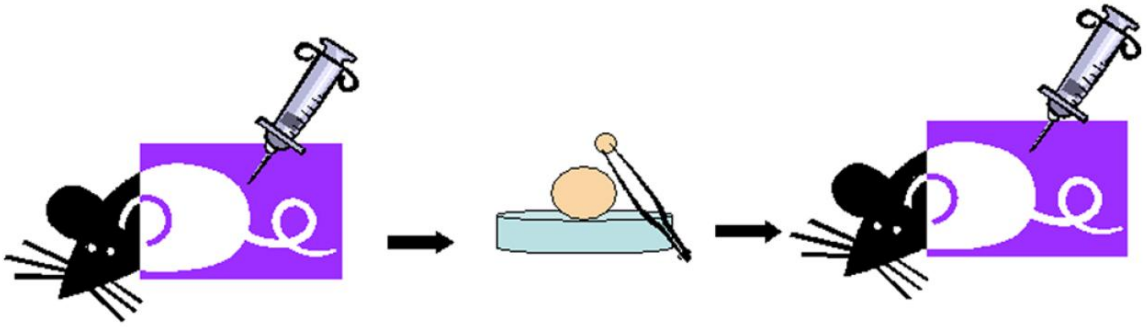

Fig. 28: A cartoonist's view of multi-passage experiments. In MPE experiments, tumors grow following the subcutaneous implantation on the back of a lab animal (usually mice) of ~106 tumor cells (from cell cultures or from surgical resection). Tumor cells are then passaged from one mouse to another by harvesting them from a growing tumor and implanting a given number of them into another healthy animal. Once the tumor has grown above a certain volume it can be harvested again. This passage of tumor cells is repeated for multiple rounds (McCredie et al. [10] report the case of a spontaneous mammary tumor in a C3H mouse, from which the first syngenic transplant was done in 1946 and which has been serially transplanted in the C3H/HeJ strain, reaching in 1971 the 900th generation!). The idea of taking a very small fraction of a spontaneous tumor mass and repeateadly transplanting it in a new host seems to reproduce the ideal situation of unlimited resources, and therefore should give us some insight about unrestricted tumor growth.

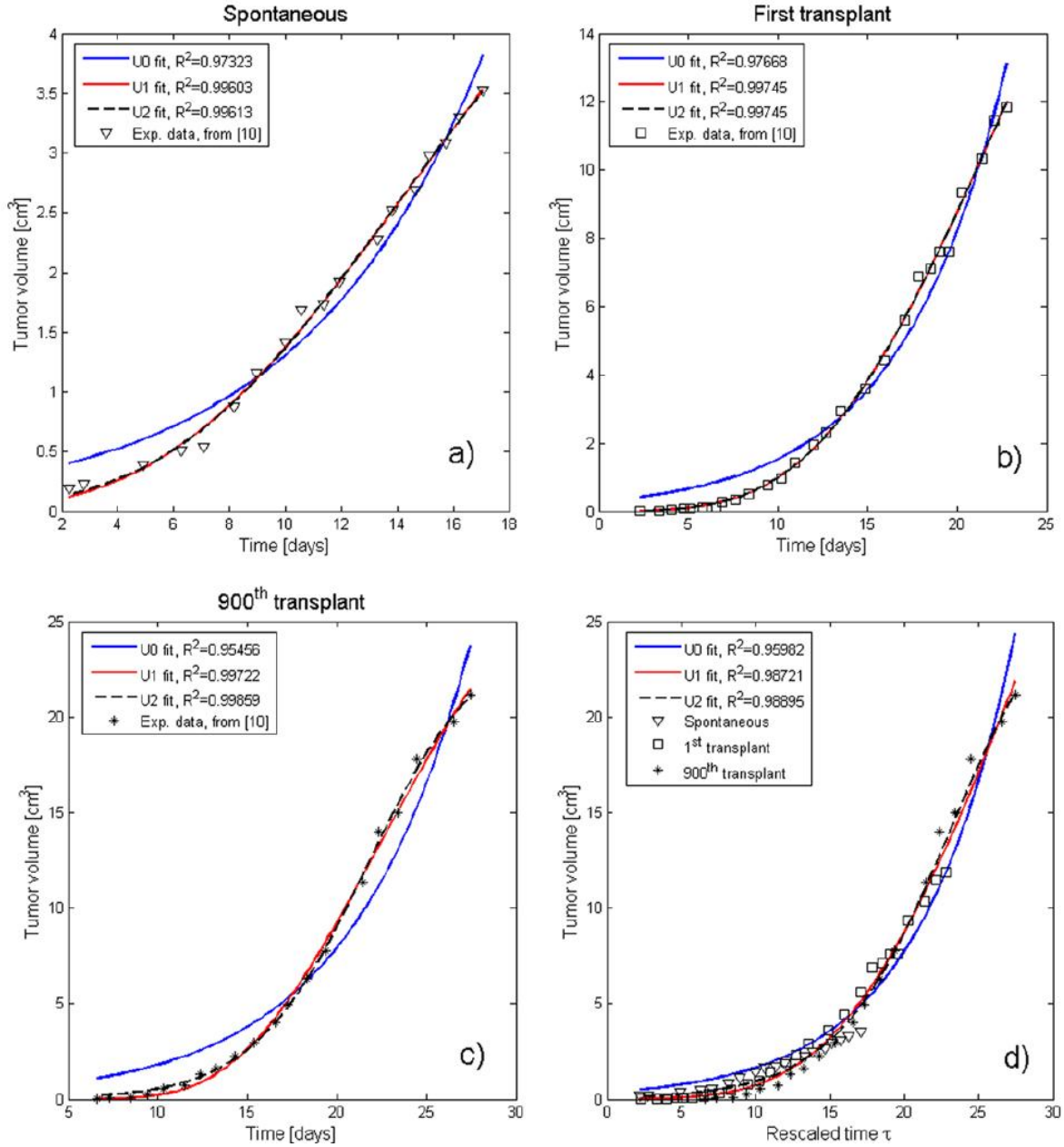

Fig. 29: MPE results from McCredie et al. [10]. As many as 900 transplants of cells from the tumoral line C3H rat mammary carcinoma have been performed, but the curves corresponding to only the original one, the first and the last (900th) transplant have been reported: (A–C), respectively. For all of them the fits of the data corresponding to the classes U0, U1, and U2 have been included. There is an obvious improvement when one goes from U0 to U1 and a much smaller one from U1 to U2. The latter, in fact, yelds an almost perfect agreement with the experimental data. As in the case of Steel's data, in (D) the growth curves are normalized and displayed as a single group of data vs. the rescaled time t. Here a U2 curve gives an excellent fit to the regrouped data. It is indeed remarkable that after as many as 900 transplants the tumor still grows with the same law (a part from the time ''rescaling'').

4.33 UNITO - Cancer growth and chemotherapy

Model description:
U1 & U2 predictions for chemotherapy dosage

4.33.1 Study 1: Tumor growth instability and its implications for chemotherapy

[CAS09] The chemotherapy late intensity schedule is revised to account for tumor growth instability, where a small tumor cell fraction emerges that exhibits a higher proliferation rate than the parent strain. Modeling this instability as simplified two-population dynamics it was found that: 1) if this instability precedes the onset of treatment, the slope of the linear increase of the drug concentration for the standard "Norton-Simon late intensity schedule" changes and the initial value of the dose strongly depends on the balance of the two tumor cell populations and on their distinct growth rates; and, 2) if the instability trails the initial treatment, the effective chemotherapeutic drug concentration changes as well. Both cases point towards necessary improvements of the "Norton-Simon late intensity" schedule.

4.34 FORTH PIHNA-ECM-LQ

Model description:
The PIHNA-ECM-LQ mathematical model describes the vascular and invasive phases of tumor growth considering the complex interactions between cancer cells and the host-tissue microenvironment. Specifically, the tumor microenvironment consists of the vasculature that provides oxygen to cancer cells, tumor-induced angiogenic factors (e.g., VEGF) as well as the macromolecules of the extracellular matrix (ECM) and matrix degrading enzymes (e.g., Matrix Metalloproteinases), which degrade the ECM locally. Depending on oxygen supply, cancer cells can be proliferative, hypoxic or necrotic. Furthermore, cancer cell populations can invade the surrounding tissue driven by chemotaxis towards higher oxygen or haptotaxis towards higher ECM concentrations. The model can also accommodate the effect of radiotherapy on cancer population, which is based on the Linear Quadratic Model (LQ) approximation.

4.34.1 Study 1: Quantifying the Role of Angiogenesis in Malignant Progression of Gliomas: In Silico Modeling Integrates Imaging and Histology

[SWA11] Gliomas are uniformly fatal forms of primary brain neoplasms that vary from low- to high-grade (glioblastoma). Whereas low-grade gliomas are weakly angiogenic, glioblastomas are among the most angiogenic tumors. Thus, interactions between glioma cells and their tissue microenvironment may play an important role in aggressive tumor formation and progression. To quantitatively explore how tumor cells interact with their tissue microenvironment, it was incorporated the interactions of normoxic glioma cells, hypoxic glioma cells, vascular endothelial cells, diffusible angiogenic factors, and necrosis formation into a first-generation, biologically based mathematical model for glioma growth and invasion. Model simulations quantitatively described the spectrum of in vivo dynamics of gliomas visualized with medical imaging. Furthermore, it was investigated how proliferation and dispersal of glioma cells combine to induce increasing degrees of cellularity, mitoses,

hypoxia-induced neoangiogenesis and necrosis, features that characterize increasing degrees of "malignancy," and it was discovered that changes in the net rates of proliferation (r) and invasion (D) are not always necessary for malignant progression. Thus, although other factors, including the accumulation of genetic mutations, can change cellular phenotype (e.g., proliferation and invasion rates), this study suggests that these are not required for malignant progression. Simulated results are placed in the context of the current clinical World Health Organization grading scheme for studying specific patient examples. This study suggests that through the application of the proposed model for tumor–microenvironment interactions, predictable patterns of dynamic changes in glioma histology distinct from changes in cellular phenotype (e.g., proliferation and invasion rates) may be identified, thus providing a powerful clinical tool. Cancer Res; 71(24); 7366–75. _2011 AACR.

Malignant progression separates primary and secondary GBMs according to proliferation and invasion kinetics

Fig. 30 shows the time course of the radial expansion of the simulated abnormality seen on T2 MRI for 2 different choices of the model parameters—a high r and low D case (case +; Fig. 30 B) and a lower r and higher D case (case +; Fig. 30 C). These 2 simulated cases differ in their time course for appearance on imaging, as well as their in silico grade at the time of first detection (assumed here to be 1 cm in radius on T2 MRI). In fact, these 2 cases represent in silico "primary" and "secondary" glioblastomas (pGBM and sGBM, respectively) in the sense that from the time of detectability on T2 MRI (assumed to be 1 cm in radius), case * maintained a grade IV in silico grade, whereas case + was considered a lower grade until it was over 2 cm in radius on T2 MRI (22).

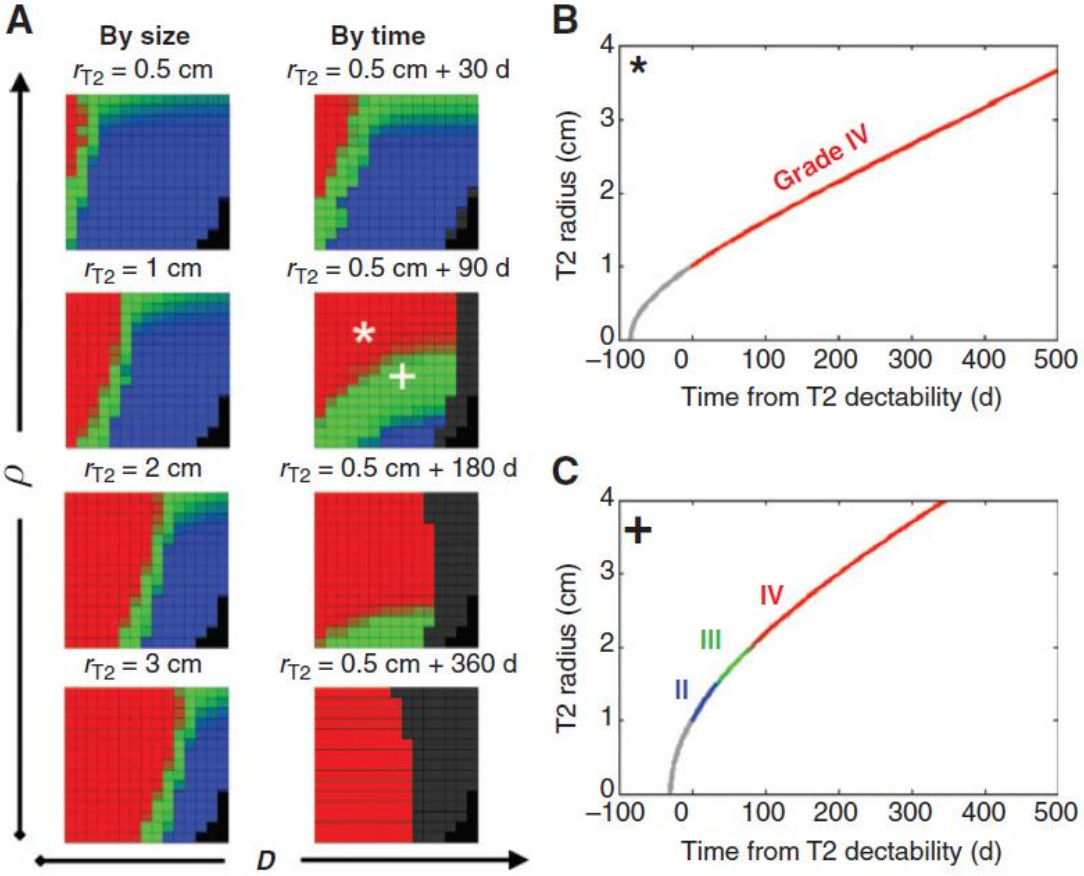

Fig. 30: A, maps of tumor grade as a function of tumor size (on T2 MRI) or of time. The blackened boxes indicate that the T2 visible portion of the simulated lesion has grown to a size sufficient to fill the whole brain. B, case * combination (high r, low D) produces a "primary" GBM (i.e., GBM from its first detectability),

whereas comparatively (C) case þ combination (low r, high D—relative to case *) produces a "secondary" GBM (i.e., "progressing" from lower grade).

4.34.2 Study 2: A SPATIAL MODEL OF TUMOR-HOST INTERACTION: APPLICATION OF CHEMOTHERAPY

[HIN09] In this paper chemotherapy was considered in a spatial model of tumor growth. The model, which is of reaction-diffusion type, takes into account the complex interactions between the tumor and surrounding stromal cells by including densities of endothelial cells and the extra-cellular matrix. When no treatment is applied the model reproduces the typical dynamics of early tumor growth. The initially avascular tumor reaches a diffusion limited size of the order of millimeters and initiates angiogenesis through the release of vascular endothelial growth factor (VEGF) secreted by hypoxic cells in the core of the tumor. This stimulates endothelial cells to migrate towards the tumor and establishes a nutrient supply sufficient for sustained invasion. To this model it was applied cytostatic treatment in the form of a VEGF-inhibitor, which reduces the proliferation and chemotaxis of endothelial cells. This treatment has the capability to reduce tumor mass, but more importantly, it was able to determine that inhibition of endothelial cell proliferation is the more important of the two cellular functions targeted by the drug. Further, it was considered the application of a cytotoxic drug that targets proliferating tumor cells. The drug was treated as a diffusible substance entering the tissue from the blood vessels. Our results show that depending on the characteristics of the drug it can either reduce the tumor mass significantly or in fact accelerate the growth rate of the tumor. This result seems to be due to complicated interplay between the stromal and tumor cell types and highlights the importance of considering chemotherapy in a spatial context.

Spatially-dependent concentrations

The model presented in this paper examines cell types in terms of spatially-dependent cell densities, and chemical species in terms of spatially-dependent concentrations. This does not permit analysis of small-scale structures, particularly the vascular networks simulated in many angiogenesis models. However, it does allow for a large-scale perspective, and gives a broader range of options for interactions.

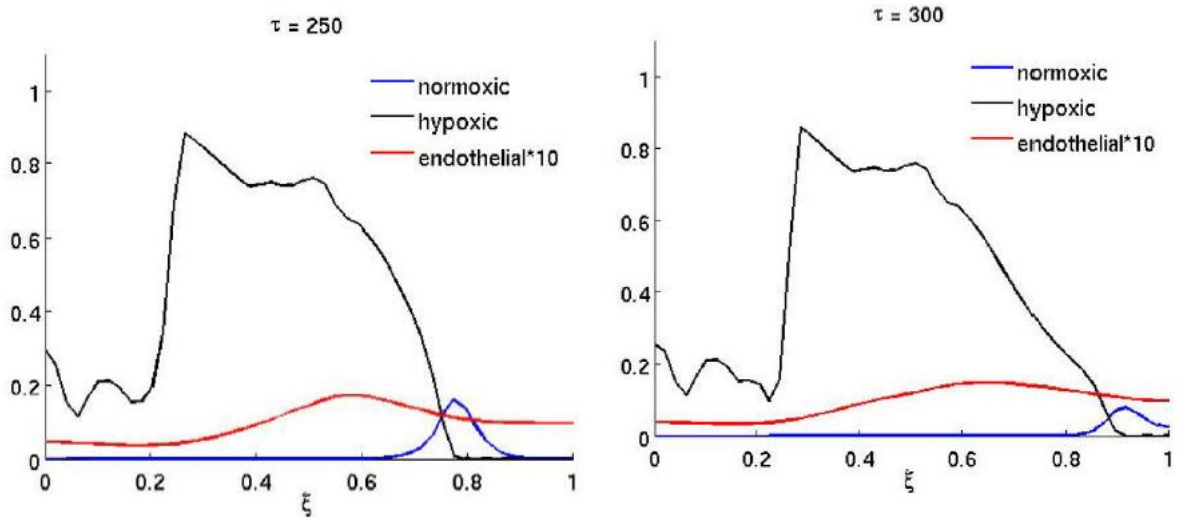

Fig. 31: The spatial distribution of normoxic, hypoxic and endothelial cells during and after antiangiogenic therapy when the proliferation αm of the endothelial cells is reduced by a factor of 10 while $200 \leq \tau \leq 300$ (all other parameters are as in the baseline scenario).

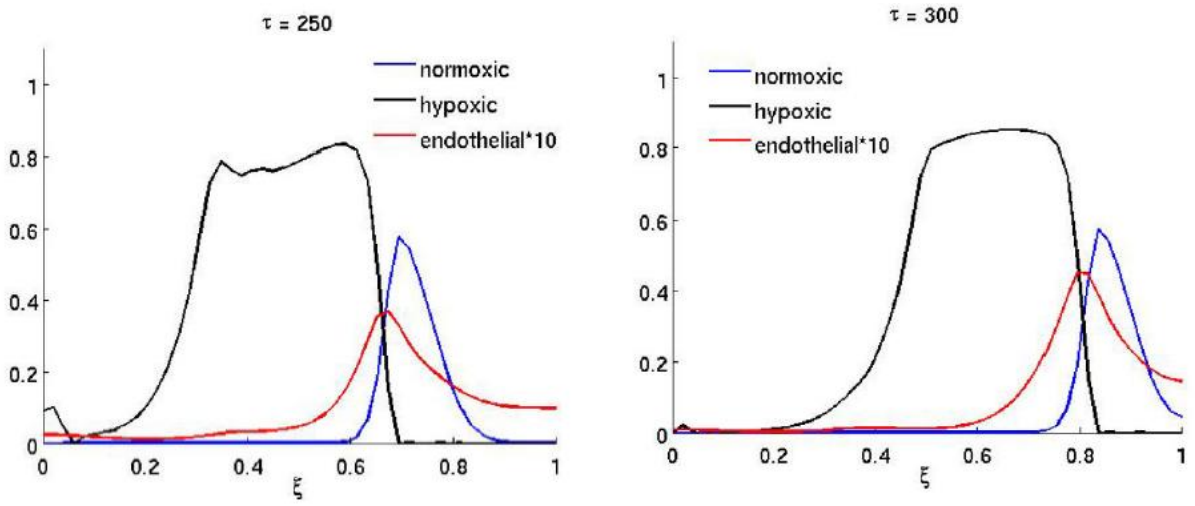

Fig. 32: Shows the result of the treatment if the anti-angiogenic drug only affects the endothelial cell chemotactic sensitivity χm (the duration of the treatment is as above). In this case the growth dynamics are quite similar to the baseline scenario, but on the other hand if only proliferation is affected the dynamics are similar to the full treatment. This suggests that inhibiting the proliferation of endothelial cells is the more important of the two effects the drug has.

A more complete model would include the pharmacokinetics and pharmacodynamics of the drug and also treat the effect of the drug on endothelial cells in more detail, but our approach serves as a first attempt at incorporating the effects of an anti-angiogenic drug into a detailed spatial model of tumor-host interaction.

4.34.3 Study 3: Solving the PIHNA model while accounting for radiotherapy

[RON12] Glioblastoma is the most aggressive type of glioma. During the last decades, several models have been proposed for simulating the growth procedure of glioma. One of the latest proposed models builds upon the proliferation – diffusion model by incorporating the angiogenic net rates and different concentration of cell populations (normoxic, hypoxic and necrotic). This proliferation- invasion- hypoxia- necrosisangiogenesis model (PIHNA) does not take into account radiotherapy. This work presents the mathematical foundation for solving PIHNA model in two dimensions with incorporated radiotherapy effect using the Linear Quadratic Model, which uses radiobiology parameters.

Row (a) of Fig. 33 presents the spatial concentration of normoxic, hypoxic and necrotic cells after 30 fictitious days of free glioma growth simulation. The computed graphs are depicted on a 40x40 grid (where L = 1cm and xo= (20,20)). The row (b) depicts the respective graphs for the second case on the 30th day, assuming that radiotherapy treatment was applied for 10 days after 20 days of free growth (by applying the parameters of the previous section)

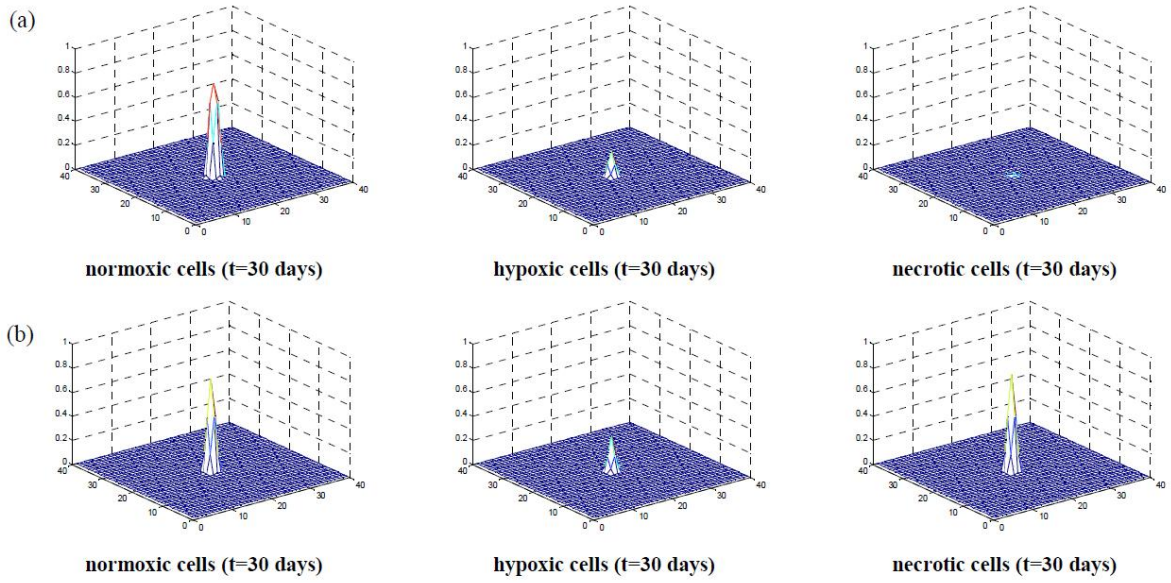

Fig. 33: The distribution of concentration for the three different populations of glioma cells (normoxic, hypoxic and necrotic cells) after applying the PIHNA model (a) and the PIHNA-LQ model (b). The graphs are extracted on the 30th day of simulation.

4.35 FORTH - Cell-level tumor invasion

Model description:
This mathematical model describes tumor growth invasion at cell-level linking genotypes with phenotypes and their interactions with the extracellular space. Specifically, cells are discrete entities that follow specific rules in response to their microenvironment and in accordance to their genotype-phenotype characteristics while the components of the extracellular space are treated as continuous variables.

4.35.1 Study 1: Hybrid Model for Tumor Spheroids with Intratumoral Oxygen Supply Heterogeneity

[TZE12] Tumor growth involves numerous biochemical and biophysical processes related to the invasion of surrounding tissue and metastasis. Such phenomena occur at different scales of time and space. The desire to understand the interactions of these complex processes has given rise to various computational models allowing for multiple variable modeling using continuous, discrete and the most recent hybrid approaches. This paper presents a hybrid mathematical model of solid tumor invasion that incorporates both continuous macro-scale and discrete cell-level descriptions. Cell-based description reflects individual cell movement and state, while the continuous part formulates the nutrient supply of the tumor. In the presented model, apart from the usage of homogenous oxygen supply, intratumoral nutrient sources are introduced.

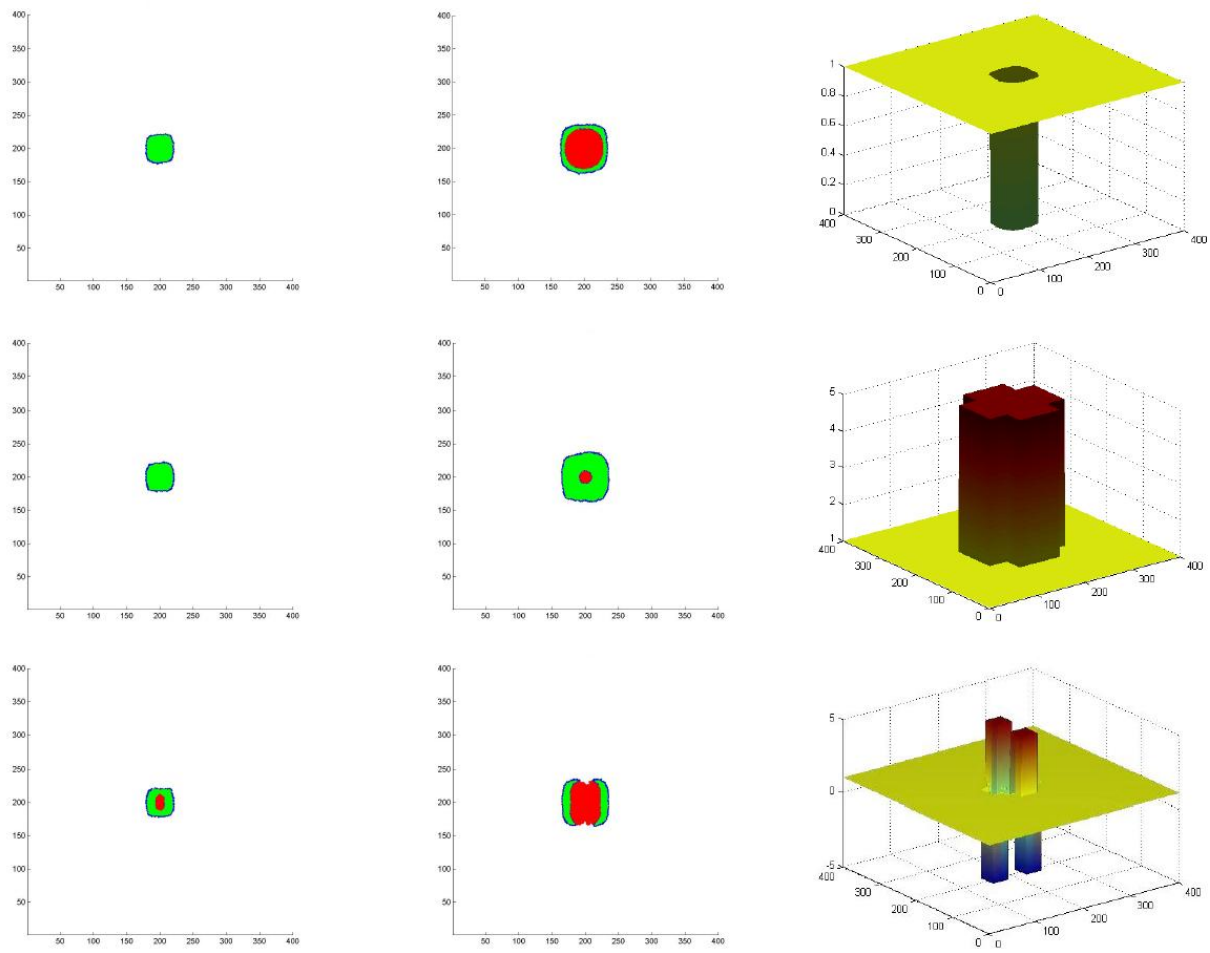

Fig. 34: Each row contains the results from the respective experiment: the first row contains the results from the first experiment, the second row from the second experiment and the third row from the third experiment. The first column depicts cancer cells after 15 iterations (5 fictious days). The central column illustrates cancer cells after 30 iterations (10 fictious days). Blue, green and red coloured cells indicate active living cells, quiescent living cells and dead cells, respectively. The third column represents the source/sink weights after 30 iterations.

4.36 UBERN - Brain Biomechanics

Model description:
Calculates strain/stresses in the brain tissues

4.37 UPENN - Bioinformatics analysis of somatic cancer mutations

Model description:
This model seeks to classify cancer mutations as driver or passenger using machine learning.

4.38 UPENN - Modeling signal

Model description:
Signal transduction in the signaling pathways will be studied using a set of coupled ode/pde equations. The code will be primarily written MATLAB with the information about the network provided using the SMBL framework.

4.39 UPENN - Modelling endocytosis

Model description:
It will be used phenomenological model based numerical modelling to understand the process of endocytosis in membranes. For this purpose it will be used a custom code based on Dynamically triangulated Monte carlo, written in Fortran and C++ .

4.40 ICCS - Molecular models formulated in General SBML

Model description:
The General Case of an SBML model

4.41 ICCS - Differentially Expressed Genes

Model description:
A Statistical Model that identifies the differentially expressed genes between two phenotypes (e.g. patient groups).

4.42 ICCS - Differentially Expressed Pathways

Model description:
A Statistical Model that identifies the differentially expressed pathways between two phenotypes (e.g patient groups).

4.43 ICCS - Phenotype Prediction Based on Gene Expression

4.44 ICCS - Drug Sensitivity Prediction based on Gene Expression

4.45 ICCS - A molecular pathway based model of the cell cycle [for the case of Acute Lymphoblastic Leukemia (ALL)]

Model description:
A kinetic Systems Biology oriented model that simulates the biochemical dynamics of the G1 phase of the cell cycle in precursor-B ALL cells.

4.45.1 Study 1: A systems biology dynamical model of mammalian G1 cell cycle progression

[HAB07] The current dogma of G1 cell-cycle progression relies on growth factor-induced increase of cyclin D:Cdk4/6 complex activity to partially inactivate pRb by phosphorylation and to sequester p27Kip1- triggering activation of cyclin E:Cdk2 complexes that further inactivate pRb. pRb oscillates between an active, hypophosphorylated form associated with E2F transcription factors in early G1 phase and an inactive, hyperphosphorylated form in late G1, S and G2/M phases. However, under constant growth factor stimulation, cells show constitutively active cyclin D:Cdk4/6 throughout the cell cycle and thereby exclude cyclin D:Cdk4/6 inactivation of pRb. To address this paradox, we developed a mathematical model of G1 progression using physiological expression and activity profiles from synchronized cells exposed to constant growth factors and included a metabolically responsive, activating modifier of cyclin E:Cdk2. Our mathematical model accurately simulates G1 progression, recapitulates observations from targeted gene deletion studies and serves as a foundation for development of therapeutics targeting G1 cell-cycle progression.

Fig. 35: Dynamical model of the mammalian G1 cell-cycle progression. (A) The mathematical model is represented in the DCL. Cdks and pRb are boxes, with circles inside denoting possible states. As an example we show the various Cdk2 states as vectors of integers (box read in the order of top to bottom and left to right). Proteins with a single internal state are represented by ovals. Transitions between states are represented by filled circles for binding and unbinding, and by squiggles that can also denote degradation of bound components or conformational change. The diagram describes Cdk4 and Cdk2 binding to p27. Cdk2 binds cyclin E or A, Cdk1 binds cyclin A and Cdk2/1 can undergo a conformational change by the activating 'modifier'. pRb is hypo- to hyperphosphorylated by active forms of Cdk4 (light green) and Cdk2/Cdk1 complexes, respectively (dark green). Hyperphosphorylated pRb unbinds E2F; E2F promotes the synthesis of cyclin E, A, Emi and itself. Cyclin A is degraded by APC/C when not bound to Emi. (B–E) Simulations (solid lines) of the model fit to data from six representative parameter sets that meet the deletion criteria (dots with error bars). Time zero refers to the synchronized entry of the cells into early G1. (B) Active Cdk2, total p27 and total cyclin E. (C) hyperphosphorylated E2F and pRb and (D) total Emi and total cyclin A. (E) In silico prediction of Cdk2/1 inhibition: hyperphosphorylated pRb at 16 h with respect to Cdk2/1 inhibition, normalized to control (0% inhibition) for the population of six models that best fit the data and meet the deletion criteria.

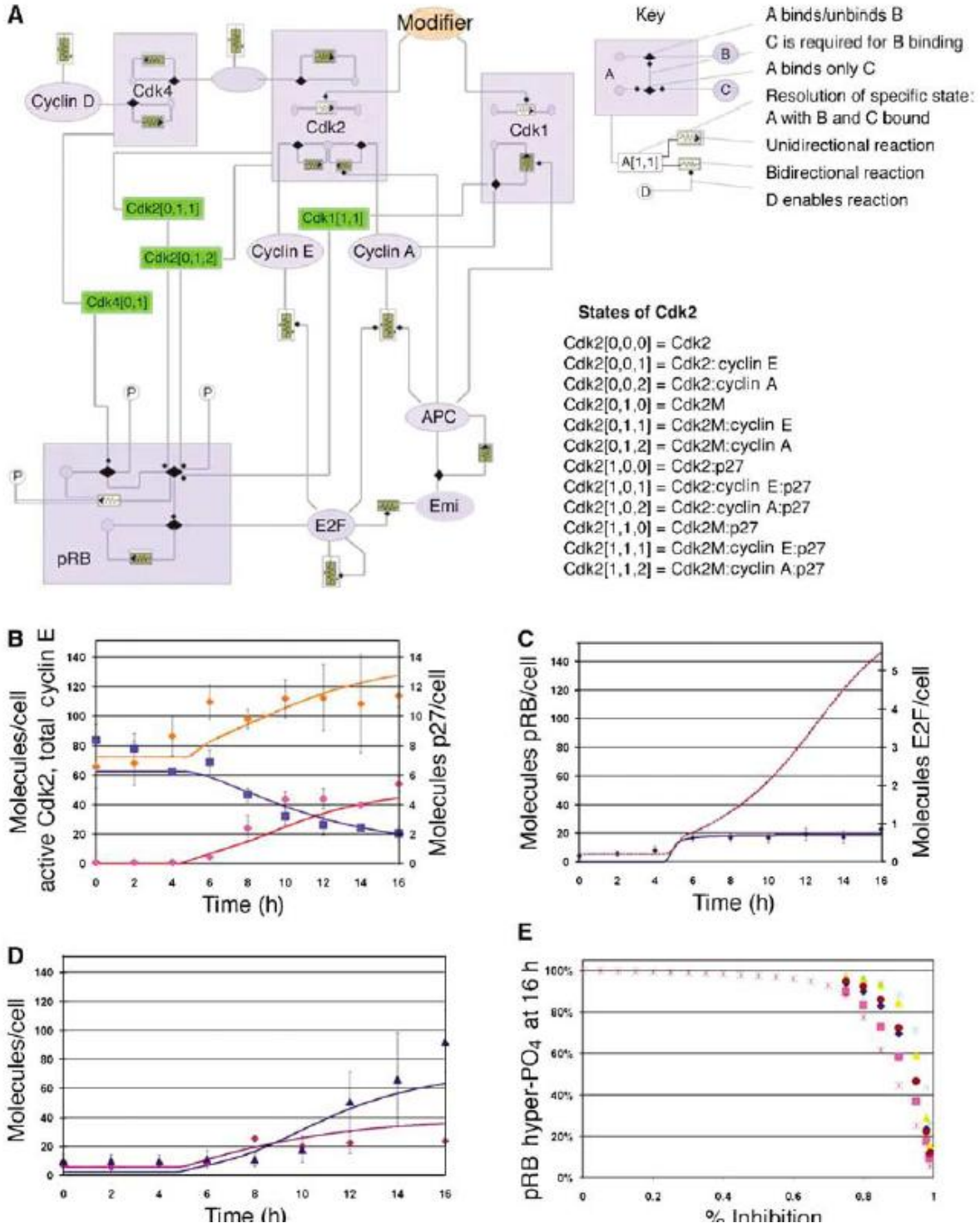

4.46 ICCS - (code developer) Radiation cell killing

Model description:
The models aims at estimating the cell killing by irradiation based on the Linear Quadratic or LQ Model.

4.47 ICCS - Epirubicin pharmacodynamics

Model description:
The model simulates epirubicin pharmacodynamics assuming an exponential law.

4.47.1 Study 1: An advanced discrete state–discrete event multiscale simulation model of the response of a solid tumor to chemotherapy: Mimicking a clinical study

This study has been referred in 4.7.1 chapter

4.47.2 Study 2: Translating Multiscale Cancer Models into Clinical Trials: Simulating Breast Cancer Tumor Dynamics within the Framework of the "Trial of Principle" Clinical Trial and the ACGT Project.

[KOL08] The potential of cancer multilevel modeling has been particularly emphasized over the past years. Integration of multiscale experimental and clinical information pertaining to cancer via advanced computer models seems to considerably accelerate optimization of cancer treatment in the patient individualized context. However, a sine qua non prerequisite for such models to reach clinical practice is to be thoroughly tested through clinical trials for validation and optimization purposes. This is one of the major goals of the European Commission funded "Advancing Clinico-Genomic Trials on Cancer" (ACGT) project. This paper presents a discrete state based, four dimensional, multiscale tumor dynamics model that has been specially developed by the In Silico Oncology Group in order to mimick the Trial Of Principle (TOP) clinical trial concerning breast cancer treated with epirubicin. The TOP trial constitutes one of the ACGT clinical trials. A substantial part of the model can address other tumor types as well. The actual pseudoanonymized imaging, histopathological, molecular and clinical data of the patient are exploited. Special emphasis is put on the effect of cancer stem/clonogenic, progenitor, differentiated and dead cells, the cell category transition rates and the cell category relative populations within the tumor from the treatment baseline onwards. The importance of adaptation of the cell category relative populations to the cell category transition rates for free tumor growth is revealed and the concept of a pertinent nomogram is introduced. A method which ensures adaptation of these two sets of entities at the beginning of the simulation execution is proposed and subsequently successfully applied. Convergence and code checking issues are addressed. Indicative parametric/sensitivity studies are presented along with specific numerical findings. The model's behavior substantiates its potential to serve as the basis of a treatment optimization system following an eventually succesful completion of the clinical validation and optimization process.

Fig. 36 shows the number of total cells as well as the number of stem and limp cells (both proliferating and dormant). In the case of treatment (therapy) these populations include both surviving cells and cells affected by the drug (and therefore destined to die) but not yet dead.

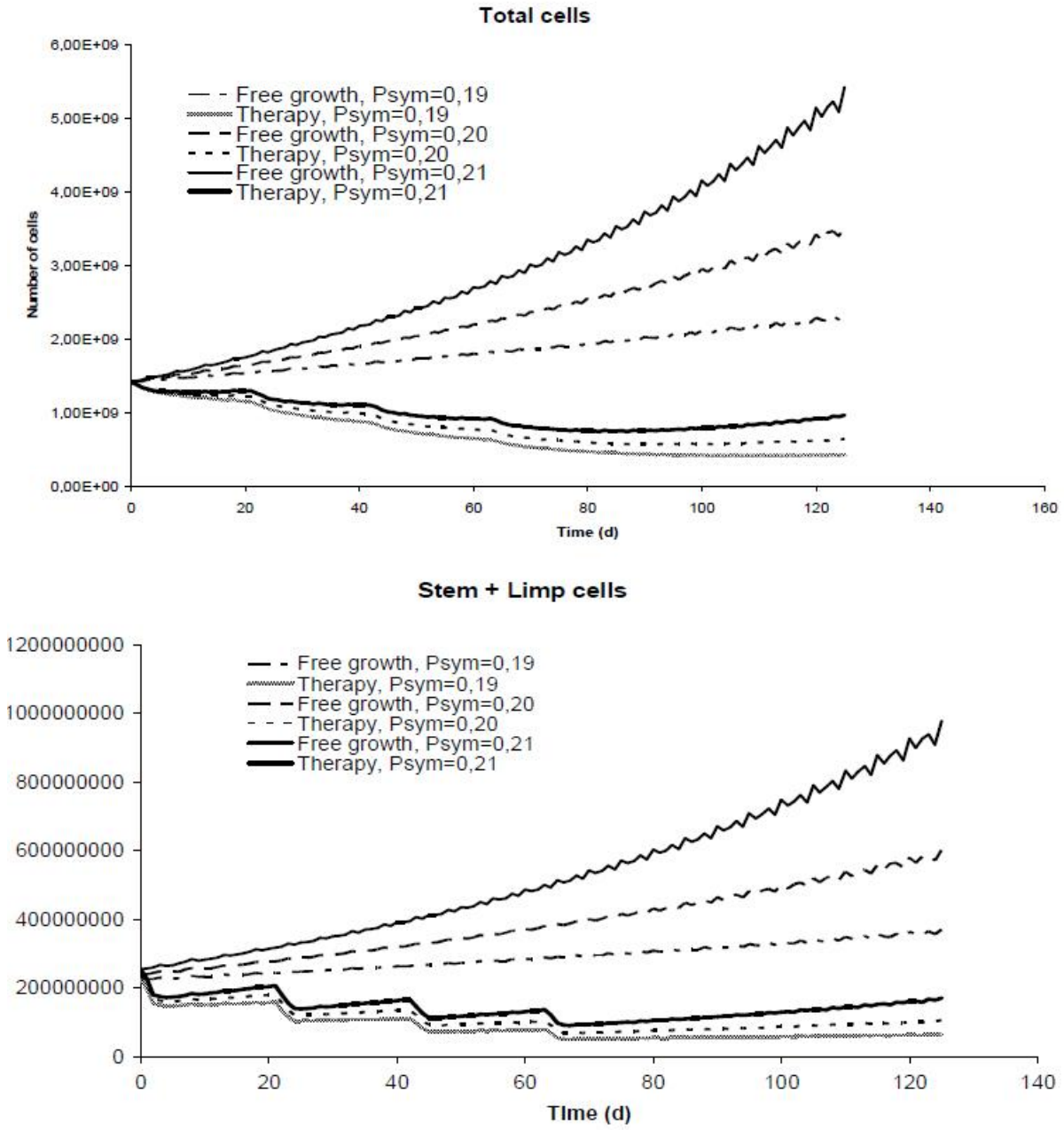

Fig. 36: Number of total tumor cells (Upper Panel) and number of stem and limp (both proliferating and dormant) tumor cells (Lower Panel) as a function of time for the following values of symmetric division fraction Psym: 0.19, 0.20 and 0.21. A homogeneous spherical tumor of diameter equal to 14 mm is considered. Free growth and response to therapy are simulated. Epirubicin is administrated according to the fractionation scheme. The dose of each fraction is 100mg/m2.

4.48 ICCS - Prednisolone PK parameters regression model

Model description:

A regression model that describes the relationship between un-bound Prednisolone PK parameters and patient covariates.

4.49 ICCS - Oral Prednisone PK model

Model description:
A model that simulates the Pharmacokinetics of orally administrated Prednisone.

4.49.1 Study 1: Towards Patient Personalization of an Acute Lymphoblastic Leukemia Model during the Oral Administration of Prednisone in Children: Initiating the ALL Oncosimulator

[OUZ12] In the present study, methods aiming at supporting the personalization of an Acute Lymphoblastic Leukemia (ALL) Model (ALL Oncosimulator), already in development by the In Silico Oncology Group, National Technical University of Athens, are provided. Specifically, a population pharmacokinetic model for orally administered prednisone in children with ALL is developed, and the ability of classification algorithms to predict the prednisone response using gene expression data is studied.

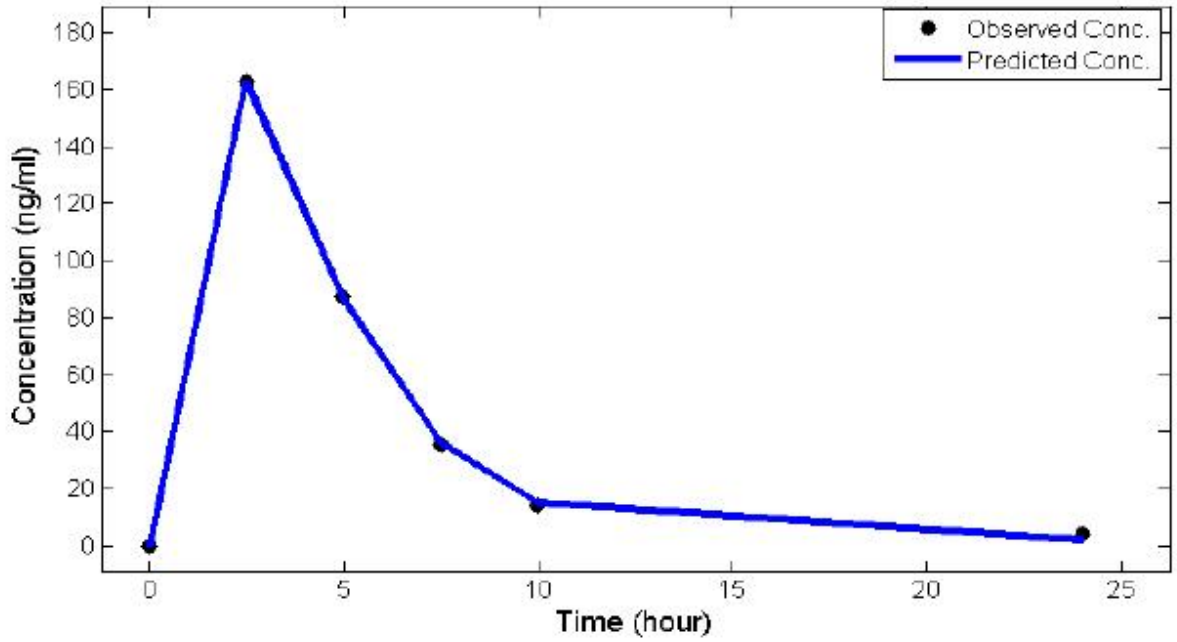

Fig. 37: The results of the proposed pharmacokinetic model simulation after the parameter estimation procedure. The solid black circles refer to the measurements and the blue line refers to the predicted concentrations of the drug in the Central Compartment.

5 Brain tumour image analysis

5.1 Glioma diagnosis

Image analysis for the glioma application has been subdivided into two separate parts: Registration and segmentation. While registration deals with the alignment of several brain images in a common frame of reference in order to be able to jointly process and evaluate these images, segmentation partitions one image into multiple segments of similar properties. These segments should be meaningful for further analysis. Both, registration and segmentation are important parts of image analysis within the CHIC project and play a significant role when comparing treatment outcome on patient images with simulated data.

A glioma is a type of cancer that starts in the brain or spine and arises from glial cells. The most common site of gliomas is the brain. Gliomas are mainly classified by cell type or by grade.

Gliomas according to cell type can be 1) ependymomas, 2) astrocytomas, 3) oligodendrogliomas and 4) mixed gliomas. Continuing, gliomas according to World Health Organization (WHO) grading system can be WHO-1, WHO-2, WHO-3 and WHO-4. The higher the grade, the more aggressive the tumour.

High-grade gliomas are highly-vascular tumours and have a tendency to infiltrate and invade into adjacent tissue. They have extensive areas of necrosis and hypoxia. Often tumour growth causes a breakdown of the blood-brain barrier in the vicinity of the tumour. As a rule, high-grade gliomas almost always recur even after complete surgical excision. On the other hand, low-grade gliomas grow slowly, often over many years, and can be followed without treatment unless causing clinical symptoms.

The diagnosis of gliomas can be done by MRI, CT, angiogram or biopsy, with MRI being the most common non-invasive method. When a high-grade glioma is diagnosed, immediate treatment is necessary because it exhibits a very aggressive and invasive behavior.

The most common problem with diagnosis and treatment of gliomas is this invasive behaviour. Generally, there are cells diffused within a large area, without being visualized in the MRI images. As you can see in the example of Fig. 38 (left), there are glioma cells that are diffused within the brain, these cells are beyond the main tumour mass and cannot be visualised by the commonly imaging techniques, as the example of Fig. 38 (right) indicates.
This can be more clearly understood by studying radiotherapy results in gliomas: Even if the clinician treats 2cm beyond the imaged bulk tumour, Glioblastoma Multiforme (GBM), is very possible to recur.

Different modalities of imaging techniques (e.g. T1 MRI, T2 MRI, Flair MRI, CT, PET etc) are required when diagnosing gliomas. Even so, it is very difficult for a radiologist to define the exact margins of bulk tumour. A real example indicating the major problem of defining the exact margins of a glioma by clinicians is given in Fig. 38. Even with 4 different modalities (T1, T1 enhanced, T2, T2 flair), glioma boundaries are not easily discernible and within each boundary different pathophysiological information is contained. The clinician and the modeller need to get these multi-modal boundaries in order to gather information concerning the individual tumour properties.

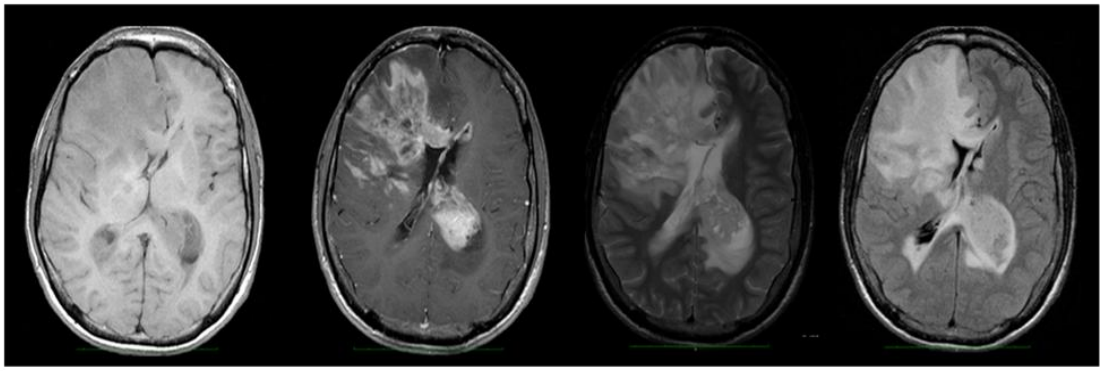

Fig. 38: Different modalities taken with different MRI techniques. From left to right: T1, T1-enhanced, T2, T2 flair.

Magnetic resonance images (MRI) of the brain are acquired using different protocols, e.g. T1 weighted images, T1 weighted images with contrast enhancement of the active tumour region and T2 weighted images. In order to be able to make use of the acquired images, different regions in the images have to be delineated. The regions of interest usually correspond to the different tissue types, which are present in the brain. In healthy brains these tissues are white matter (WM), grey matter (GM) and cerebrospinal fluid (CSF). In pathologic images, there also exists the tumour region with its different subregions. The tumour subregions include the active tumour part exerting mass effect on the surrounding tissues, the necrotic part and the infiltrative and edema part.

The aim is to segment these different parts of healthy and pathologic tissues using (semi-) automatic methods. Segmentation of the different tumour regions is most important for comparing the patient data to a cellular simulator, while segmentation of the different brain tissues is required for the biomechanical simulations.

The tumour regions can be manually segmented on each image slice with reasonable effort. However, manual segmentation of the brain tissues (WM, GM, CSF) in a 3D image is an extremely tedious and time-consuming task. Therefore, we decided to tackle the problem of brain tissue segmentation in tumour-bearing MRI images first.

All the CHIC partners involved in glioma cancer prediction and prognosis using MRI-based bio-markers will be part of the target group.

5.2 Brain Tissue Segmentation

Numerous segmentation methods have been proposed for the clustering of pixels in brain images, following either supervised or unsupervised approaches. Supervised classification requires input from the user, typically a set of pixel class samples. In order to classify CSF, GM, WM and brain lesions k-NN classifiers have been employed, followed by a connected components filtering algorithm for result refinement [CAR13]. Other classifiers that have been used for brain tissue classification include discriminative Random Decision Forest [YI09] classification and Kohonen neural networks [AGU10].

On the other hand, unsupervised approaches often rely on a Gaussian approximation of the pixel intensity distribution for each tissue type [DUG04]. An additional unsupervised method was proposed, which models neighbouring pixels interactions using a Markov-Random field (MRF) statistical model [VAN99].

An alternative to statistical parametric approaches is the use of unsupervised, nonparametric schemes. One such approach is the Mean-shift algorithm [COM02], which uses adaptive gradient ascent in order to detect local maxima of data density in feature space.

5.3 Unified healthy and pathological tissue segmentation via hierarchical classification

The aim of segmentation is to partition a medical image consisting of different gray level values into distinct, anatomically or physiologically meaningful regions. In the literature, there exist many different approaches for this purpose, ranging from statistical to geometrical approaches.

Brain tumors exhibit several subregions like necrotic and active tumor region, as well as edema region. These different subregions can only be distinguished if several MRI modalities are considered simultaneously. In the case of the images available from the database, we have the T1-weighted image (T1), the T1-weighted image with contrast enhancement (T1c), the T2-weighted image (T2) and the T2-flair weighted image (T2f) available. One slice showing the 4 modalities for one patient from the database is depicted in Fig. 39. From left to right the T1, T1c, T2 and T2f image are shown. In order to take advantage of the full data, all four modalities have to be fused for further processing. The easiest way to take the information from all four modalities into account at the same time is by using classification methods. Therefore, the partner at University of Bern developed a machine-learning based classification approach for brain segmentation, which is extended and refined for the case of 3D medical gray level images. The method is outlined in more detail in the following.

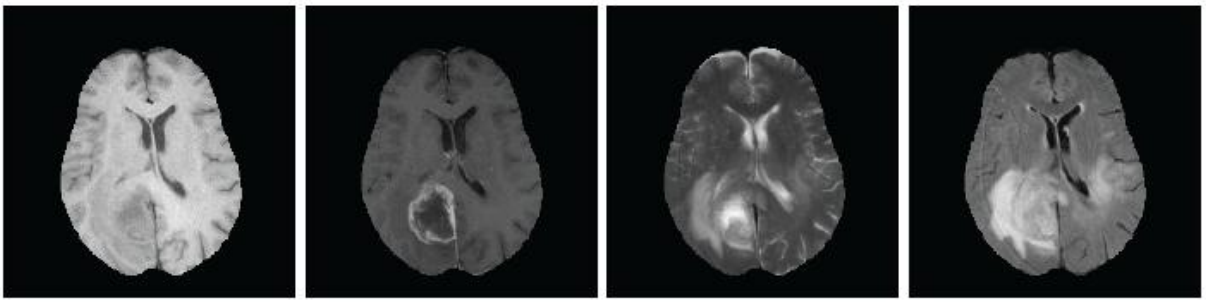

Fig. 39: Axial slice of four MRI modalities of one patient. From left to right: T1, T1c, T2, T2flair

In a first step, it is beneficial to strip the skull from all the images because this allows for more accurate results in the following classification step. Skull-stripping is performed using in-house developed methods. Subsequently, the images from all four modalities have to be aligned in a common frame of reference. For this purpose we make use of the registration method. Noise is removed from all images with the help of an anisotropic diffusion filter [PER90]. This filter allows for edge-preserving smoothing because the smoothing term is adapted to the local contrast of the image. Once this is done, we correct for the bias-field using established methods [SLE98]. Gray levels obtained from the MR images should be as similar as possible across different patients in order to allow for meaningful comparisons. However, as MRI is not a quantitative imaging technique, additional measures have to be taken in order to achieve this. Therefore, we rescale the gray level values in all images to a meaningful range first and then apply histogram matching for each modality separately.

After preprocessing, the segmentation task can be tackled. Segmentation is done using a soft-margin SVM classifier [SCH02]. SVMs are discriminative classifiers, originating from

machine learning. They require a training step to find a separating hyperplane for the data in the feature space. SVMs solve the optimization problem

$$\min_{w,b,\xi} \frac{1}{2} w^T w + C \sum_{i=1}^{l} \xi_i$$
$$\text{Subject to } y_i (w^T \Phi(x_i) + b) \geq 1 - \xi_i \text{ with } \xi_i \geq 0 \quad (9)$$

where (x_i, y_i) are the instance-label pairs of the dataset and w is the normal vector of the separating hyperplane. C is a penalty parameter for the error term and b is the offset of the hyperplane. Slack variables ξ are used for soft-margin classification. The appealing property of SVMs is that they offer the possibility to use a kernel function $K(x_i, x_j) = \Phi(x_i)^T \Phi(x_i)$ for transforming the data into a higher-dimensional feature space, where the data can be linearly separated efficiently with a maximum margin. Slack variables x_i are used for soft-margin classification. Parameter selection for the SVM classifier is done using grid-based cross-validation on the training data. In order to extend the inherently binary SVM classifier to a multiclass problem, we use a one-against-one voting strategy.
Features for the SVM classifier are extracted from the multispectral imaging data. The most prominent features for distinguishing pathologic and healthy tissues, as well as all their subregions, are the image intensities in the different modalities. Additionally, we use the first order texture features according to [TUC98] because they can be computed fast and easily. This yields a 28-dimensional feature vector x, which consists of the voxel-wise concatenation of the multimodal intensities I and multimodal textures T at each voxel i, as shown in the following equation.

$$x(i) = \left[I_{T1}(i), I_{T1c}(i), I_{T2}(i), I_{T2f}(i), T_{T1}(i), T_{T1c}(i), T_{T2}(i), T_{T2f}(i) \right] \quad (10)$$

Although being quite powerful, SVMs have the drawback of treating each image voxel separately as iid random variables. This assumption is obviously not correct for images, where neighboring voxels tend to be strongly correlated. We account for that by applying a retrospective regularization on the label result. Regularization is performed using a Markov Random Field (MRF), which takes the neighbor relationships of each voxel into account. Markov Random Fields offer the possibility to formulate the regularization as an energy minimization problem. To this end we use a second-order MRF with two energy terms.

$$E = \sum_i V(y_i) + \sum_{ij} w(y_i, y_j) D_{pq} \quad (11)$$

The first term denotes the data energy, which is only dependent on the data at the current point, whereas the second term constitutes the smoothness energy, which takes the neighborhood information into account. The data potentials can be calculated directly from the output produced by the SVM classifier. The smoothness energy is computed depending on the labels of neighboring voxels.

After the first coarse classification into tumor and healthy tissues, a strong regularization is employed. In a second stage, regularization is applied on the image that has been subclassified into the different tumor and healthy subregions.

Optimizing MRFs is a challenging and time-consuming task, especially when many voxels and multiple labels are involved. Most optimization algorithms for MRFs like Iterative Conditional Modes (ICM) yield only approximate solutions and can be trapped in local minima. Speed is another important issue for large multilabel problems. In order to deal with these difficulties, we employ a recent optimization algorithm, which is based on graph-cuts.
The developed algorithm is tailored to standard clinical acquisition protocols, which exhibit high intra-slice resolution coupled with large inter-slice spacing. Additionally to the tumor and its subregions, the algorithm also yields the segmentation of the healthy tissues into gray matter, white matter and cerebrospinal fluid.

Fig. 40 shows one slice of a patient image from the available database when interpatient classification is applied. The first row shows a coarse segmentation into tumor and healthy regions, while the second row depicts the final fine segmentation result. The manually defined ground truth is shown in the left column, the middle column shows the result with regularization and the right column shows the result without regularization.

Quantitative analysis of the algorithm has been carried out on 10 datasets from the available database using intrapatient classification as well as interpatient classification with leave-one-out cross-validation. The Dice similarity coefficients (the Dice similarity coefficient measures the mean overlap with the ground truth, values of 0 indicate no overlap, 1 indicates perfect overlap.), show good overlap for the gross tumor volume, including all pathologic tissue regions, while the task of subdividing the tumor regions appears to be more challenging.

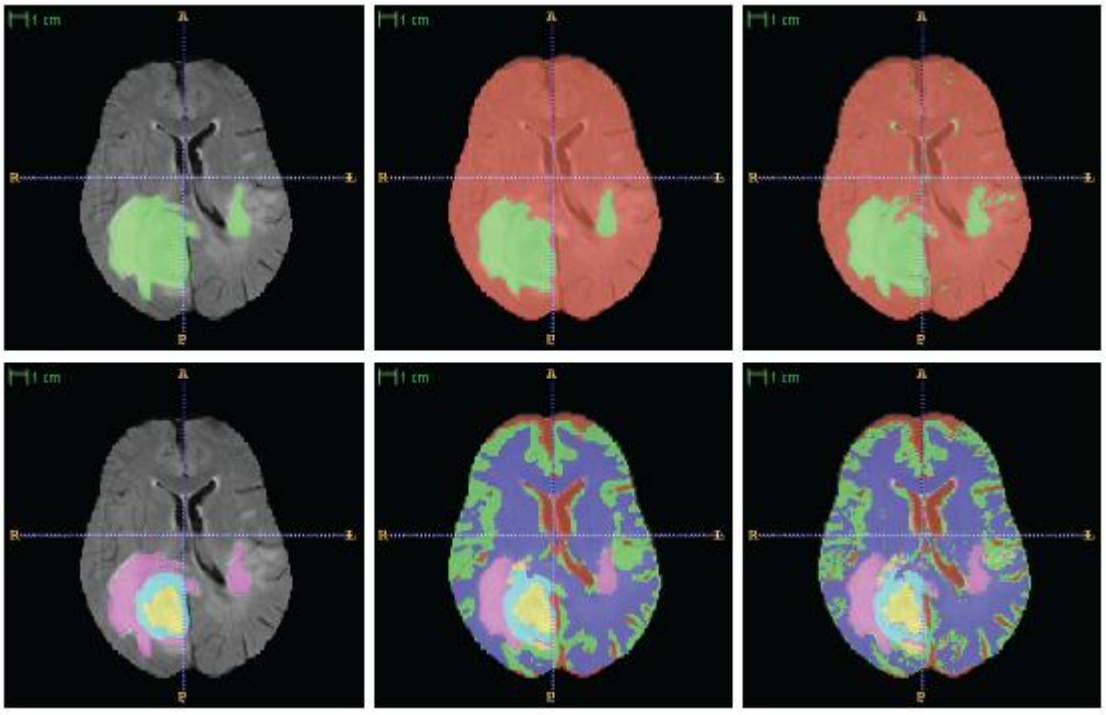

Fig. 40: Classification result for one patient from the ContraCancrum database. Upper row: coarse classification, lower row: fine classification including tumor and healthy tissue subregions

In general, all CHIC partners involved in assessment of glioma to teraphy and/or reocurrence prediction and using multimodal volumetric information from MRI data will be targeted in these requirements.

6 Magnetic Resonance Imaging (MRI)

The ability of Magnetic Resonance Imaging (MRI), when combined with registration and segmentation techniques, to identify and demonstrate tumor morphology and the relationships of malignant lesions to neighbouring structures provides relevant clinical information for clinical management and surgical planning. The last years, sequential sets of magnetic resonance images and the development of small molecular weight paramagnetic contrast agents have a major impact in the assessment and monitoring of tumor treatment response.

Dynamic contrast-enhanced magnetic resonance imaging (DCE-MRI), which relies on fast MRI sequences obtained before, during and after the intravenous administration of a gadolinium (Gd) based contrast agent has been widely used in the study of tumor angiogenesis, a process where neovascularization is developed within a tumor. DCE-MRI is able to quantify the leakage of the contrast agent, from the neovascularization into the tissue, by quantitative analysis of the DCE-MRI data through the use of pharmacokinetic models. These models provide independent indices of angiogenic activity, and therefore act as prognostic indicators in a broad range of tumor types. A number of physiological parameters of vascularity (volume transfer constant between tumor and vessels, also named as ktrans, and extravascular extracellular volume fraction ve) coming from the pharmacokinetic models play an important role in quantitatively assessing tumor vascularity within a region, where neo-vascularity/leaky vessels are associated with higher ktrans values, while response to therapy has been correlated with a drop in ktrans values between imaging sessions 0.

Several pharmacokinetic (PK) models can be used while the most reliable are Tofts [ESS12] and Patlak [TOF91] 0(briefly discussed in the following chapters). Finally, several studies have been conducted and compare the results from different pharmacokinetic models using specific clinical trial(s?) ([PAT83], [HAR04], [DON10], [BAR08], [SAM06], [TOF97], [SOU11])

Diffusion imaging is based on the self-diffusion of water molecules in the tissue. There are several indexes that can quantify diffusion such as ADC (Apparent Diffusion Coefficient), DTI (Diffusion Tensor Imaging) and FA (fractional Anisotropy) where each of them describes a different mechanism. The general procedure to acquire the data is to change the so called ‘b-value’ a quantity that depends on the strength of the gradients (G), the duration of the gradients (Δ) and the amount of time passing between the gradients (δ). Changing the b-value the contrast of the DW image is a function of the apparent diffusion coefficient (D) which can be estimated with acknowledgment of two or more measurements on different b-values.

One application of Diffusion Imaging is the tumor characterization. In tumor areas the diffusion is lower than the healthy tissue and this can be used in the delineation of tumor margins. Also a marker to assess tumor response to therapy is to observe changes in the diffusivity pattern of a tumor (see Fig. 41). Finally, there is a lot of discussion whether DW Imaging can evaluate tumor grade with enough specificity so as to be useful as a clinical context.

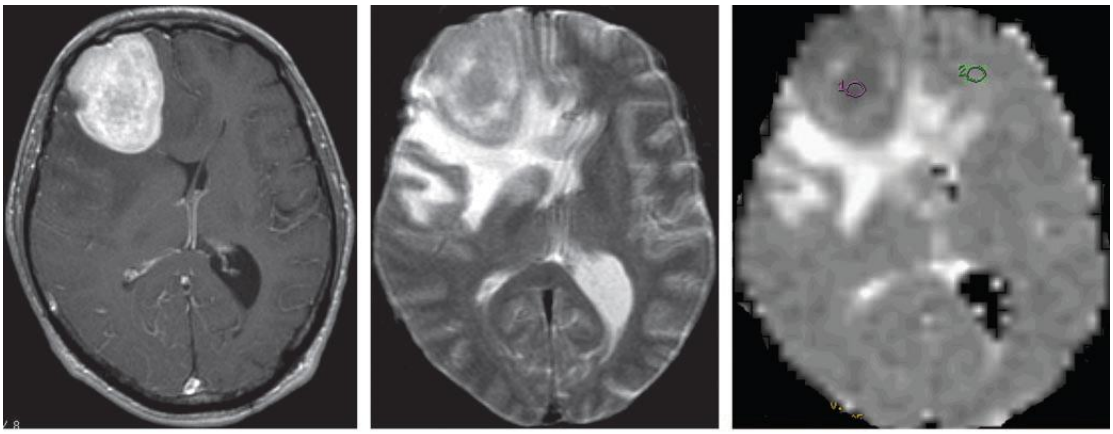

Fig. 41: Low mean ADDC representing metastasis from primary lesion outside the central nervous system in a 62- year old man with large B-lymphoma. (a) Transverse contrast-enhanced T1-weighted MR image shows large right frontal lobe enhancing lesion with mass effect. (b) Transverse T2-weighted MR image shows signal intensity of central portion of mass is only slightly higher than that of gray matter, suggesting high cell density. (c) Transverse ADC map shows mass has lower signal intensity than normal tissue. Mean ADC in the mass region of interest (1) was 65% of that of normal tissue [PRO06].

6.1 Data requirements

DCE-MRI analysis follows a pipeline procedure where several imaging parameters, high temporal and spatial resolution data are required. Typical sequences and requirements in case of using T1 weighted images in DCE-MRI analysis are given in the table below.

	T1-Weighted (DCE)
Sequence	SPGR/MP RAGE/FLASH/FFE (Typically 3D)
Temporal resolution	~3–6 s
Total acquisition time	3–5 min
Spatial resolution	1-mm in-plane × 5-mm slices
Geometric artifact	Low impact
Model parameters	k^{trans}, v_p, v_e, IAUC

Fig. 42: Table 1 Typical sequences used and minor practical requirements [ESS12]

A general scheme for the acquisition protocol is available using dynamic MRI series prior, during and after the injection of a contrast agent, which can be given either in DICOM or any other medical imaging format (i.e. ANALYZE, NIFTI, etc.). In case of having DICOM format, parameters required in the pharmacokinetic models such as the repetition time (TR), flip angles (FA), and the acquisition time for each MRI slice, are retrieved directly from the DICOM file header (DICOM Tags). On the other hand, when alternative medical imaging formats are available for analysis, this piece of information is rarely included in the header of the imaging data and needs to be given additionally.

In order to apply pharmacokinetic models of contrast distribution to imaging-based data the first essential step is to use the signal changes observed in the dynamic acquisition to calculate quantitative parametric images of contrast concentration at each time point. Since the relationship between signal intensity and contrast concentration may be non-linear this

adds an additional complication and often requires the measurement of the pre-contrast T1 values for each of the voxels to be studied. In the case 3D MRI data volumes on different flip angles prior the contrast agent (CA) administration are (2 to 7 different angles in the range 5^o to 60^o) are important.

DCE-MRI analysis is based on measurements taken from a specific region of interest (ROI) in the 3D MRI. This region can be either taken by user-defined annotations or by automated techniques (segmentation of the malignant region). Moreover, the conversion of the signal intensities of the MRI to contrast agent concentration requires the identification of an appropriate large blood vessel. This allows the measurement of the contrast concentration changes in the plasma over time, which is commonly referred to as the arterial input function (AIF).

Finally, optional clinical information has to be given by the hematocrit level of the patient (default value is 0.45) and the type of the contrast agent (CA) that is used.

6.2 The Implementation

The circulatory system consists of capillary vessels like arterioles and venules. These transfer pipes are permeable to some substances that exist in the blood, while the bigger vessels are not permeable, in order to deliver nutrients to different tissues of the body and pick up the metabolites produced by these tissues. The permeability is due to the several pores that are present on these pipes. However, in tumors there are several of these pores also in bigger vessels. DCE-MRI is able to quantify the permeability of the vessels by the measurement of ktrans, which is the transfer constant (sec-1) between blood plasma and extravascular extracellular space (EES) and indicates the volume of blood which flows out of the vessels, ue which is the volume of EES per unit volume of tissue and indicates the volume of blood which flows out of the vessels, and kep which is the rate constant between EES and blood plasma (sec-1). These three parameters are related by the expression:

$$k_{ep} = \frac{k_{trans}}{u_e} \qquad (12)$$

In general, ktrans is representative of the steepness of the slope and ve is correlated with the level of plateau. In Fig. 43, two different curves are shown from the analysis in DCE-MRI data. The first curve corresponds to a vessel with high permeability and the steep slope followed by the plateau is obvious, which means fast extravasation of the contrast agent and rapid accumulation in the tissue. The second curve is representative of a vessel with low permeability. Notice the constant and smoother curve almost without plateau that corresponds to a slow but constant extravasation of the contrast agent.

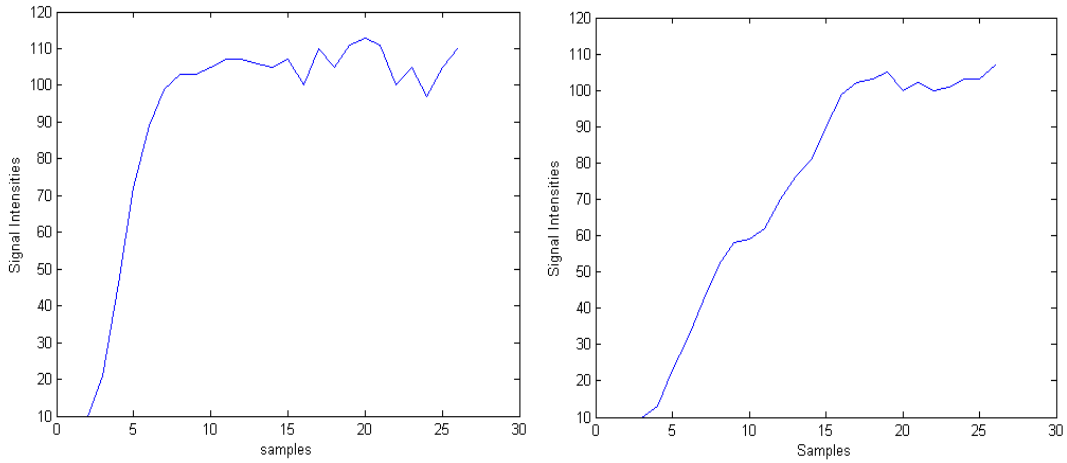

Fig. 43: Signal intensities for two different pixels. The first graph represents the SI for a pixel with high ktrans while the second represents the SI for a pixel with low ktrans

Tissue physiological parameters (ktrans, ue) are often used for treatment response combined with other parameters such as Apparent Diffusion Coefficient (ADC), Cerebral Blood Flow (CBF), Cerebral Blood Volume (CBV) and Fractal Dimension (FD). There are several studies that combine different imaging biomarkers to assess response to therapy after the administration of different agents ([BAR08], [LIT10], [HAH08], [YAN07], [ADR07]).
Tofts et al. [TOF91] assumed that when the contrast agent is injected into the blood stream and is able to pass across the blood vessel endothelium, it will move to the tissue's extracellular space at a rate that is proportional to the difference in concentration between the plasma and the tissue:

$$\frac{dC_t}{dt} = k^{trans}\left(C_p - \frac{C_t}{u_e}\right) \qquad (13)$$

where Ct is the concentration in the tissue and Cp is the concentration in the plasma (AIF) (see Fig.).

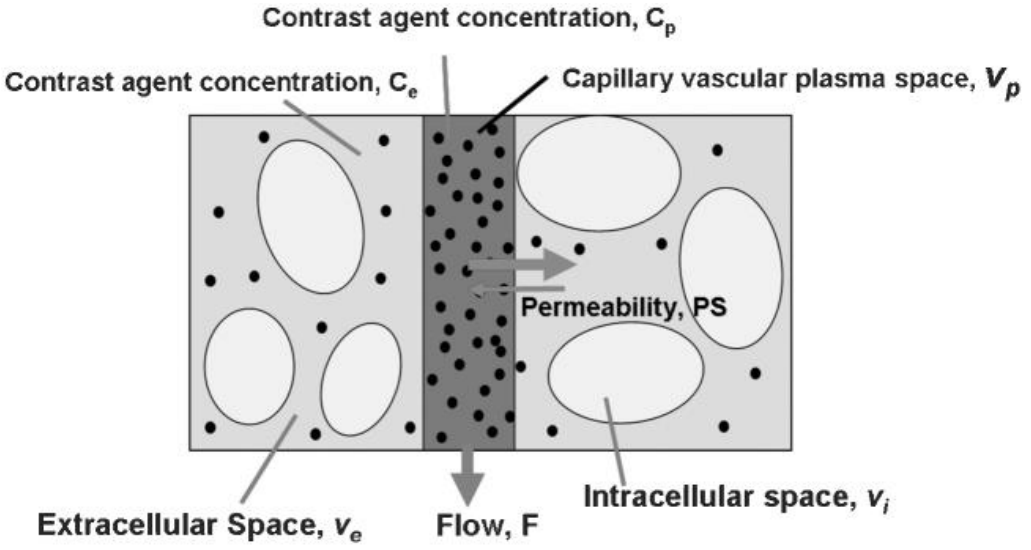

Fig. 44: Graphical representation of the contrast distribution occurring within an individual voxel of tissue. Contrast Agent passes from the blood into the interstitial tissues and the figure shows the standard mathematical abbreviations used to describe each of the individual tissue spaces.

The solution of Eq. [13] is:

$$C_t(t) = C_p * (k^{trans} \cdot e^{-t \cdot k^{trans}/u_e}) = k^{trans} \int_0^t C_p(t') \cdot e^{-k^{trans}/u_e \cdot (t-t')} dt' \qquad (14)$$

and with knowledge of Ct (from converting signal intensities (SI) of DCE-MRI data to concentration) and Cp (measurement of AIF either from data or assuming a theoretical value) we can perform a parameter estimation algorithm to Eq. [TOF91] and fit the ktrans, ue values. A major issue in the topic is whether the arterial input function (AIF) should be determined from the MRI data ([HAN12], [HAN96], [RAG10], [YAN07]) or considered theoretically [SOU12]. There is also a lot of discussion whether SI should be converted to CGD. Several studies have shown that the CA concentration is not linearly dependent on DCE-MRI data ([HAN96], [WEI84], [TWE91], [LI00]). Fig represents the measurement of the AIF from an artery and the corresponding concentration.

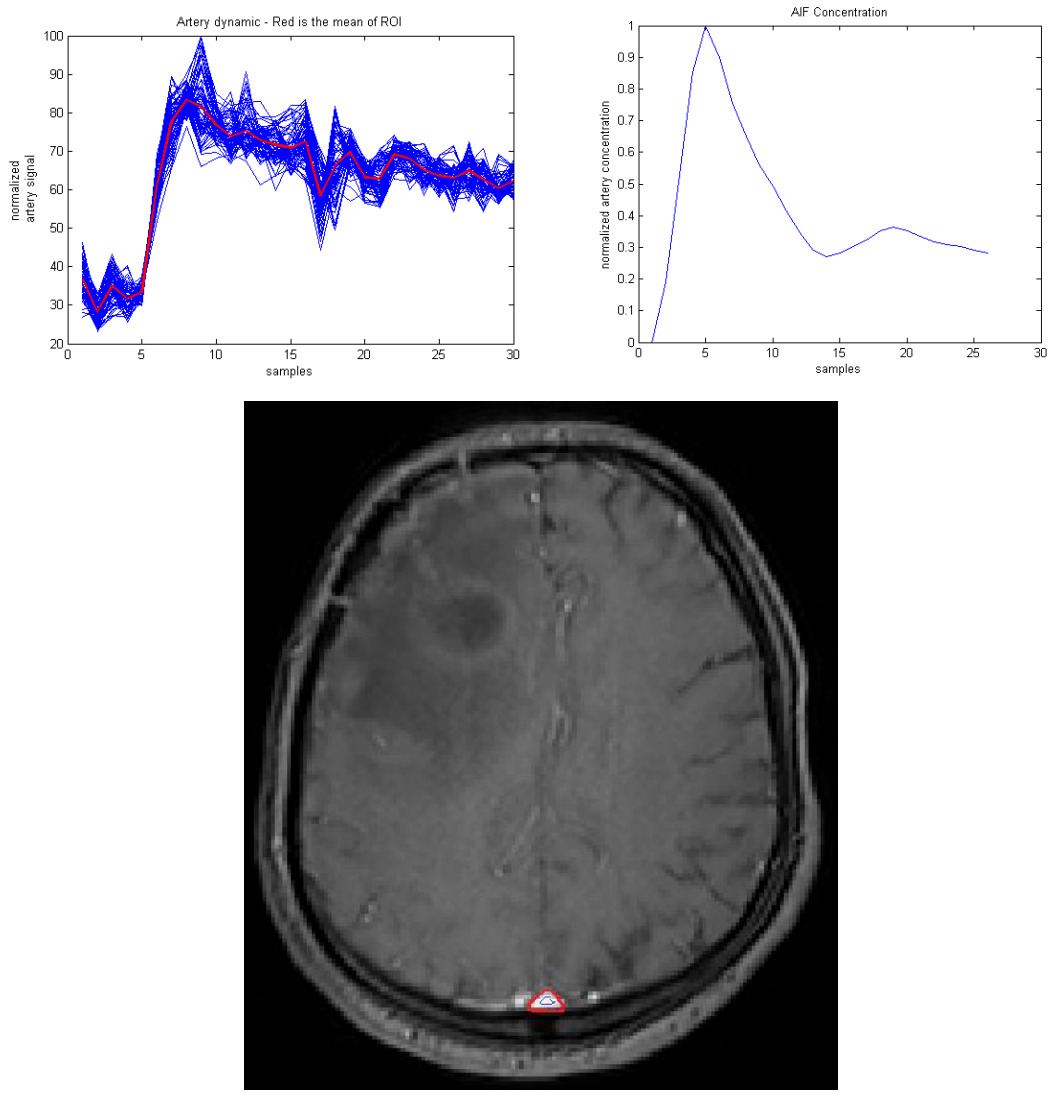

Fig. 45: a) blue lines are the signal intensities for each pixel in the ROI of artery, red line is the mean signal, b) conversion of the mean artery signal to concentration; notice the second pass of the Gd (second peak) and the nonlinearities in comparison with the SI c) Artery selection from a slice of dynamic images.

The VPH tool developed in p-medicine take as input the patient's DCE MRI imaging data and perform physiological modelling and extraction of tissue physiological parameters that are

computed from PK models of contrast agent kinetics. It is applicable in several anatomical areas including the brain, prostate and breast and can be used to assist the evaluation of treatment response [HAH08]. Fig. 16 depicts the results in a ROI of an MRI image slice and the corresponding ktrans values, exhibiting high permeability values in the malignant region.

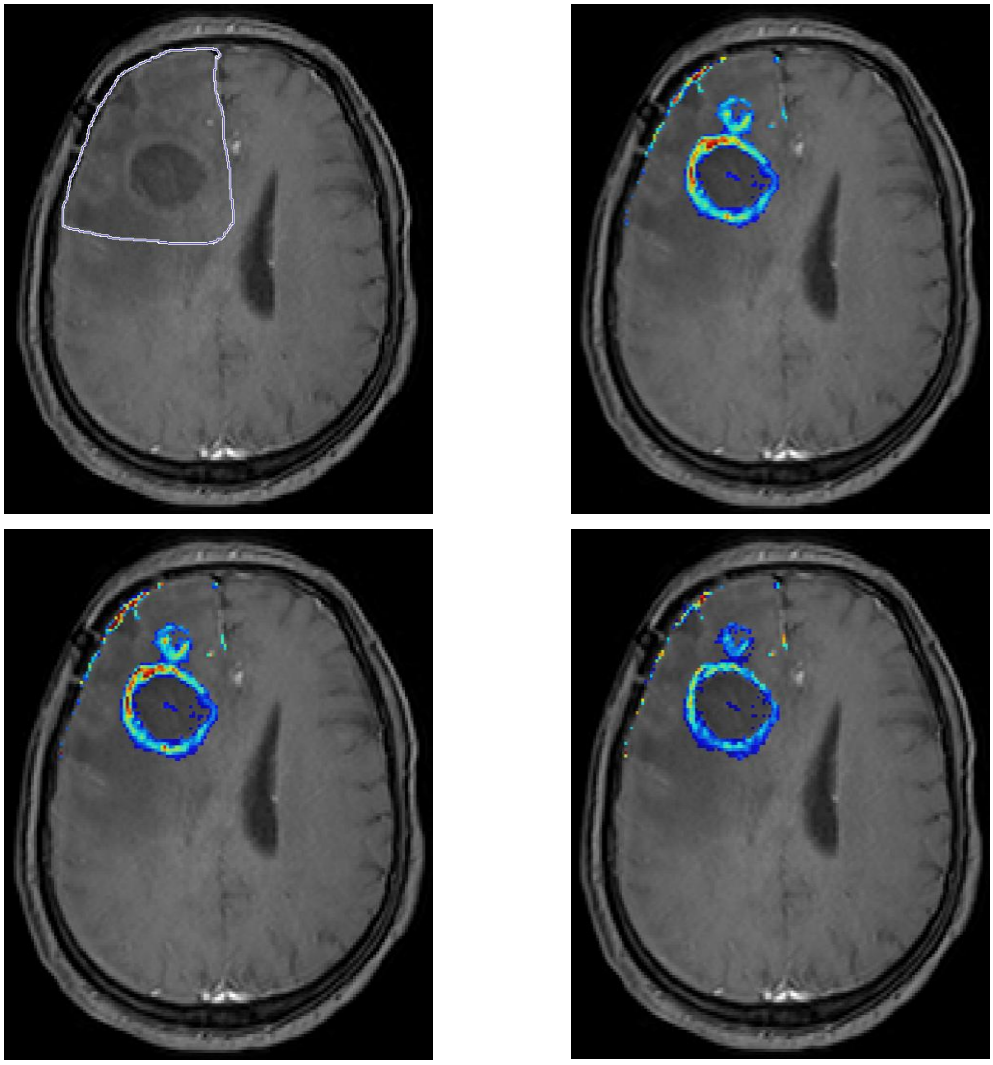

Fig. 16: Quantitative results in brain MRI data. a) selection of ROI, b) AUC, c) ktrans, d) vp.

7 Conclusion

It is worthwhile to point out that the analysis given in Section 4-6 was based on the initial collection of the models that will be included in the CHIC model repository. This initial model collection will of course be subject to further scrutiny with the continuous progress the project. However, through the requirement analysis towards the initial model collection, we are able to draw conclusions on the common requirement of visualization and image processing techniques. We will further refine these requirements where necessary in the duration of the project.

7.1 Summarised requirement on visualization

The user requirement investigation shows that following visualization techniques are needed across different cancer models

- **2D Graphs** such as curves, lines, histograms, that can be used to display data patterns. For example, we need to use 2D line graph to show time evolution of total number of geometrical cells involved in the tumor, and time evolution of number of cells of different types in the whole simulation over time, all of which are important measures for the prediction of tumor volume/population change.

  Combined 2D plot graphs are also needed for visualizing the results of several code executions. Coordinated views or side by side views can be used to allow comparison, for example, the data between different patients.

  Network graph techniques can be used to explore the links between the data and their attributes, as well as the overall structure of the data.

- **3D Rendering** such as surface and volume visualizations will be need to visualize cancer disease such as shapes of tumors, which will be important in the prediction of change of overall tumor shape. The 3D rendering can also be coupled with **animated views** that allow us to expose concealed geometry**,** and **animated evoluation** to show longitudinal information of the disease, such as the simulation of tumor growth over simulated time.

  Volume visualization can be used for the representation of 3D and 4D(3D+time) structural and temporal information from the results of tumor modeling and simulation. We need to look into a range of adequate visual techniques for the portrayal of volumetric structures.

  Similar to the 2D case**, combined views** in one panel also needed to compare the shape of tumors before and after the treatment.

  Colour coded views are often needed for showing geometric cells. 2D cut through is often used as a means to explore internal structures of objects (e.g. tumor) under concerns.

- **Data selection** techniques will be important in terms of allowing users to search and interact with the data.

- **Data and dimension reduction** is important as the result of cancel models often reside in high dimensional space. Techniques that present high dimensional information include parallel coordinates with properly arranged order of the data attribute for visual exploration of data pattern; subspace clustering showing data patterns in a relevant sub feature space allowing avoidance of the influences from irrelevant dimensions.

- **User interaction** constitutes the key for a user centered exploration . Standard interaction techniques will be implemented, including selection, panning, highlighting & brushing, zoom in/out(e.g. focus & context), which will be incorporated with a number of data analysis techniques (filtering, aggregation). The focus here should be on the user, i.e. how to develop the most effective interaction techniques to support user interaction and knowledge exploration from the data.

In addition to the visualization of results from individual models, visualization in CHIC also need to:

- visualize the structure of the models and data repository to allow an overall picture of the model/data repository.
- visualize information associated to the models, e.g. parameters. The information can be regarded as a set of multi-dimensional data.
- visualize the data in the data repository. The data visualization here will cover two individual aspects, namely visualization of the information of the data (which can be viewed as a net of multi-dimensional data in a similar way to the models); and visualization of the data itself.

Given the amount of the data for visualization, we need to develop scalable visualization techniques to support the visualization of large scale data. These will include data removal and filtering techniques that allow users to focus on their selected targeted data; aggregation techniques that allow users to combine details and create different levels of overviews in hierarchies and support users to perform "overviews first and details on demand".

7.2 Summarised requirement on image processing

Image processing and image analysis is heavily demanded in most of the cancer models in the model repository. A number of basic image processing functions include:

- Multi modality image formatting and transformation - The available imaging data are usually 3D DICOM MRI (e.g. in the case of nephroblastoma) or CT data sets (e.g. in the case of lung cancer). Different modalities of imaging techniques (e.g. T1 MRI, T2 MRI, Flair MRI, CT, PET etc) are often required. The DICOM data set, should be converted to a raw file format (raw+mhd). In this file, different subregions of interest should be noted with distinct color numbers (eg white-255 for tumor area, black -0 for normal tissue). The information about the size of the image will be included in mhd file.
- Image filtering techniques to allow a range of basic operations on images.
- Cropping - in order to reduce computational requirements, the requested three-dimensional representation should not correspond to the entire image scan, but to a "region of interest" centered on the tumor, with available space around it to permit growth simulations. The amount of this extra space can be defined based on the maximum dimension of the tumor: an extra space equal to half the maximum direction of the tumor is used along the 3 dimensions of the cartesian coordinate system.
- Segmentation - Segmentation is a very important task in this project. Areas of interest should be annotated by the clinicians by using appropriate software. These areas might be Tumor and necrotic/cystic areas within. Tumor delineation (external boundary of tumor) is the minimum requirement for all the types of tumors that will be addressed, such as brain tissues, white-grey matter, CSF, and skull boundaries for the glioblastoma cases, neighbor organs at risk, healthy and pathological tissue segmentation.

- Registration - Registration of images acquired at different time points or/and position is needed. Fusion of different imaging methods (T1, T2, DW MRI) might be needed to extract valuable information.
- Resampling - Usually voxels in imaging data sets are non-isotropic, i.e. their dimensions differ in the x-,y- and z-direction. The 3D images need resampling because the voxels defined in the ICCS discrete models are cubic. Voxels of 1 or 2 mm acne (resolution) are commonly used (depending on the computational time demands). In case the resulting voxel grid is of higher resolution, interpolation is also needed to have a smooth transition from slice to slice.
- Diagnosis from medical image – for example, The diagnosis of gliomas can be done by MRI, CT, angiogram or biopsy, with MRI being the most common non-invasive method. When a high-grade glioma is diagnosed, immediate treatment is necessary because it exhibits a very aggressive and invasive behavior.
- Treatment monitoring – for example, sequential sets of magnetic resonance images and the development of small molecular weight paramagnetic contrast agents have a major impact in the assessment and monitoring of tumor treatment response.

8 References

[ADR07] JDL. Adrianus, EM. Vivian van den Boogaart, JM. Tim, M. Lubberink: Use of H215O-PET and DCE-MRI to Measure Tumor Blood Flow. The Oncologist vol. 13 no. 6 631-644, 2007

[AGU10] Aguila R. P. Automatic segmentation and classification of computed tomography brain images: An approach using one-dimensional Kohonen networks. Int. J. Comp. Science 2010; 27-35.

[AND09] K. Andrews, M. Wohlfahrt, G. Wurzinger: Visual graph comparison. In Proceedings of International Conference on Information Visualisation, pp. 62–67. 16 pp. 81–88. 16, 2009

[ARG12] KD. Argyri, DD. Dionysiou, GS. Stamatakos: Modeling the Interplay Between Pathological Angiogenesis and Solid Tumor Growth: the Anti-angiogenic Treatment Effect, 1 - 4, 2012

[BAR08] DP. Barboriak, JR. MacFall, BL. Viglianti, D. Dewhirst: Comparison of three physiologically-based pharmacokinetic models for the prediction of contrast agent distribution measured by dynamic MR imaging. J. Magn. Reson. Imaging, 27: 1388–1398, 2008

[BAT99] DIG. Battista, P. Eades, R. Tamassia, IG. Tollis: Graph Drawing: Algorithms for the Visualization of Graphs. Prentice Hall, 1999

[BAU11] S. Bauer, L. Nolte, M. Reyes: Fully automatic segmentation of brain tumor images using support vector machine classification in combination with hierarchical conditional random field regularization. In: Fichtinger, G., Martel, A., Peters, T. (eds.) MICCAI International Conference on Medical Image Computing and Computer-Assisted Intervention. Lecture Notes in Computer Science, vol. 14, pp. 354-61. Springer Berlin Heidelberg, Toronto, 2011

[BAU12] S. Bauer, C. May, D. Dionysiou, G. Stamatakos, P. Buchler, M. Reyes: Multi-Scale Modeling for Image Analysis of Brain Tumor Studies. IEEE Transactions on Biomedical Engineering 59(1), 25-29, 2012

[BOY01] Y. Boykov, O. Veksler, R. Zabih, Fast approximate energy minimization via graph cuts, IEEE Trans. PAMI, 23(11):1222-1239, 2001

[BOY04] Y. Boykov, V. Kolmogorov. An experimental comparison of min-cut/max-flow algorithms for energy minimization in vision. IEEE Trans. PAMI, 26(9):1124–1137, 2004

[CAR13] Cárdenes R., Warfield S. K., Macías E. M., Santana J. A. and Ruiz-Alzola J. An efficient algorithm for multiple sclerosis segmentation from brain MRI. Int. Workshop Comput. Aided Syst. Theory (EUROCAST) 2003; 542-551.

[CAS06] P. Castorina, PP. Delsanto, C. Guiot: A Classification Scheme for Phenomenological Universalities in Growth Problems, Phys Rev Lett. 96(18):188701, 2006

[CAS09] P. Castorina, D. Carcò, C. Guiot, TS. Deisboeck: Tumor growth instability and its implications for chemotherapy, Cancer Res. 2009 Nov 1;69(21):8507-15. doi: 10.1158/0008-5472.CAN-09-0653. Epub 2009

[Ced00] Cedilnik, A., Rheingans, P. (2000). Procedural Annotation of Uncertain Information. In Proc. of the IEEE Conference onVisualization, pp. 77–83, 2000

[Cle88] W. S. Cleveland and M. E. McGill, editors. Dynamic Graphics for Statistics. Statistics /Probability Series. Wadsworth & Brooks/Cole, Pacific, Grove, CA, USA, 1988

[COM02] Comaniciu D. and Meer P. Mean-shift: A robust approach towards feature-space analysis. IEEE Trans. Pattern Ana. Mach. Intell 2002; 23: 603-619.

[CON12] JP. O'Connor, Jackson A, Parker GJ, Roberts C, Jayson GC.: Dynamic contrast-enhanced MRI in clinical trials of antivascular therapies. Nat Rev Clin Oncol 9:167-77, 2012

[DIO04] DD. Dionysiou, GS. Stamatakos, NK. Uzunoglu, KS. Nikita, A. Marioli: A four-dimensional simulation model of tumour response to radiotherapy in vivo: parametric validation considering radiosensitivity, genetic profile and fractionation. J Theor Biol. 230(1), 1-20, 2004

[DIO08] DD. Dionysiou, GS. Stamatakos, D. Gintides, N. Uzunoglu, K. Kyriaki: Critical parameters determining standard radiotherapy treatment outcome for glioblastoma multiforme: a computer simulation. Open Biomed Eng J. 2:43-51, 2008

[DON10] SB . Donaldson, CM. West, SE. Davidson, BM. Carrington, G. Hutchison, AP. Jones, SP. Sourbron, DL. Buckley: A comparison of tracer kinetic models for *T*1-weighted dynamic contrast-enhanced MRI: Application in carcinoma of the cervix. Magn Reson Med, 63: 691–700, 2010

[DUG04] Dugas-Phocion G., González Ballester M. Á., Malandain G., Lebrun C. and Ayache N. Improved EM-based tissue segmentation and partial volume effect quantification in multi-sequence brain MRI. Int. Conf. Med. Image. Comp. Assist. Int. (MICCAI) 2004; 26-33.

[ELM08] N. Elmqvist, TN. Do, H. Goodell, N. Henry, JD. Fekete: Zame: Interactive large-scale graph visualization. In Proceedings of IEEE Pacific Visualization Symposium, pp. 215–222. 2008

[ELM10] N. Elmqvist, J. D. Fekete, Hierarchical Aggregation for Information Visualization: overview, techniques and design guidelines, IEEE TVCG 2010

[PRO06] JM. Provenzale, S. Mukundan, DP. Barboriak, Diffusion-weighted and perfusion MR imaging for brain tumor characterization and assessment of treatment response, Radiology, 239(3):632-49, 2006

[ESS12] M. Essig, MS. Shiroishi, TB. Nguyen, M. Saake, JM. Provenzale, D. Enterline, N. Anzalone, A. Dörfler, A. Rovira, M. Wintermark, M. Law: Perfusion MRI: The Five Most Frequently Asked Technical Questions", American Journal of Roentgenology, DOI:10.2214/AJR.12.9543, 2012

[FEK02] J.-D. Fekete and C. Plaisant. Interactive information visualization of a million items. In Proceedings of the IEEE Symposium on Information Visualization, pages 117–124, 2002

[FEL04] P.F. Felzenszwalb, D.P.Huttenlocher, Efficient belief propagation for early vision, In CVPR, 2004

[FER10]B. J. Ferdosi, et al. Find and visualizing relevant subspaces for clustering high-dimensional astronomical data using connected morphological operators, IEEE Symposium on visual analytics science and technology, Salt Lake City, 2010

[GEO08] EC. Georgiadi, GS. Stamatakos, NM. Graf, EA. Kolokotroni, DD. Dionysiou, A. Hoppe, NK. Uzunoglu: Multilevel cancer modeling in the clinical environment: Simulating the behavior of Wilms tumor in the context of the SIOP 2001/GPOH clinical trial and the ACGT project, 1-8, 2008

[GEO12] EC. Georgiadi, DD. Dionysiou, N. Graf, GS. Stamatakos: Modeling Nephroblastoma Treatment Response Cases with In Silico Scenarios. Advanced Research Workshop on In Silico Oncology and Cancer Investigation - The TUMOR Project Workshop (IARWISOCI), 1 - 4, 2012

[GEO12] ECh. Georgiadi, DD. Dionysiou, N. Graf, GS. Stamatakos: Towards in silico oncology: adapting a four dimensional nephroblastoma treatment model to a clinical trial case based on multi-method sensitivity analysis. Comput Biol Med. 42(11):1064-78, 2012

[GIA12a] SG. Giatili, GS. StamatakosA detailed numerical treatment of the boundary conditions imposed by the skull on a diffusion–reaction model of glioma tumor growth. Clinical validation aspects. Vol 218, Is 17, 8779–8799, 2012

[GIA12b] SG. Giatili, GS Stamatakos: The Continuous Mathematics Based Glioblastoma Oncosimulator: Application of an Explicit Three Dimensional Numerical Treatment of the Skull-Glioblastoma Neumann Boundary Condition on Real Anatomical Data, Advanced Research Workshop on In Silico Oncology and Cancer Investigation - The TUMOR Project Workshop (IARWISOCI), 2012 5th International, 1-5, 2012

[GLI09] AS. Gliozzi, C. Guiot, PP. Delsanto: A New Computational Tool for the Phenomenological Analysis of Multipassage Tumor Growth Curves. PLoS ONE 4(4): e5358, 2009

[GOO11] A. Gooya, A., K. Pohl, M. Bilello, G. Biros, C. Davatzikos: Joint Segmentation and Deformable Registration of Brain Scans Guided by a Tumor Growth Model. In: Fichtinger, G., Martel, A., Peters, T.M. (eds.) Medical Image Computing and Computer-Assisted Intervention MICCAI 2011. pp. 532-540. Springer LNCS, Toronto 2011

[GRE09] M. Greilich, M. Burch, S. Diehl: Visualizing the evolution of compound digraphs with TimeArcTrees. Computer Graphics Forum 28, 3, 975–982, 2009

[HAB07] T. Haberichter, B. Mädge, RA. Christopher, N. Yoshioka, A. Dhiman, R. Miller, R. Gendelman, SV. Aksenov, IG. Khalil, SF. Dowdy: A systems biology dynamical model of mammalian G1 cell cycle progression. Molecular Systems Biology, 3:84, 2007

[HAH08] OM. Hahn, C. Yang, M. Medved, G. Karczmar, E. Kistner, T. Karrison, E. Manchen, M. Mitchell, MJ. Ratain, WM. Stadler: Dynamic Contrast-Enhanced Magnetic Resonance Imaging Pharmacodynamic Biomarker Study of Sorafenib in Metastatic Renal Carcinoma, Journal of Clinical Oncology, October 1, 2008 vol. 26, 2008

[HAH99] P. Hahnfeldt, D. Panigrahy, J. Folkman, L. Hlatky: Tumor development under angiogenic signaling: a dynamical theory of tumor growth, treatment response, and postvascular dormancy. Cancer Res. 1;59(19):4770-5, 1999

[HAN12] T. Fritz-Hansen, E. Rostrup, HB. Larsson, L. Søndergaard, P. Ring, O. Henriksen: Pattern analysis accounts for heterogeneity observed in MRI studies of tumor angiogenesis. Magn Reson Med, 36(2):225-31, 2012

[HAN96] T. Fritz-Hansen, E. Rostrup, HB. Larsson, L. Søndergaard, P. Ring, O. Henriksen: Measurement of the arterial concentration of Gd-DTPA using MRI: A step toward quantitative perfusion imaging. Magn Reson Med, 36: 225–231. 1996

[HAR04] HA. Haroon, , D. Buckley, TA. Patankar, GR. Dow, SA. Rutherford, D. Balériaux, A. Jackson: A comparison of Ktrans measurements obtained with conventional and first pass pharmacokinetic models in human gliomas. J. Magn. Reson. Imaging, 19: 527–536, 2004

[HER00] I. Herman, G. Melancon, M. Marshall: Graph visualization and navigation in information visualization: A survey. IEEE Transactions on Visualization and Computer Graphics 6, 1, 24–43. 2000

[HIN09] P. Hinow, P. Gerlee, LJ. McCawley, V. Quaranta, M. Ciobanu, S. Wang, JM. Graham, BP. Ayati, J. Claridge, KR. Swanson, M. Loveless, AR. Anderson A spatial model of tumor-host interaction: application of chemotherapy. Math. Biosci. Eng. 6(3):521-545, 2009

[HUB12] ME. Hubbard, HM. Byrne: Multiphase modelling of vascular tumour growth in two spatial dimensions. Journal of Theoretical Biology, 2012

[HUE07] R. Huey, GM. Morris, AJ. Olson, DS. Goodsell: A Semiempirical Free Energy Force Field with Charge-Based Desolvation. J Comput Chem, 30;28(6), 1145-52, 2007

[INS85] A. Inselberg. The plane with parallel coordinates. The Visual Computer, 1(2):69–91, 1985.

[JEN08] Jens N. Kaftan and Andr{\'e} A. Bell and Til Aac, Proceedings of the Third International Conference on Computer Vision Theory and Applications, VISAPP 2008

[Kei10] Daniel Keim (Scientific Coordinator of VisMaster), Jörn Kohlhammer (Coordinator of VisMaster), Geoffrey Ellis and Florian Mansmann, Mastering the information age: solving problems with Visual Analytics, Eurographics Association, 2010.

[KOL06] V. Kolmogorov, Convergent tree-reweighted message passing for energy minimization, IEEE Trans. PAMI, 28(10):1568-1583, 2006

[KOL08] EA. Kolokotroni, GS. Stamatakos, DD. Dionysiou, EC. Georgiadi, C. Desmedt, NM. Graf: Translating Multiscale Cancer Models into Clinical Trials: Simulating Breast Cancer Tumor Dynamics within the Framework of the "Trial of Principle" Clinical Trial and the ACGT Project. BioInformatics and BioEngineering, 2008. BIBE 2008. 8th IEEE International Conference on, 1 - 8, 2008

[KOL11] EA. Kolokotroni, DD. Dionysiou, NK. Uzunoglu, GS. Stamatakos: Studying the growth kinetics of untreated clinical tumors by using an advanced discrete simulation model. Mathematical and Computer Modelling, 54:1989-2006, 2011

[KRI09]H.P. Kriegel, et al. Clustering High-Dimensional Data: A Survey on Subspace Clustering, Pattern-based clusgtering and Correlation clustering, ACM Transaction on Knowledge Discovery from Data, 3(1), 2009

[Lan10] T. von Landesberger, A. Kuijper, T. Schreck, J. Kohlhammer, J.J. van Wijk, J.-D. Fekete, D.W. Fellne, Visual analysis of large graphs, Eurographics, 2010, State of The Art Report, 2010

[LAN11] T.von. Landesberger, A. Kuijper, T. Shreck, J. Kohlhammer, J. J. van Wijk, J.E. Fekete, D. W. Fellner, Visual Analysis of Large Graphs, Eurographics, STAR-State of The Art Report, 2011

[LEE07] IM. Van Leeuwen, HM. Byrne, OE. Jensen, JR. King: Elucidating the interactions between the adhesive and transcriptional functions of beta-catenin in normal and cancerous cells. J Theor Biol. 247(1), 77-102. 2007

[LES06] J. Leskovec, C. Faloutsos: Sampling from large graphs. In Proceedings of 12th ACM SIGKDD Int. Conference on Knowledge Discovery and data mining (2006), pp. 631–636, 2006

[LI00] KL. Li, XP. Zhu, J. Waterton, A. Jackson: Improved 3D quantitative mapping of blood volume and endothelial permeability in brain tumors, J. Magn. Reson. Imaging, 12: 347–357. 2000

[LIT10] GJS.Litjens, M. Heisen, J. Buurman, B.M. Haar Romeny: Pharmacokinetic models in clinical practice: What model to use for DCE-MRI of the breast?, Biomedical Imaging: From Nano to Macro, IEEE International Symposium, vol., no., pp.185-188, 14-17, 2010

[MAR07] K. Marias, D. Dionysiou, V. Sakkalis, N. Graf, RM. Bohle, PV. Coveney, S. Wan, A. Folarin, P. Büchler, M. Reyes, G. Clapworthy, E. Liu, J. Sabczynski, T. Bily, A. Roniotis, M. Tsiknakis, E. Kolokotroni, S. Giatili, C. Veith, E. Messe, H. Stenzhorn, YJ. Kim, S. Zasada, AN. Haidar, C. May, S. Bauer, T. Wang, Y. Zhao, M. Karasek, R. Grewer, A. Franz, G. Stamatakos: Clinically driven design of multi-scale cancer models: the ContraCancrum project paradigm. Interface Focus. 1(3):450-61. 2007

[MOR09] GM. Morris, R. Huey, W. Lindstrom, MF. Sanner, RK. Belew, DS. Goodsell, AJ. Olson: AutoDock4 and AutoDockTools4: Automated Docking with Selective Receptor Flexibility. J Comput Chem, 30(16) 2785-91, 2009

[NEU06] P. Neumann, MS. Carpendale, A. Agarawala: Phyllotrees: Phyllotactic patterns for tree layout. In Proceedings of the Joint Eurographics and IEEE TCVG Symposium on Visualization, Eurographics, pp. 59–66, 2006

[OUZ12] EN. Ouzounoglou, DD. Dionysiou, M. Stanulla, GS. Stamatakos: Towards Patient Personalization of an Acute Lymphoblastic Leukemia Model during the Oral Administration of Prednisone in Children: Initiating the ALL Oncosimulator. Advanced Research Workshop on In Silico Oncology and Cancer Investigation - The TUMOR Project Workshop (IARWISOCI), 2012 5th International, 1-4, 2012

[Pal93] Nikhil R Pal, Sankar K Pal, A review on image segmentation techniques, Pattern Recognition,Volume 26, Issue 9, 1277–1294, 1993

[PAT83] CS. Patlak, RG. Blasberg, JD. Fenstermacher: Graphical evaluation of blood-to-brain transfer constants from multiple-time uptake data, 1983

[PER90] Perona P. and Malik J. Scale-Space and Edge-Detection using Anisotropc Diffusion. IEEE Transactions on Pattern Analysis and Machine Intelligence 1990; 12: 629-639.

[PIR11] H. Piringer, Large Data Scalability in Visual Analysis, PhD Dissertation, 2011.

[POL11] J. Poleszczuk, M. Bodnar, U. Foryś: New approach to modeling of antiangiogenic treatment on the basis of Hahnfeldt et al. model. Math Biosci Eng. 8(2):591-603. doi: 10.3934/mbe.2011.8.591, 2011

[Pot10] Potter, K., Kniss, J., Riesenfeld, R., Johnson, C. R. (2010). Visualizing Summary Statistics and Uncertainty. Computer Graphics Forum 29, 3, 823–832, 2010

[RAG10] DK. Ragan: Measurement of the vascular input function in mice for DCE-MRI". UT GSBS Dissertations and Theses.Paper 11, 2010

[RON12] A. Roniotis, V. Sakkalis, E. Tzamali, G. Tzedakis, M. Zervakis, K. Marias: Solving the PIHNA model while accounting for radiotherapy. Advanced Research Workshop on In Silico Oncology and Cancer Investigation - The TUMOR Project Workshop (IARWISOCI), 5th International, 1 - 4, 2012

[SAM06] S-Samuel. Walker, MO. Leach, DJ. Collins: Evaluation of response to treatment using DCE-MRI: the relationship between initial area under the gadolinium curve (IAUGC) and quantitative pharmacokinetic analysis, Phys. Med. Biol. 51 3593, 2006

[SCH02] Schoelkopf B. and Smola A. J. Learning with kernels: support vector machines, regularization, optimization, and beyond. MIT Press. 2002

[SCH09] HJ. Schulz, H. Schumann, S. Hadlak: Pointbased tree representation - a new approach for large hierarchies. In Proceedings of IEEE Pacific Visualization Symposium, 2009

[SHN92] B. Shneiderman. Tree visualization with tree-maps: A 2-D space-filling approach. ACM Transactions on Graphics, 11(1):92–99, 1992

[SLE98] Sled J. G., Zijdenbos P. and Evans C. A nonparametric method for automatic correction of intensity nonuniformity in MRI data. IEEE transactions on medical imaging, 1998; 17(1): 87-97. doi: 10.1109/42.668698.

[SOU11] SP. Sourbron, DL. Buckley: On the scope and interpretation of the Tofts models for DCE-MRI. Magn Reson Med, 66: 735–745, 2011

[SOU12] SP. Sourbron, DL. Buckley: Tracer kinetic modelling in MRI: estimating perfusion and capillary permeability, Physics in Medicine and Biology vol 57 R1, 2012

[STA02] GS. Stamatakos, DD. Dionysiou, EI. Zacharaki, NA. Mouravliansky, KS. Nikita, NK. Uzunoglu: In silico radiation oncology: combining novel simulation algorithms with current visualization techniques. Proceedings of the IEEE, 90:11, 1764 - 1777, 2002

[STA06] GS. Stamatakos, VP. Antipas, NK. Uzunoglu: A spatiotemporal, patient individualized simulation model of solid tumor response to chemotherapy in vivo: the paradigm of glioblastoma multiforme treated by temozolomide. IEEE Trans Biomed Eng, 53(8):1467-77, 2006

[STA07] GS. Stamatakos, EC. Georgiadi, N. Graf, EA. Kolokotroni, DD. Dionysiou: Exploiting Clinical Trial Data Drastically Narrows the Window of Possible Solutions to the Problem of Clinical Adaptation of a Multiscale Cancer Model. PLoS ONE 6(3): e17594, 2007

[STA10] GS. Stamatakos, EA. Kolokotroni, DD. Dionysiou, ECh. Georgiadi, C. Desmedt. An advanced discrete state–discrete event multiscale simulation model of the response of a solid tumor to chemotherapy: Mimicking a clinical study. J Theor Biol, 266(1), 124-39, 2010

[STE07] U. Sternberg, R. Witter, AS. Ulrich: All-atom molecular dynamics simulations using orientational constraints from anisotropic NMR samples. J Biomol NMR, 38(1), 23-39, 2007

[SWA11] KR. Swanson, RC. Rockne, J. Claridge, MA. Chaplain, EC. Alvord, AR. Anderson : Quantifying the Role of Angiogenesis in Malignant Progression of Gliomas: In Silico Modeling Integrates Imaging and Histology, Cancer Res. 71(24):7366-75, 2011

[SZE08] R. Szeliski, R. Zabih, D. Scharstein, O. Veksler, V. Kolmogorov, A. Agarwala, M. Tappen, C. Rother, A comparative study of engery minimization methods for Markov Random Fields with smoothness based priors, IEEE Trans. PAMI, 30(6), 1066-1080, 2008

[TOF91] PS. Tofts, AG. Kermode: Measurement of the blood–brain barrier permeability and leakage space using dynamic MR imaging: 1. Fundamental concepts" Magn. Reson. Med. Vol. 17 357–67, 1991

[TOF97] PS. Tofts: Modeling tracer kinetics in dynamic Gd-DTPA MR imaging. J. Magn. Reson. Imaging, 7: 91–101, 1997

[TUC98] Tuceryan M. and Jain A. K. Texture analysis. In C. H. Chen, L. F. Pau, & P. S. P. Wang (Eds.), Handbook of Pattern Recognition and Computer Vision (2nd ed., 1998; 304: 207-248). World Scientific Publishing Co.

[TWE91] MF. Tweedle, P. Wedeking, J. Telser, CH. Sotak, CA. Chang, K. Kumar, X. Wan, SM. Eaton: Dependence of MR signal intensity on Gd tissue concentration over a broad dose range, Magn Reson Med, 22: 191–194, 1991

[TZE12] G. Tzedakis, E. Tzamali, V. Sakkalis, A. Roniotis, K. Marias: Hybrid Model for Tumor Spheroids with Intratumoral Oxygen Supply Heterogeneity. Advanced Research Workshop on In Silico Oncology and Cancer Investigation - The TUMOR Project Workshop (IARWISOCI), 2012 5th International, 1 - 4, 2012

[Utt05] J. M. Utts. Seeing Through Statistics. Brooks/Cole, 3rd edition, 2005.

[VAN99] Van Leemput K., Maes F., Vandeurmeulen D. and Suetens P. Automated model-based tissue classification of MR images of the brain. IEEE Trans. Med. Imag. 1999; 18: 897-908.

[VER08] R. Verma, E. Zacharaki, Y. Ou, H. Cai, S. Chawla, S. Lee, E. Melhem, R. Wolf, C. Davatzikos: Multiparametric tissue characterization of brain neoplasms and their recurrence using pattern classification of MR images. Academic radiology 15(8), 966-77, Aug 2008

[VIO01] P. Viola, M. Jones, Rapid Object Detection using a Boosted Cascade of Simple Features, CVPR, 2001

[vLan09] VT. Landesberger, M. Görner, R. Rehner, T. Schreck: A system for interactive visual analysis of large graphs using motifs in graph editing and aggregation. In Proceedings of Vision Modeling Visualization Workshop, 331–339., 2009

[WAI05] M. Wainwright, T. Jaakkola, A. Willsky, Map estimation via agreement on trees: Message-passing and linear programming, IEEE Trans. Information Theory, 51(11): 3697-3717, 2005

[WEI84] HJ. Weinmann, M. Laniado, W. Mützel: Pharmacokinetics of GdDTPA/dimeglumine after intravenous injection into healthy volunteers, Physiological Chemistry and Physics and Medical NMR 16(2):167-172, 1984

[WEL08] M. Wels, G. Carneiro, A. Aplas, M. Huber, J. Hornegger, D. Comaniciu: A discriminative model-constrained graph cuts approach to fully automated pediatric brain tumor segmentation in 3-D MRI. Medical image computing and computer-assisted intervention : MICCAI. International Conference on Medical Image Computing and Computer-Assisted Intervention 11(Pt 1), 67-75, 2008

[YAN07] C. Yang, GS. Karczmar, M. Medved, WM. Stadler: Multiple reference tissue method for contrast agent arterial input function estimation. Magn Reson Med, 58: 1266–1275, 2007

[YAN07] TE. Yankeelov, M. Lepage, A. Chakravarthy, EE. Broome, KJ. Niermann, MC. Kelley, I. Meszoely, IA. Mayer, CR. Herman, K. McManus, RR. Price, JC. Gore: Integration of quantitative DCE-MRI and ADC mapping to monitor treatment response in human breast cancer, Magnetic Resonance Imaging, Volume: 25, Issue: 1, Pages: 1-13, 2007

[YAN10] Q. Yang, L. Wang, N. Ahuja, A Constant-Space Belief Propagation algorithm for stereo matching, In CVPR, 2010

[Yi07] JS. Yi, YA. Kang, J. Stasko, J. Jacko: Toward a deeper understanding of the role of interaction in information visualization. IEEE Transactions on Visualization and Computer Graphics 13, 6 (2007), 1224–1231, 2007

[YI09] Yi Z., Criminisi A., Shotton J. and Blake A. Discriminative, semantic segmentation of brain tissue in MR images. Int. Conf. Med. Image. Comp. Assist. Int. (MICCAI) 2009; 558-565.

[ZAC09] E. Zacharaki, C. Hogea, D. Shen, G. Biros, C. Davatzikos: Non-diffeomorphic registration of brain tumor images by simulating tissue loss and tumor growth. NeuroImage 46(3), 762-774, 2009

[ZAU03] RJ. Zauhar, G. Moyna, L. Tian, Z. Li, WJ. Welsh: Shape Signatures: A New Approach to Computer-Aided Ligand- and Receptor-Based Drug Design. J Med Chem, 18;46(26), 5674-90, 2003